Doctor of Philosophy

A STUDY ON FORCE CONTROL MECHANISM AND ALGORITHM FOR DEBURRING ROBOT

Graduate School of University of Ulsan

Department of Mechanical and Automotive Engineering

May 2018

Nguyen Chi Thanh

A STUDY ON FORCE CONTROL MECHANISM AND ALGORITHM FOR DEBURRING ROBOT

Advisor: Professor Yang Soon Yong

A Dissertation

Submitted to the Graduate School of the University of Ulsan in Partial Fulfillment of the Requirements for the Degree of

Doctor of Philosophy

by

Nguyen Chi Thanh

Graduate School of Mechanical and Automotive Engineering

University of Ulsan, South Korea

May 2018

NGUYEN CHI THANH 의

공학박사 학위 논문을 인준함

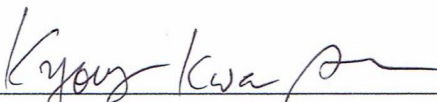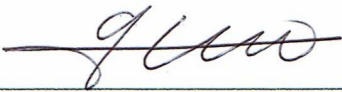| 심사위원장 | 안경관 | (인) |
심사위원	양순용	(인)
심사위원	이병룡	(인)
심사위원	김용석	(인)
심사위원	임태형	(인)

울산대학교 대학원

기계자동차공학과

2018 년 5 월

A STUDY ON FORCE CONTROL MECHANISM AND ALGORITHM FOR DEBURRING ROBOT
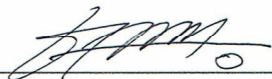
This certifies that the dissertation of

NGUYEN CHI THANH is approved.

Committee Chairman: Prof. Ahn Kyung Kwan

Committee Member: Prof. Yang Soon Yong

Committee Member: Prof. Lee Byung Ryong

Committee Member: Prof. Kim Yong Seok

Committee Member: Dr. Lim Tae Hyung

Graduate School of Mechanical and Automotive Engineering

University of Ulsan, South Korea

May 2018

ACKNOWLEDGMENTS

Thank all you come into my life.

Ulsan, South Korea

May 2018

Nguyen Chi Thanh

ABSTRACT

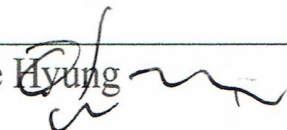The research carries out a study on the force control mechanism and algorithm for the deburring robot. The interaction between the robot and workpieces is the main objective to study through the robot motion and contact force.

On the manufacturing technologies, the force control device for deburring robot, the intelligent deburring control (IDC) device is produced as a controllable stiffness mechanism. The IDC device consists of two pneumatic cylinders with a magnetic position sensor, pneumatic valve system, and an acceleration sensor. This device is modeled as the mas-damper-spring system in which the deburring tool is a mass component. The IDC device operates as an elastic suspension system, the automatic controller was required in the process of designing and manufacturing of IDC device. Therefore, the force control and interactive control were considered and studied. Through many steps of research, the realization of target impedance model is the main object to implement the simulation and experiment to evaluate the system response and theory. The objective of this research is to evaluate the position/force control for contact robotics by using the unified position/force control method and estimate the various perspectives on force control and robotics. The contact performance between the robot and workpieces is investigated by synthesizing the transient processes of robot motion and contact force. In which, the relation between contact force and robot motion is analyzed by unified position/force control method. In the transient processes, the stabilization of contact force is determined through the stabilization of robot motion. The position/force stabilization characteristics – based target impedance model is realized for building modeling of contact force is a function in accordance with robot motion deviation as position, velocity acceleration and for evaluating the affections of mass, damping, and stiffness parameters on the responses of the contact

force such as overshoot ratio, settling and steady state. The combination of IDC device and robot impedance control can improve the performance of deburring patterns, compensate the actual position, and contact force.

KEYWORDS

Deburring automation robot system, Intelligent Deburring Control (IDC) device, Pneumatic System, Surface Processing, Mathematical Modeling, Constant contact force, Environment Stiffness, Target Impedance Model, Unified Position/Force Approach, Impedance Control, MATLAB, Arduino

TABLE OF CONTENTS

LIST OF TABLES

LIST OF FIGURES

LIST OF ABBREVIATIONS

Nº	Short name	Full name
1	IDC	Intelligent Deburring Control
2	ACFM	Adjustable Constant-Force Mechanism
3	CAD	Computer-Aided Design
4	IPBIC	Improved Position-Based Impedance Control
5	ILC	Iterative Learning Control
6	XML	Extensible Markup Language
7	STL	STereoLithography
8	DOF	Degrees of Freedom
9	PID	Proportional–Integral–Derivative
10	ATC	Auto Tool Changer

CHAPTER I INTRODUCTION

I.   Background

From the middle of the 1980s, along with the automation development in the world, some of the mechanisms of active and passive deburring robot's end-effector were introduced with the suitable control proposals [1-5]. In which, [1] Kazerooni et al. developed a control strategy for precision deburring to guarantee burr removal while compensating for robot oscillations and small uncertainties in the location of the part relative to the robot. [2] Yoshikawa proposed a dynamic hybrid control approach, based on the dynamic equation of robot manipulators and a description of the end-effector constraint, which considers the manipulator dynamics. [3] Stepien et al. described the design and implementation of a microprocessor-based system to control the interaction forces between a five-axis articulated robot and a workpiece. The control system worked in parallel with a robot controller by calculating position corrections that allowed forces to be controlled in the desired manner. These corrections were successfully interfaced to the controller's position control loop on an individual-axis level. Stable force-control algorithms were designed in spite of limitations imposed by flexibility in the robot drive train. For multi-degree-of-freedom force control, it is shown that each axis can be considered autonomous, obviating the need for a multivariable approach. [4] Kazerooni et al. presented the design, construction, and control of a wide bandwidth, active end-effector can be attached to the end-point of a commercial robot manipulator. The end-effector behaves dynamically as a two-dimensional, Remote Center Compliance (RCC). The compliance in this active end-effector is developed electronically and can therefore be modulated by an on-line computer. [5] Bone et al. described the development of an active end effector based force control system for deburring using a PUMA-560 robot. This includes an analysis of the dynamics of the robot arm, positioning errors and the deburring process.

In the 1990s, the numbers of researches increased comparing to last decade [6-33].

2

From the 1990s' early, the deburring processes were focused in many sections. Such as compliance control with the passive compliance end-effector or the 2D planar control table. Some of deburring mechanisms and control proposals were mentioned. In which, [6] Kramer et al. began developing the robotic deburring system with passive compliance end-effector to compensate the positional errors and to provide for simultaneous edge tracking and force control. [7] Choudhary presented a simple heuristic approach for force-position-velocity control of an industrial machine in a computer integrated manufacturing environment. [8] Her et al. realized an automated robotic deburring acting on the workpiece was mounted on the 2D control table. [9] Bone et al. designed force control system by minimizing the normal chamfering force variance online. [10] Liu et al. implemented an adaptive control for a deburring robot can adapt to the deburring process in a manner very similar to a human worker. [11] Elbestawi et al. built a control system incorporating of sensor fusion for inspection, adaptive control parameters and learning control for robotic deburring. [12] Li et al. presented the adaptive feedforward control approach which is based on the adaptive zero phase error tracking control algorithm for robot force control system. [13] Dornfeld positioned the deburring tool by using vision feedback for burr size and location determination, and the sensor feedback by combined force and acoustic emission sensing. [14] Liu used the fuzzy force control to compensate positional inaccuracies and to adjust the feed-rate according to unknown burr size in a systematic way.

In the middle of this decade, the acting force mechanism, motion planning, model structure, control algorithm, and teaching method for robots were studied in diverse ways, such as [15] Ali et al. considered a manipulator as a mass-spring-dashpot system. The inertia, stiffness, and damping of this system can be changed to control the response of the manipulator to different kinds of input interaction forces. [16] Jeon et al. applied learning algorithm to hybrid force and position control of robot manipulators. [17] Liu et al. built a task-level adaptive controller for performing a

claw of complex tasks by robots. The design of the adaptation mechanism that updates the controller parameters (including reference inputs and feedback gains) is based on a set of teaching data taken from a human's demonstrations. [18] Hwang et al. presented a global motion planner for tracing curves in three dimensions with robot manipulator tool frames. This planner generates an efficient motion satisfying three types of constraints: constraints on the tooltip for curve tracing, robot kinematic constraints, and robot-link collision constraints. [19] De Luca et al. proposed a suitable model structure that handles the more general case in which purely kinematic constraints on the robot end-effector live together with dynamic interactions. Feasible end-effector configurations are parameterized from the environment point of view, using a minimal set of coordinates. [20] Tabarah et al. developed two algorithms are for the optimal motion coordination of a pair of industrial robots engaged in contact operations such as part machining or deburring. In the first algorithm, the two robots jointly grasp a tool and move it in such a way that it performs a prescribed contact operation along the surface of a workpiece. In the second algorithm, one robot grasps the tool while a second robot grasps and maneuvers the workpiece; both robots move simultaneously relative to each other so that the tool maintains contact with the workpiece while tracking a prescribed trajectory along its surface at a constant speed. [21] Shimokura et al. discussed a new method for teaching a deburring robot based on demonstration of human skillful motion. The robot is controlled to adjust the tool feed rate in accordance with the various burr characteristics, such as burr size and material properties. This dynamic change of tool feed rate is motivated by the effective human skill in performing a deburring task. The relationship between the tool feed rate and burr characteristic is obtained from the human demonstration data and is stored in a computer as an associative memory. [22] Bone et al. described the sensing and control elements of a system for automated robotic edge deburring. The deburring path, generated by a task planner automatically, is corrected online by an active end e ector with the objective of controlling the chamfer depth. [23] Schimmels applied method for accurate positioning using compliance and constraint is applied to material removal

processes. Accurate forte guidance is achieved through the use of an end-effector mounted jig in conjunction with the proper design of the compliance of the manipulator and the material removal tool. The compliance of the manipulator is designed so that: 1) an initial unique relative position/orientation of the jig with respect to the workpiece edge is attained despite manipulator positioning error; and 2) the unique relative position initially established is maintained while moving along the workpiece edge. [24] Ferretti et al. investigated the robustness properties of explicit force control with respect to contact stiffness applied considering different control laws to an industrial robot affected by joint compliance. A theoretical analysis, performed on the well-known linear fourth-order model of a single joint robot interacting with the environment, shows that, differently from the case of P or PD control, integral control ensures increasing stability with increasing contact stiffness. [25] Tomastik et al. proposed the concept requires the robot for positioning of the cutter and the around-the-arm end-effector capable of measuring the orthogonal force between cutter and workpiece, measuring cutter position with respect to end-effector frame of reference, and actively controlling the cutter-applied orthogonal force. [26] Bone et al. presented the test method for quantifying the performance of a vision and force sensor based robotic deburring system at high feed rates and on stainless steel parts. [27] Abou-El-Ela et al. introduced a new approach to motion control of robot manipulators in deburring and chamfering applications. The information about the interaction between the end-effector and the workpiece during the machining procedure was obtained by model-based evaluation of the cutting tool signals. The main design objective of the proposed hybrid fine motion control scheme is to compensate for limited uncertainties in the workpiece location relative to the prescribed robot trajectory.

In the last of the 1990s, the algorithm of hybrid force/position control, the deburring method optimization, controlling the robot behavior as human skills, the varied types of deburring tool and modeling of burr information were approached. [28] Joly et al.

showed that in hybrid position/force control as well as in multi-robot cooperation and teleoperation, the desired behavior of the system can be defined in terms of a massless mechanism whose joints act as ideal position or force sources. [29] Hekman et al. presented the method for optimizing the horizontal feed rate when using depth of cut manipulation to improve part parallelism in grinding. In vertical spindle surface grinding, achievable single pass tolerances are often limited by the grinding wheel and machine compliance. [30] Hsu et al. proposed an adaptive fuzzy hybrid force/position controller, which can update fuzzy rules to compensate for the robot dynamics along with the force dynamics induced by the contact between the cutting tool and the part's edge and identify the actual desired contact force. [31] Aertbeliën et al. discussed a method for transferring the skill of a human operator to a control strategy that can cope with these changes in parameters. The human skill is transferred by an indirect learning method. The human actions are modeled as an impedance controller whose parameters are adapted by observations of the deburring process state. A neural network learns the non-linear relation between the process state and the controller parameters. [32] Stango et al. focused on edge deburring operations that utilize polymer/abrasive filamentary brushes. Either the burr geometry resembles burrs or flash that was produced during the metal cutting or die casting operations, respectively. Master Curves are introduced as machining descriptors, which characterize the incremental burr removal performance of the brush/workpiece system. [33] Lee et al. presented the generalized burr model based rapid deburring pass planner utilizing the identified burr shape information with a laser vision sensing.

In the early half of the 2000s, the various issues were developed. Mostly the hybrid force/position control was improved by using intelligent control algorithm. Moreover, the dynamic modeling and novel methodologies also were proposed. [34] Su et al. proposed a training scheme, called the evolution-based virtual training scheme, in extracting knowledge for robotic deburring tasks. An evolution strategy was employed to search for the best set of fuzzy rules. This learning scheme had been applied

successfully in adjusting the parameters of impedance controllers required in deburring operations. [35] Hsu et al. proposed an adaptive fuzzy hybrid position/force controller, which can update fuzzy rules to compensate for robot dynamics along with the force dynamics induced by contact between a cutting tool and a part's edge and can identify the actual desired contact force. [36] Chen et al. presented a novel trajectory planning, which allows for arbitrary planning of trajectory with a large distance inside the constrained surface. When the manipulator contacts with the environment, the robot controller compensates for the trajectory in real time by applying an innovative geometrical projection method. To demonstrate the feasibility and effectiveness of the proposed method, a Cartesian robot arm on which a grinding tool is rigidly mounted performs precision deburring and chamfering on unknown contours. [37] L. Chen et al. developed a force-control model for edge deburring with filamentary brushes. The model is based upon experimentally obtained ''master curves,'' that is, material removal data that corresponds to the actual machining performance of the brush/work part system during the incremental burr removal process. [38] Pagilla et al. provided an experimental study of the planar impact of a robot manipulator on a surface. Using the data collected from a series of experiments, it investigates post impact behavior for different pre-impact conditions such as the configuration of the robot, angle, and velocity of impact, etc. Understanding the post-impact behavior for various pre-impact conditions can result in the design of improved transition control strategies to stabilize the manipulator onto the surface. [39] They also considered control of robotic surface finishing processes such as deburring, grinding, chamfering, and polishing. A complete dynamic model that describes the dynamic behavior of the robot for surface finishing tasks is developed. A complete surface finishing task is divided into three phases (free motion phase, a transition phase, and constrained motion phase) depending on the location of the robot end-effector with respect to the constraint surface. [40] Goradia et al. proposed a new hybrid force/position controller, implemented in a moving reference frame, which could control the interaction force along arbitrary directions. [41] Valente et al. proposed a complete framework for an efficient robotic deburring

7

implementation. The framework aims to integrate all the steps of the robotic implementation, since the trajectory programming to the trajectory control. As an intermediate step, a new version of Malkin's model is proposed in order to evaluate the contact between the deburring tool and the workpiece. [42] Ziliani et al. presented a mechatronic methodology for the robotic deburring of workpieces of unknown shape. The combined design of the milling tool and of a hybrid force/velocity controller, which is based on measurements provided by a force/torque sensor, allows being obtained the high performances.

In the rest of this decade, the compliant motion mechanisms and intelligent active vibration control were developed for the deburring process. Besides, some of the new deburring tools with modeling and interaction control algorithm were focused. Along with that, the diverse types of the deburring tool were also developed. The detail here is, [43] Wang et al. developed a process force model taking into account the burrs effect and an adaptive algorithm for robotic deburring. The burrs, cavity, deflection of the end-effector and the tool worn can be distinguished by the adaptive algorithm, hence the reference force and the feed-rate can be adjusted respectively to obtain better quality deburred contour and improve machining efficiency. An impedance control with the algorithm is proposed for the robotic deburring process. [44] Robetsson et al. described the design and implementation of a platform for fast external sensor integration into an industrial robot control system (ABB S4CPlus). An easily reconfigurable control structure was achieved, which is able to control contact forces with a sampling bandwidth of an order of magnitude higher than for conventional robot control systems. [45] Wang et al. proposed an intelligent compliance control strategy by employing a fuzzy impedance controller and a fuzzy velocity controller for improving the constrained motion control performance and the quality of the deburred surface. For the improvement of force control performance, impedance parameters can be modified according to the difference between the actual and the desired position by the fuzzy adaptation mechanism. The feed rate in the tangential direction is adjusted

for the special burrs and defects to get a smooth surface. An empirical force model taking into consideration the burrs affection is developed to predict the cutting force. [46] Kim et al. discussed the modeling and control of a robotic manipulator with a new deburring tool, which integrates two pneumatic actuators to take advantage of a double cutting action. A coordination control method was developed by decomposing the robotic deburring system into two subsystems: the arm and the deburring tool. A decentralized control approach was pursued in which suitable controllers were designed for the two subsystems in the coordination scheme. Robust feedback linearization was utilized to minimize the undesirable effect of external disturbances, such as static and Coulomb friction and nonlinear compliance of the pneumatic cylinder stemming from the compressibility of air. [47] Nagata et al. proposed a sanding system based on an industrial robot with a surface following controller for the sanding process of wooden materials constructing furniture. Handy air-driven tools can be easily attached to the tip of the robot arm via a compact force sensor. [48] Buckmaster et al. presented a mechanism of compliant motion control for robust robotic surface finishing. With the emergence of stable and responsive robotic compliant motion control, introducing robotic grinding and deburring to the industry may soon be feasible. Technical needs for this transition include means to accommodate imprecise fixturing, a method for simple, intuitive and dependable programming, and the ability to monitor process progress online. [49] Kim et al. developed a robotic deburring method based on a new pneumatic tool, which considers the interaction among the tool, the manipulator and the workpiece and couples the tool dynamics and a control design that explicitly considers deburring process information. The developed deburring method adopts a new active tool design based on a pneumatic actuator with a passive chamber, which aims at providing compliance and eliminating and/or reducing the chatter caused by air compressibility. [50] Wang et al. presented four different force control technologies to address the specific problems inherent in assembly, grinding/polishing, deburring and milling respectively. The benefits of force control technologies are clearly demonstrated through increased robot

dexterity, simplified robot programming, great reduction of cycle time, and improved surface accuracy. [51] Choi et al. proposed the interaction force model to accomplish the de-burring task by using the dual-arm manipulation. A methodology to control the interaction force without using a force/torque sensor is proposed. Finally, the feasibility and effectiveness of the suggested method of interaction force control were shown through simulations for the given de-burring task. [52] Liao et al. developed a dual-purpose compliant toolhead for both polishing and deburring through the integration of tool pressure sensing with tool extension sensing. For the polishing control, a PID controller is applied for pressure tracking through pressure sensing. For the deburring control, another PID controller is applied to maintain the desired tool length through tool extension sensing. [53] Zhu et al. presented the passivity analysis and control design of a pneumatic actuator controlled by a four-way proportional valve. A pseudo-bond graph model is presented and used to prove the closed-loop passivity of a pneumatic actuator. The resulting passive closed-loop pneumatic system is able to interact with any passive environment in a safe and stable manner. Additionally, the formulation is able to produce a desired interaction force by using pressure sensors in the actuator chambers instead of external force sensing. [54] Daniali et al. proposed an intelligent active vibration control design to reduce the vibration of robot end-effector in contact task. The proposed neuro-fuzzy controller is a self-tuning system based on the reinforcement learning. A fuzzy critic was used to evaluate the performance of the controller to produce a proper reinforcement signal updating parameter of the neuro-fuzzy controller. [55] Lee et al. developed the teaching and playback method, which was applied to the 2DOF manipulator for the robotic deburring task. The method included techniques for reducing redundant teaching points and protecting the tool from damage. By comparing the teaching with the playback technique, which plays back the recorded control output, it had computational advantages and more possibilities to apply the planning algorithm.

In the recent years, the algorithms, based on the position control and path planning, were studied for impedance control. In addition, the novel constant force mechanisms and control solutions were focused for constant force control for the deburring robots. [56] Xi et al. developed an adaptive controller for the pressure tracking of the pressurized toolhead in order to maintain the constant contact stress for the polishing process. This was a new polishing control method, which combines the adaptive control theory and the constant stress theory of the contact model. By using an active pneumatic compliant toolhead, a recursive least-squares estimator is developed to estimate the pneumatic model, and then a minimum-degree pole-placement method is applied to design a self-tuning controller. [57] Osada et al. proposed the original bilateral controller, which had the gain components on the line used to transfer the force signal between master and slave robot. These gains changed the binding force between master and slave robot to change the construct of the system. [58] Chen et al. presented an adjustable constant-force mechanism (ACFM) to passively regulate the contact force of a robot end-effector. The proposed ACFM combined the negative stiffness of a bistable mechanism and positive stiffness of a linear spring to generate a constant-force output. Through prestressing the linear spring, the constant-force magnitude can be adjusted to adapt to different working environments. The ACFM is a monolithic compliant mechanism that has no frictional wear and is capable of miniaturization. A design formulation was also proposed to find optimal mechanism configurations that produce the most constant-force. [59] Dietz et al. surveyed the use of advanced programming systems for a deburring use-case commonly found in small and medium-sized enterprises (SME) production. [60] Song et al. proposed the tool path generation based on matching between the tool paths from the CAD model to teaching point to minimize the position and orientation errors of the workpiece. The basic tool path for deburring could be generated by the computer-aided manufacturing (CAM) software with a CAD model. Using direct teaching based on impedance control, some contact points between the tool and the actual workpiece are manually selected as the teaching points, which are the minimum number of points to feature the

11

shape of the workpieces. [61] Domroes et al. intended to give an insight into the development and evaluation of force controlled machining processes with a commercially available setup. They also focused on a deburring and a grinding scenario, representing the major applications in today's robot machining. [62] Song et al. proposed a tool-path modification method based on a computer-aided design (CAD) model and direct teaching to achieve precision deburring, taking into consideration the position/orientation errors of the workpiece. In addition, based on this trajectory, impedance control is used to avoid applying an excessive contact force and a virtual wall is adapted to improve the force-control performance. [63] Parlaktaş introduced a novel constant-force mechanism and described the fundamentals of the design method. Design geometry and initial conditions are presented for the selected configurations of the compliant constant-force mechanism. [64] Posada et al. presented a novel approach to automatically program an industrial robot-based on the CAD model of the product variants and to enable online control to minimize errors during a deburring process. The operator selected the edge of the workpiece to be machined, and an automatic program generation system is designed which programs the robot for the deburring process and enables online compensation. A laser scanner sensor device is used for localizing the workpiece in the robot cell and in the online compensation to perform fine corrections of the robot's movement during the process. [65] Tian et al. presented the solutions adopted for a robotic automatic polishing platform for finishing machining on curved surfaces to reduce cost and improve quality on such manual finishing operations. [66] Xu presented a unified control framework for both set-point and time-varying force control of robot manipulator by introducing an improved position-based impedance control (IPBIC). In order to achieve essentially accurate force control, especially time-varying force tracking, a new target impedance function compensated by a force controller is presented. The essence of the improved method in realizing time-varying force tracking, as well as the coupled stability of the manipulator–environment system is investigated. To improve further the force control

performance, the Newton-type iterative learning control (ILC) is introduced upon the closed-loop system.

II.   Technologies for Contact Tasks of Robot and the Environment

The industry has successfully used robots in engaging in executing various tasks whose working environment is harmful to human beings or whose operations are repetitive and/or require high accuracy. Usually, those tasks can be programmed into the operations of robots because those tasks do not interact with the environment frequently and then human skill may not be necessary for the operations of the tasks. On the other hand, there exist tasks such as deburring, grinding, milling, assembly, etc., which may need a great deal of interactions with the environment and thus require lots of decision-making process while facing those interactions. Hence, the successful execution of those tasks largely relies on human skill in achieving satisfactory results. Actually, the human skills are very miracle, along with the development of technology in the world, many researchers, manufacturers are doing efforts to make the machines, and robots can be flexible as human but be great powerful for applying in the essential tasks in the industry, in the medicine and the surgery, and in post-manufacturing. In the trend of such purpose, the robotic deburring and advanced solutions also are focused to go forward to the most novel approaches. Due to the advancement of robotic technologies, the robot manipulators are widely used for automation of finishing processes, such as deburring and grinding. Contrary to manual operation, automated robotic finishing is an efficient, precise and cost-effective approach, which can eliminate other extra operation. Industrial robots have also been progressed remarkably and applied to several tasks such as painting, welding, handling and so on. In these cases, it is important to control precisely the position of the end-effector attached to the tip of the robot arm. On the contrary, when the robots are applied to polishing, deburring or grinding tasks, it is indispensable to use some force control strategy without damaging the object. Robots that are able to autonomously adapt

themselves to semi-unstructured tasks are nowadays a key issue in such industrial applications, where the capacity to cope with a workpiece of an unknown shape would significantly reduce the task programming phase, especially when frequent changes in the production occur.

Applications such as stub grinding and deburring represent good examples of common tasks, which would be desired to automate. Not only are manual fettling and finishing major cost elements in the production process which often lead to inconsistency in quality and delivery delays, there are also severe health aspects related to this process in today's foundry industry. In these types of material removal applications, there are two important issues, accurate control of the force between the tool and the workpiece, and starting and ending the material removal process without lowering the quality of the machining.

The burrs may cause problems in further processes, such as handling and assembling operations. The disadvantages of the manual method lead to the automation of the deburring process. Developing automated robot manipulators for deburring is becoming more important because of the high cost of manual deburring. In general, deburring tasks are done to remove burrs from the edges and to maintain the final geometry of the deburred part's edges while undergoing contour-following motion. When driving the cutting tool to perform a deburring task, the burring robot must implement two major motions. One motion applies a suitable chamfering force to the part's edges to remove burrs while avoiding damage to the part. The other motion performs contour following. This ensures that the cutting tool will remain in contact with all the burrs over the chamfer. A heuristic deburring control policy can attain the desired chamfering force by controlling the feed-rate of the cutting tool. Robotic deburring can be performed in two ways. If the part is relatively lightweight, the robot can handle can hold it against a tool that performs the actual deburring. If the part is heavy, the robot can hold the deburring tool and control its motion around the stationary part. In both ways, the relative motion between the tool and the part is of a

continuous-path type with high repeatability and accuracy.

The automated robotic deburring system has been investigated for a number of years as a replacement for manual operation, which is considered as labor intensive and low productivity method. A machining manipulator is subject to mechanical interaction with the object being processed. The robot performs the task in the constrained workspace. In the constrained task, one is concerned with not only the position of the robot endpoint but also the contact forces, which are desired to be accommodated rather than resisted. Therefore, interaction force needs to be considered in designing and controlling deburring tools. As a final finishing process, deburring is widely used in many manufacturing industries including aerospace, automobile, and dies and molds. Deburring removes the part's burrs without affecting its geometry. Traditionally, deburring has largely been a manual operation that is very labor intensive, highly skill dependent, inefficient with long process time, high cost, error-prone, and hazardous due to abrasive dust. A viable solution to overcome the abovementioned problems of manual operation is through automation. However, successful implementation of an automated deburring system requires effective control methods.

Nowadays, the development of the robotic technologies leads the automation technologies extensively is carried out in the industry. The deburring process is a post-manufacturing process, in which the cutting tools or the abrasive tools are used to remove the burrs out of the commercial products. Followings are two approaches for solving the problems of interaction when applying robotics for surface processing.

In chapter ii and iii, the IDC device, in which IDC abbreviates for Intelligent Deburring Control, is presented about the constitution, mechanism, and applications. Actually, the IDC device uses the pneumatic mechanism to control the pressure for generating the contact force, it is observed by a position sensor, pressure feedback, and incline sensor. This device – mounted between the robot end-effector and working tool

– aims to maintain the preset contact force while robot works on the surface of workpieces and is controlled by the own controller, which don't depend on the robot controller. The IDC device can be used for deburring robotics, grinding robotics, or sanding robotics… and can be useful for constraining the actual force of working tool.

In chapter iv, in order to control the constant contact force when the robot works for surface processing, the dynamic models of second-order robot and environment is investigated and the unified position/force method is studied for evaluating the affection of robot motion to the contact force. The relative equation between the motion and the force is based on the robot dynamic model and environment dynamic model. In which, the Lyapunov stability criterion and Root Locus method rules are applied to stabilizing the transient processes of the motion and the contact force. The unified position/force method showed that the stabilization of contact force is decided by the stabilization of robot motion in part. Basing on such findings, the target impedance model is realized by MATLAB System Identification Toolbox and evaluated by MATLAB/Simulink Simulation from the experimental system's specification. The results show the affection of estimated mass, damping and stiffness parameters to the responses of the contact force.

In chapter v, the experiment of impedance control is carried out for deburring robot works on the variable profile. The impedance control can control the actual force and tracks the deburring profile. And while deburring processes, the inherent properties is the cause of abnormality of force response, then the IDC device with controllable stiffness is used to compensate the motion of the robot and actual force.

CHAPTER II CONCEPT DESIGN OF

DEBURRING AUTOMATION SYSTEM

I. Technical Development Overview

1.1 Necessities of technology development

In the field of machining and surface treatment such as polishing, deburring, cutting, painting and surface treatment, after automation process the human is used to complete the finishing tasks. As for spot or arc welding, the standardization is necessary for manufacturing the number of products. Beyond there are some products with irregular shape is not done in a certain pattern, it is difficult to teach the robot automatically. When the product is not uniform, the manual operation remains to be required.

Through active research, development, and market formation of peripheral parts of industrial articulated robots, the transition from manual to automated systems is being made with radical technological improvements. We believe that the development of automation system secures the competitiveness of robot industry in the irregular tasks or in many unexplored areas.

 The surface machining automation system is mainly composed of straight lines such as steel and section steel, or in the form of a straight line in a planar shape, or simply by using an orthogonal robot. However, this type of automation system is performed within the confined work in the field of surface machining, and it is impossible to apply it to the complicated shapes of automobile body shape and plastic injection, etc.

Even though the machining device such as the surface grinder is mounted and tested on the arm of the industrial articulated robot like the deburring technology, the shape of the panel is very bendy and the teaching of the robot is very difficult. The pressure cannot be processed and the quality cannot be reached. In this situation, the automation system of the deburring technology is limited to drill and spindle type deburring technology and its utilization are also limited.

1.2   The target of technology development

a. The IDC intelligent precision deburring controller

The IDC intelligent precision deburring controller is one of the most important items, which are developed in this project. It is installed between the cutting mechanism part and the robot arm and serves as a buffer for the vehicle body and the driving system such as the suspension of the automobile.

When cutting tool and surface machining are performed on the shaping surface of the product, the shape of the product is very important.

According to the characteristics of the product, it is more practical than drill type in plastic injection or surface processing, and this product is not developed in South Korea, according to a preliminary investigation, there is no related patent. If IDC is developed early, it will be able to prevail in the domestic market and it can be applied to various fields of automated processing equipment related to articulated robots, so it can be sold not only in domestic market but also in overseas market. In addition, it can gain competitiveness based on its own technology development in the domestic market which is dependent on foreign countries which imported special specification products from Europe or Japan.

The product is flexible to operate the surface deburring system of the robot according to the shape of the automobile parts so that it can be flexibly operated when the surface of the product, plastic injection bur or gate is removed without finishing the product shape or robot teaching. We aim to develop the precision deburring technology of automobile parts through intelligent control which maintains decompression by monitoring in real time so that product quality is not damaged.
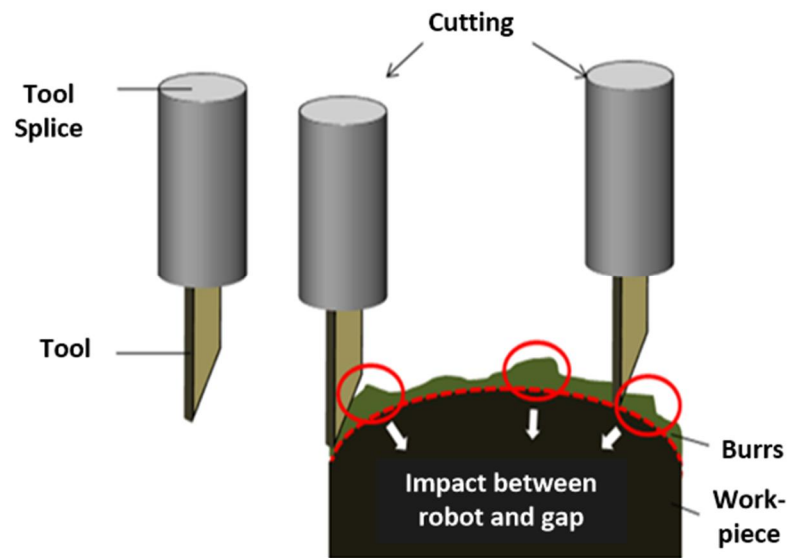
Fig. 1 Concept of deburring process.
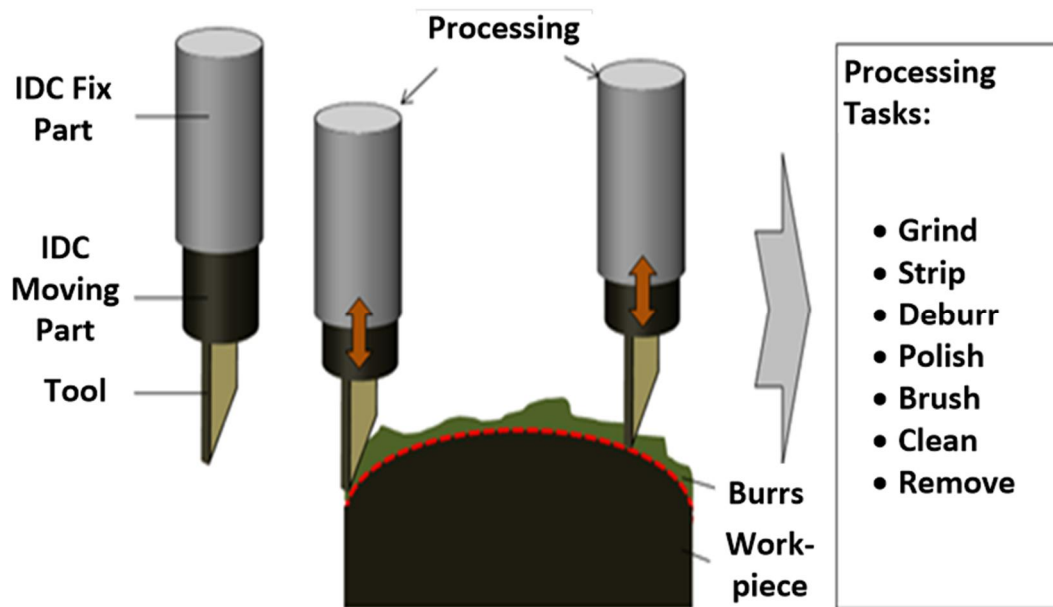
Fig. 2 Concept of surface processing using IDC device.

The figure above is a conceptual diagram that makes it easy to understand the contents of the work. The illustration shape is not the shape of the product will be developed in the future. In the conventional process, it is impossible to relax the shrinkage of the product itself as shown in the figure. Since the robot has to program the part shape with 100% teaching, it is impossible to adjust finely the tolerance of the product and the deburring machine in mm. Moreover, it is more difficult to approach when

machining the surface. However, when IDC is installed, it is possible to eliminate completely the tolerance between the deburring eliminator on the robot arm and the part shape during robot teaching or to adjust the desired pressure on the user side as desired, thus preventing damage to the product. By adjusting the processing depth of the surface of the product in millimeters, it is possible to use it in automation of surface processing.

b. Integrated automation system using the robot.

- The robot automation system is developed that consists of IDC intelligent precision deburring unit with a cutting tool and ATC (Auto Tool Changer) module.
- Realization of interlocking automation system through synchronizing between robot and IDC for constructing the interface between robot-IDC and communication interface module.

c. Scratch-resistance JIG

Development of high precision scratch resistant JIG device for firmly fixing the product that is very vulnerable to be scratch.

d. Gates and Burrs removal device.

High-precision cutting device is developed for uniform cutting of polymer products and securing the quality of the cut surface.
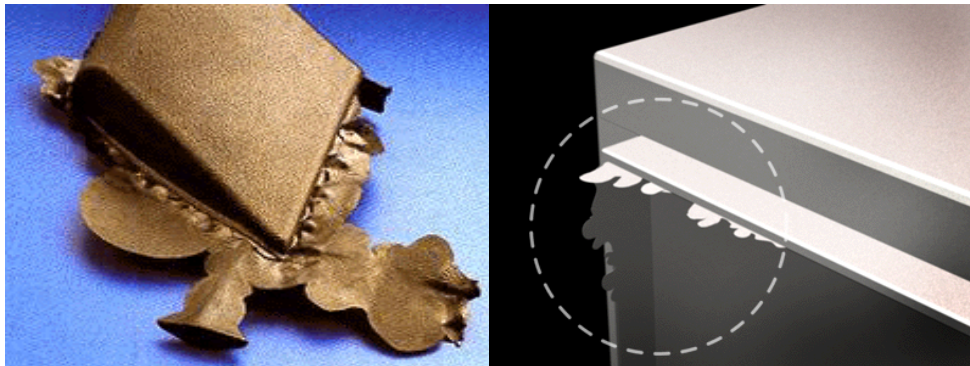
Fig. 3 The products with burrs.

21

e. Product transferring devices.

Development of the device which is capable of transferring products after removing the gates and burrs, and loading from the inside of a mold to a fixed JIG after injection without a scratch.

Development of the dedicated ATC device for changing the cutting device is used to remove the gates and burrs, and device for taking out the products.

II. Designing of IDC device.

2.1 General Purposes
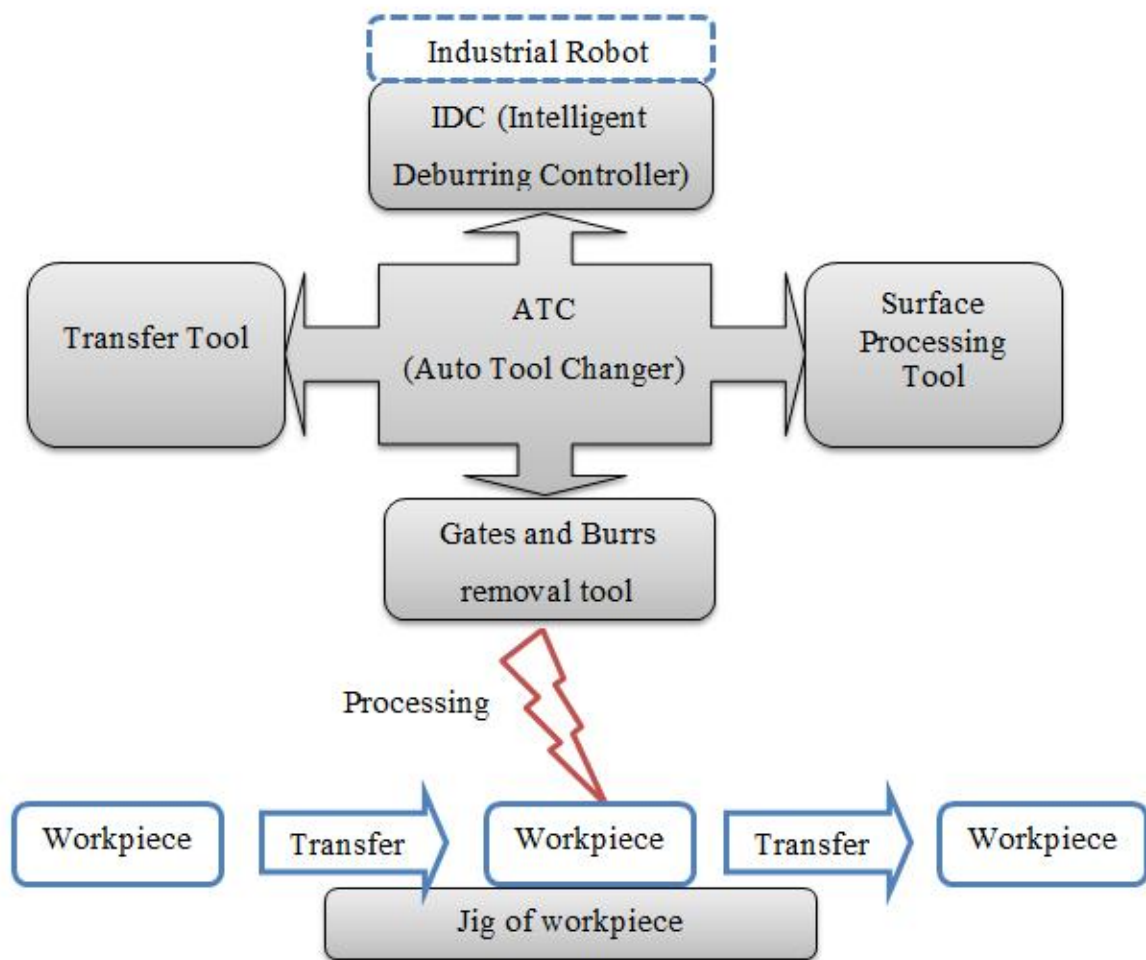
Fig. 4 The concept of deburring system

22

The deburring system is developed as Fig. 4, in which the intelligent deburring control (IDC) device is an active system to maintain the constant force. The IDC device, auto tool changer, transfer tool and the deburring tool should be made compatible with each other. The deburring tool, cutting tool or grinding tool will be changed for removing the gates or the burrs. The products are transferred for each procedure.

Fig. 5 Conceptual Diagram of Deburring Automation System.

The robot controller of the deburring automation system is designed to connect with robot interlocking panel through CC-LINK type wiring in the process control panel. The IDC controller is connected to the robot-interlocking panel through the interface. The IDC and ATC mounted on the arm of the robot are supplied with 24V power and have the output from the OUTPUT terminal in the robot-interlocking panel. The relay box is used to connect the robot-interlocking panel with the deburring robot and the JIG's signal and wiring. IDC tool is driven by air with 5 bars pressure. The command

for IDC and ATC device in the robot-interlocking panel can be changed through device net.

2.2   The interlocking system of ROBOT-IDC-cutting tool –ATC.
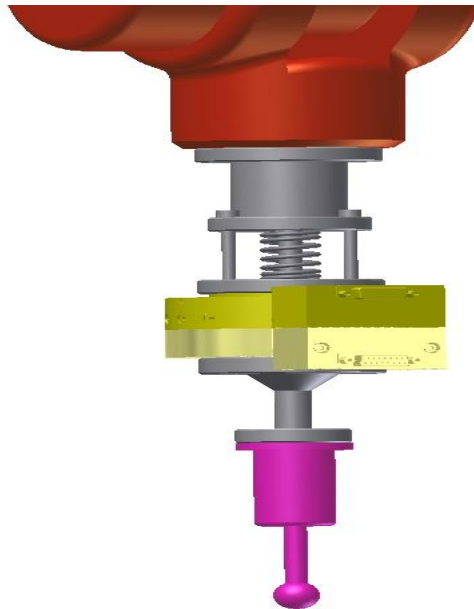
Fig. 6 ROBOT – IDC – cutting tool –ATC System.

In the development of the second year, the IDC and the cutting tool are applied as shown in the mounting concept of the 위, and it is composed of the robot-IDC-cutting tool-ATC interlocking system. Generally, ATC is not used, but considering the nature of plastic injection, the production process C / T is about 30 / s. Therefore, the goal is to develop the process so that the cutting tools can be changed for each job due to the removal of gates and burrs of plastic injection. The IDC is basically attached to the arm of the robot. When the completion signal of plastic injection material is received, unlike the robot, the transfer hanger is moved from the injection machine to the fixed JIG after the product is clamped and the robot unclamps the product to the fixed JIG do. When the product is placed on the JIG, the sensor attached to the JIG recognizes the product, and the recognized JIG clamps and fixes the product, and then transmits the fixed completion signal to the robot. After transferring the activation signal to the

PLC, the robot receives the cutting tool for the injection product, attaches it to the IDC, moves to the product fixed on the JIG, and returns to the original position after the necessary process. After that, the robot sends a job completion signal. When the JIG receiving the job completion signal receives the unclamping, the worker takes the product from the JIG, checks the quality, and loads it on the pallet.

2.3   The mechanism of IDC device.

IDC device has an important role for the precision deburring technology of automobile components. The deburring automation tool consists of a spindle or drill system. The IDC device is used to equip the deburring tool to end-effector of the robot. The conception of IDC device is proposed as Fig. 7.
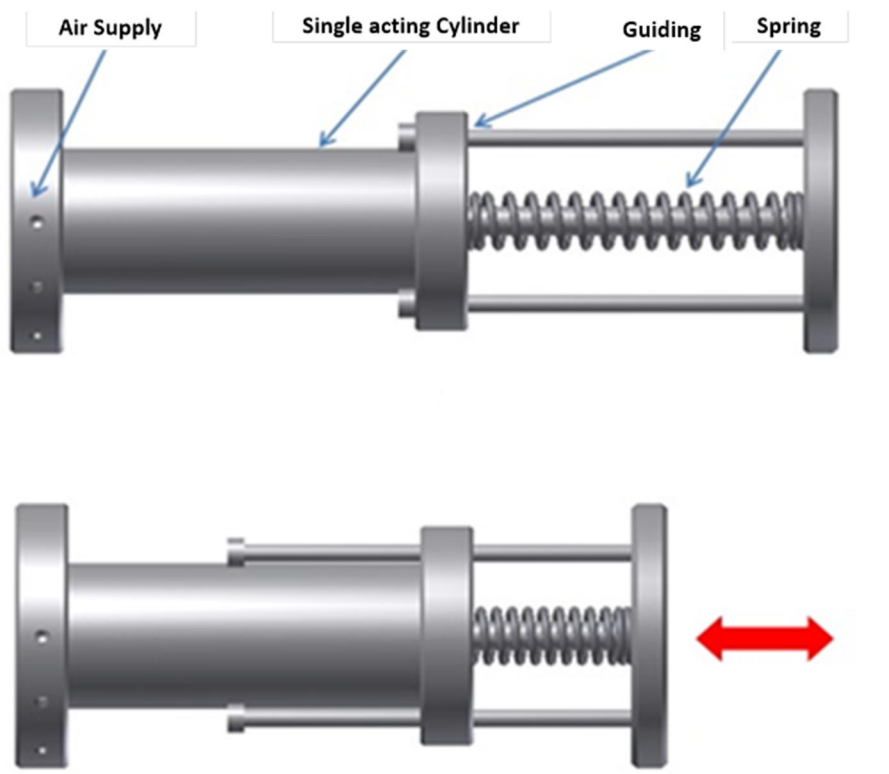
Fig. 7 The conception of IDC device.

The workpiece can be damaged when robot acts directly. In Fig. 8, the IDC can be controlled with a certain distance from the workpiece. The tolerance between the

deburring tool and the workpiece can be adjusted by IDC device. When necessary, the IDC's air pressure range is set regardless of the contour curvature. The material can be protected by interrupting and reconditioning.
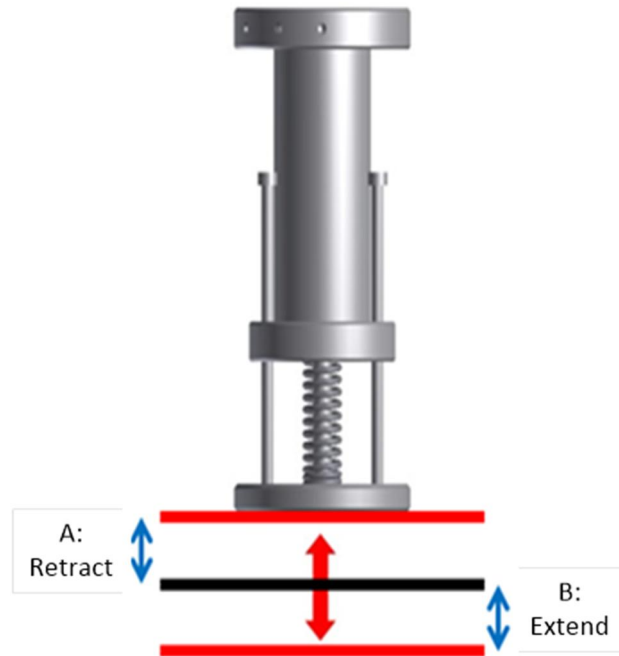
Fig. 8 Stroke of IDC device

As shown 위, when the robot operates, the black line is referred as a machined product and the IDC is the allowable stroke between A and B while reaching the critical point of the A or B stroke. The controller of IDC device receives the signal from the pressure sensor and adjusts the air cylinder pressure in the IDC device, so that the pressure can be maintained based on the midline. When such a technique is applied to the material processing, it is pushed to the material surface at a constant pressure, so that it is pressed not only the gate and burr removal but also the polishing or cutting of the body panel with a constant force on the surface.

2.4   Transfer Tool and Removing Tool ATC module.

The advantage of the jointed-arm robot with a hanger is used for transporting and bringing it out of a plastic injection of molding machine. It can protect the workers from burning due to the characteristics of a plastic injection machine with a lot of heat, and the effect of reducing the process time (CT-time cycle) can be invited, thereby exerting a definite effect on the process improvement.

- A transfer tool is developed to move the item to the desired position.
- A structure is applied to transfer the complex shape of the product in a short period of time with minimal damage to the product using vacuum adsorption system.

Fig. 9 Example of the transfer mechanism of vacuum adsorption.
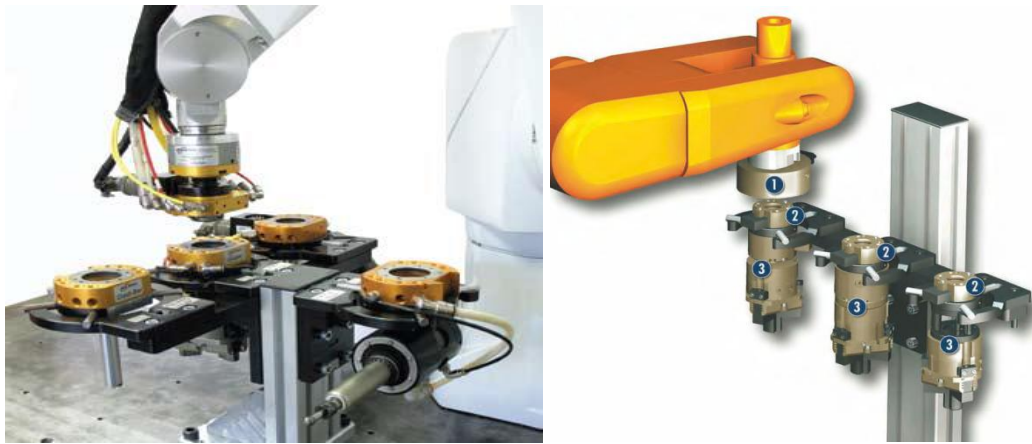
Fig. 10 Example of ATC system.

2.5 The communication interface of robot and IDC device

The driving method of the industrial articulated robot is composed of 6-axis and the servo motor is used. In the case of a kinematic robot, there is a method of connecting with external equipment by recognizing it as 7th-axis by connecting the external axis of the robot and connecting it to the output terminal and the method of starting. In the control method between the IDC controller and the robot is developed, the IDC controller is designed using CC-LINK communication method. In order to realize real-time interlocking operation through synchronous technology as well as the operation of the cutting mechanism, is constructed to perform the same role as the outer axis of the robot.

2.6 Automation synchronization system of robot and IDC device.

The robot controller is linked with the system configuration through the interlock module and device net. The communication interface of IDC controller is configured through robot interlock module and CC-LINK type. Additionally, the change in a pressure sensor that can operate on the cutting board fitted to IDC through real-time communication monitoring of the robot controller and the IDC controller provides the final step to confirm the configuration of the robot. This development is a new

technology that has not been in the spindle before and will contribute significant revenue to other business classification applications after development is completed.

2.7 Investigation of the deburring tool.

The performance of deburring efficiency and high precision is required for finishing the products. The characteristics required for the development of this technology can be largely classified into technical characteristics, quality characteristics, and cost-related characteristics. It is necessary to have the adequate deburring ability, suitability to the shape, dimensions and surface roughness of parts, stable quality of deburring, non-damage to unnecessary parts. The preparation time for deburring is short, the fixed fixture is formed, cost of operation of deburring tool and cost is economical, and facility investment should be secured. The deburring tool is applied to the development of the technology uses repetitive use of similarly shaped parts, so the strength and toughness of the tool are important.

Recently, importance and quality of finished car quality have been increasing. Generally, when assembled with burr remaining, the occurrence rate of assembly failure increases and serious injury may occur to the work during the assembly process. If the bur is removed in a strong way to avoid burrs, the product will be deformed and damaged, and the original product function will be lost. Therefore, we would like to select a cutting tool with high cutting efficiency and accuracy while minimizing damage to the product with the performance required in this technology development.

Fig. 11 Types and shapes of the deburring tool

Conventional burr removal tools use nylon brushes, wire brushes, etc., which mainly contain abrasive grains. However, since the abrasive force is insufficient, tool shape changes due to abrasion are large, burrs after burrs are removed, which is unsuitable for use in automobile injection parts. In addition, although barrel, short-lasting, and sandpaper are also used, continuous processes are not possible, and there are environmental problems caused by wastewater treatment, high equipment cost, and short life. Due to the above problems, automation of the deburring process has not progressed greatly, most of the burr-removing processes are performed manually by hand, and the increase in the processing cost is a problem. In order to develop the intelligent deburring system, it is essential to select a deburring tool with high accuracy and a stable degree.

Nylon, wire brush	Manual deburring tool	Shot blasting
Sandpaper	Deforming brush	Deburring cutter

Fig. 12 Classification of the deburring tool.

The test of the tool material was performed on the high strength SS 400 steel at a low speed (rpm) and the transfer speed (mm/min) by calculating the tool size 16 mm, rotation speed 300 rpm, and transfer speed 300 mm/min as variables in order to determine the robustness of the tool.
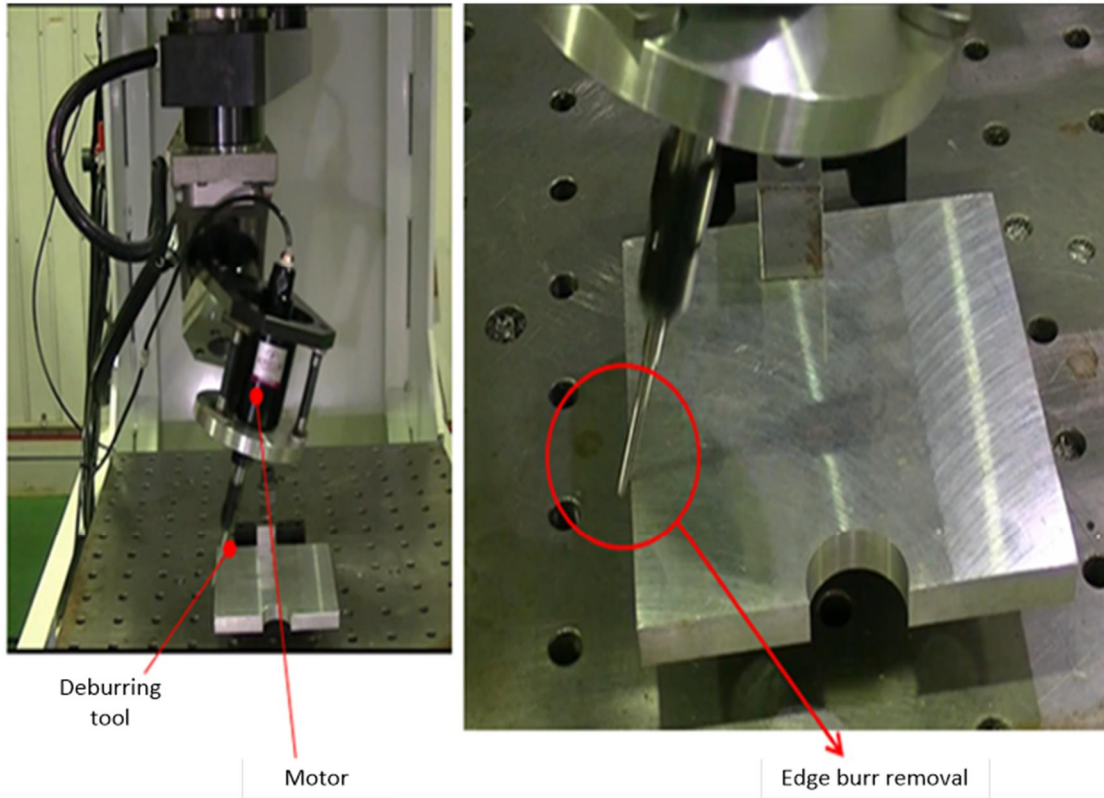
Fig. 13 Testing of the deburring tool.

Table 1 Specification of deburring tool test.

No.	Feed Rate (mm/min)	Rotation Speed (rpm)
1	100	100
2	100	200
3	100	300
4	200	300
5	300	300

□ Test Tool Specification

-. Material: S45C carbon steel

-. Tool diameter: 16mm
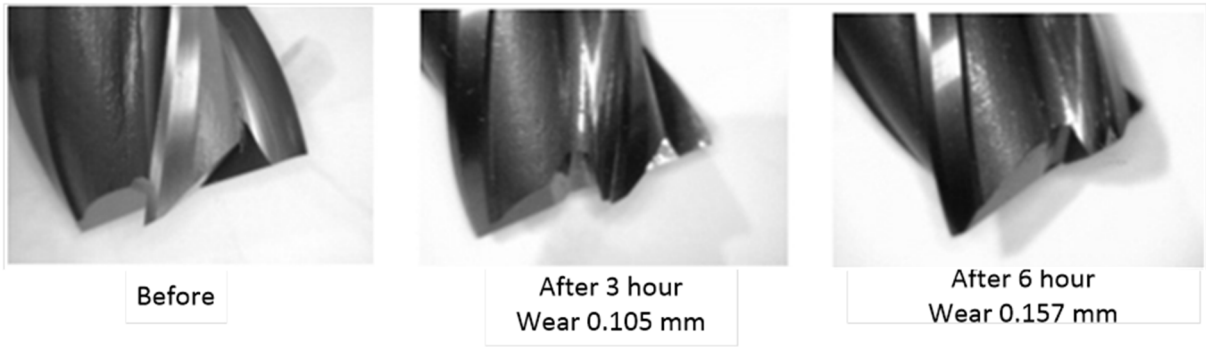
Fig. 14 Wear test for deburring tool

When cutting off the components, the surface quality is considered good, and the gate removal surface is considered good. However, a fine cut scratch has occurred, and it is deemed necessary to derive the optimization condition for the cutting-edge angle and the cutting speed for the cutting tool in the future. The quality determination of the cutting surface was carried out through visual inspection of the cutting surface and the surface roughness test, and the quality of the cutting plane was evaluated through the roughness measurement of the cutting surface. For the objective determination of the quality of the cutting surface in the future, it is required to determine the amount of deburring per hour according to the applied tool. It also intends to conduct an analysis on the loss of work stability and processing time.
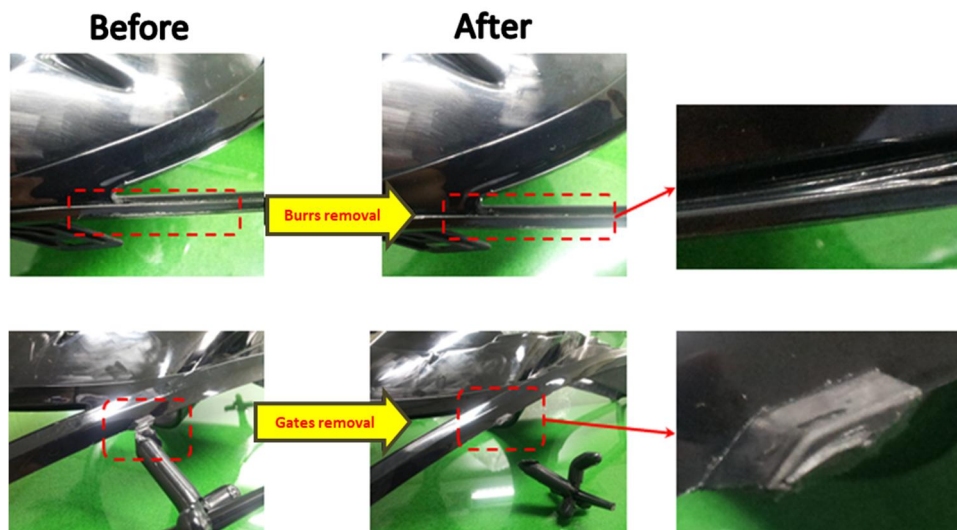
Fig. 15 Deburring test for finished products.

In order to develop a precise deburring process for our products, we will combine robot, IDC, and deburring tools.
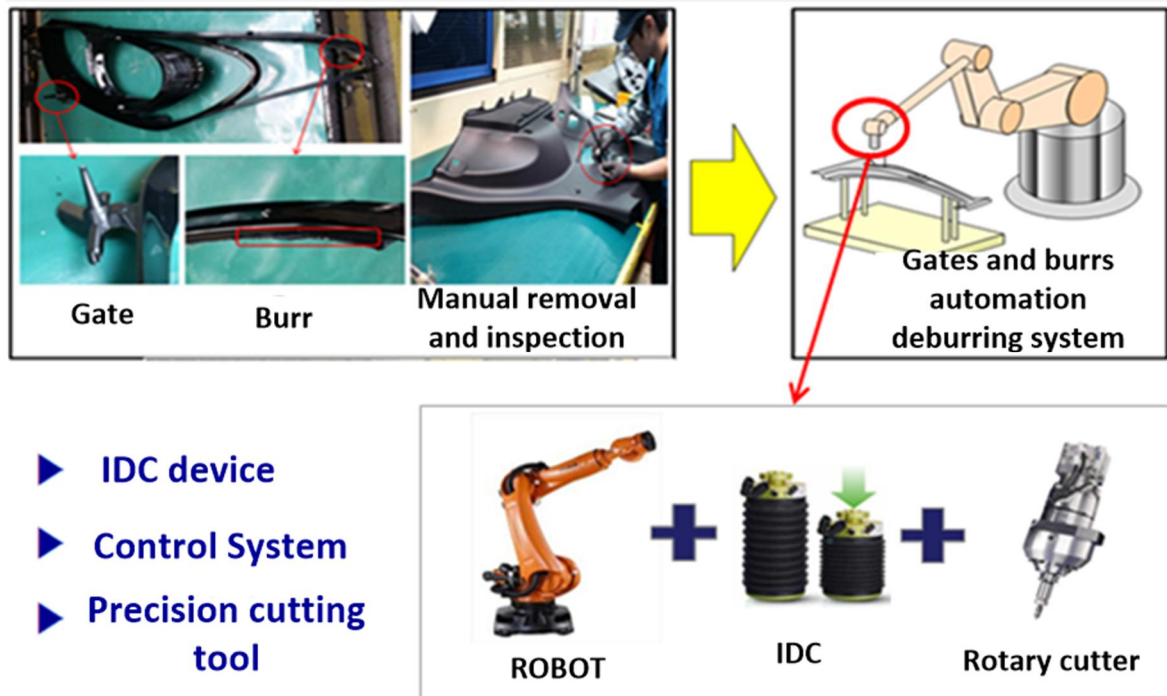
Fig. 16 The concept of deburring tool application.

Development of a gate and burr removal tool considering the characteristics of the product is carried out by replacing with an automatic tool change type according to the shape of the molding material by applying high-frequency cutting and grinding method using pneumatic. It adopts the universal mounting structure for automation and applies the universal cutting edge applicable structure, and it is developed to be easily applied to another field in the future through common use between cutting mechanism part and mechanical part.

Fig. 17 An application example of a metal deburring tool.

- Development of active load control structure that removes gate and burr of complex and irregular shape with constant cutting pressure

- Development of devices (localization and mass production), that meet the gate and burr removal conditions of the products is benchmarked for overseas products.

- Universal mounting structure for automation

- When the IDC is under load control, the constant pressure reduction stroke is arbitrarily set. When tuning the pressure, it can control the acceleration/deceleration through IDC control. The structure is designed that maintains maximum constant pressure when bent surface changes.

- Check the gate and burr removal performance of the cutting device with the intelligent precision deburring controller after fixing the product in the developed custom JIG.

2.8   The anti-scratch fixing JIG.
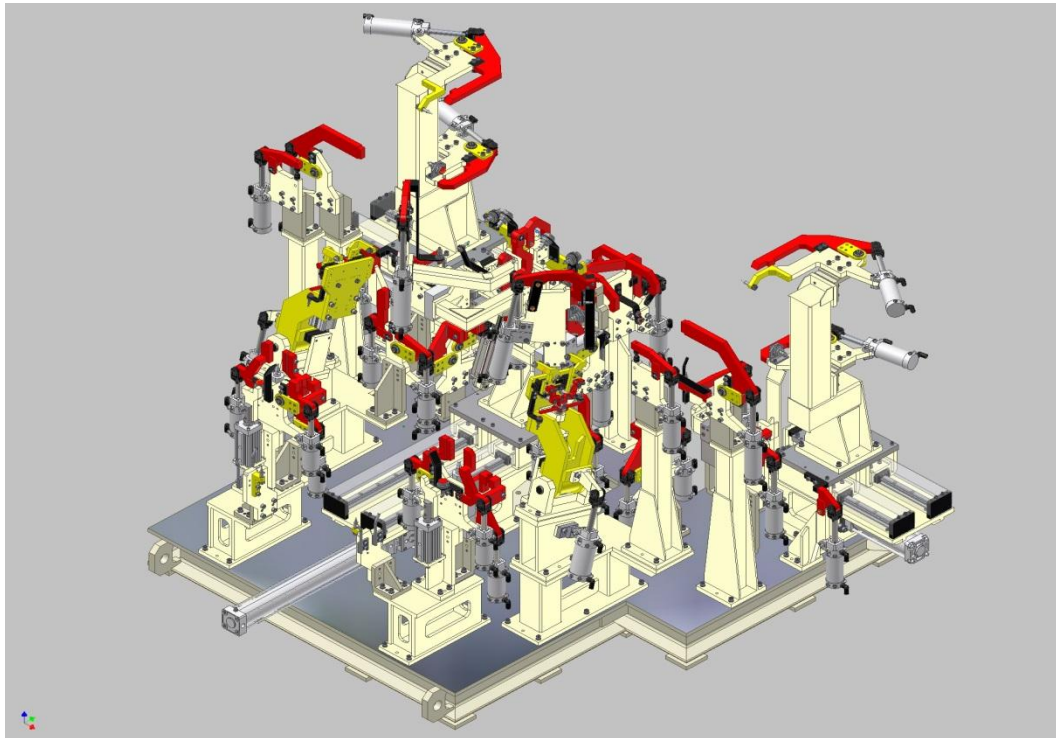
Fig. 18 An application example of auto clamping fixing JIG.

The customized fixing JIG for each selected product shows a characteristic of being soft compared to the steel material due to the characteristics of the plastic product. To this end, the JIG material and parts for scratch prevention will be applied. In addition, it is equipped with the loading sensor for the automation system, and the automatic clamping device is applied to remove the re-start which is required for the process after loading the material of the robot so that injection-loading-transfer-unloading-surface processing-loading-transfer-shipping. The non-stop process is the most effective way to prevent scratches and to improve the process time.

III.   Structure of IDC device

The IDC device is used to compensate the actual force and tolerance between the deburring tool and the products. The main components are pneumatic system and the inclination and position sensor are used for monitoring the IDC device's operation.
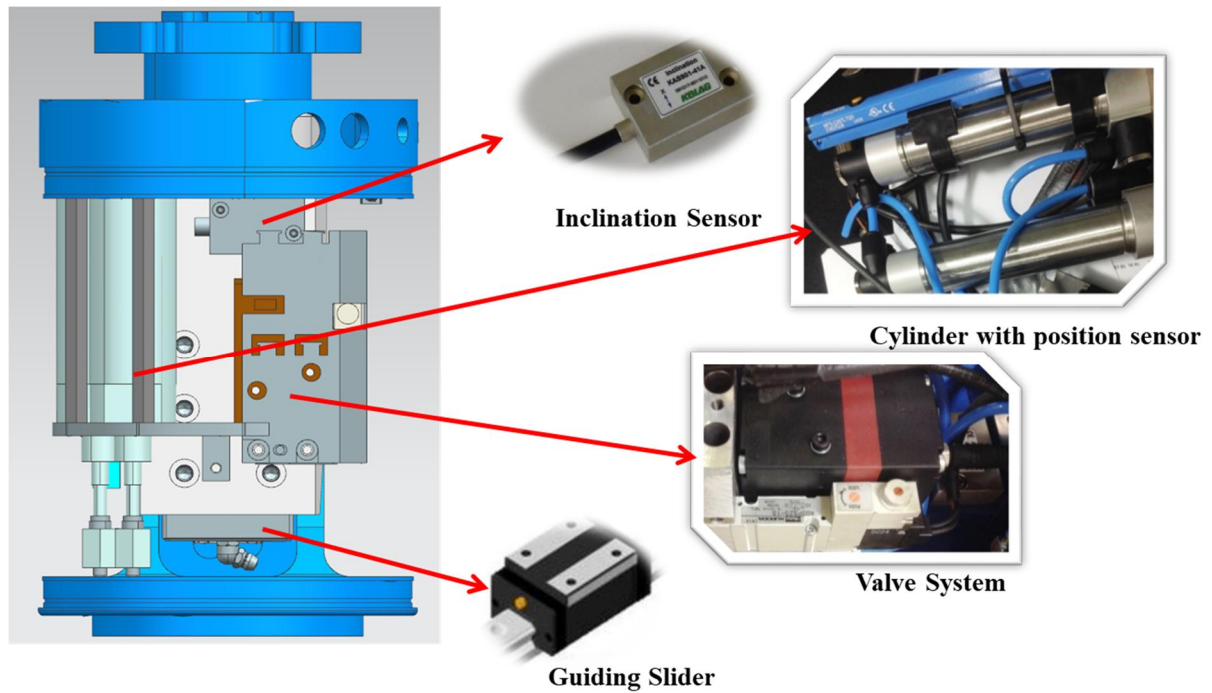
Fig. 19 The structure of IDC device.

3.1   Component manufacturing

The benchmarked products were mainly made of aluminum. The first prototype is replaced by stainless steel and galvanized steel sheets in consideration of the production cost of the product. The weight of the product will be heavy, but it will not affect performance significantly. In future mass production, aluminum will be changed to reduce the weight.
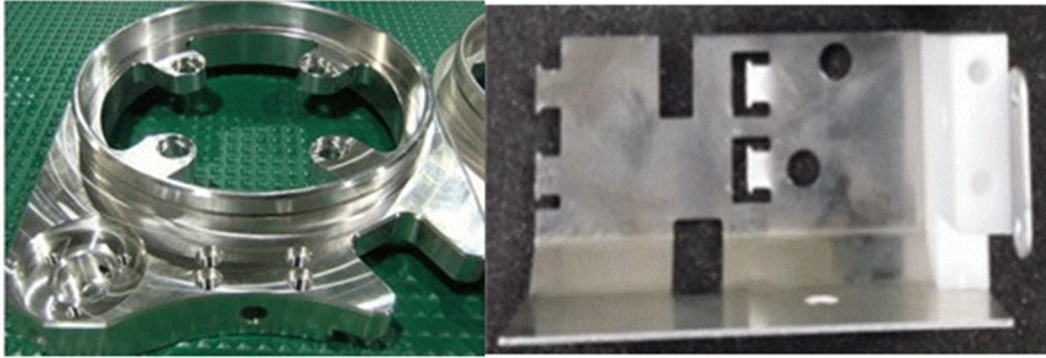
Fig. 20 A prototype of products.
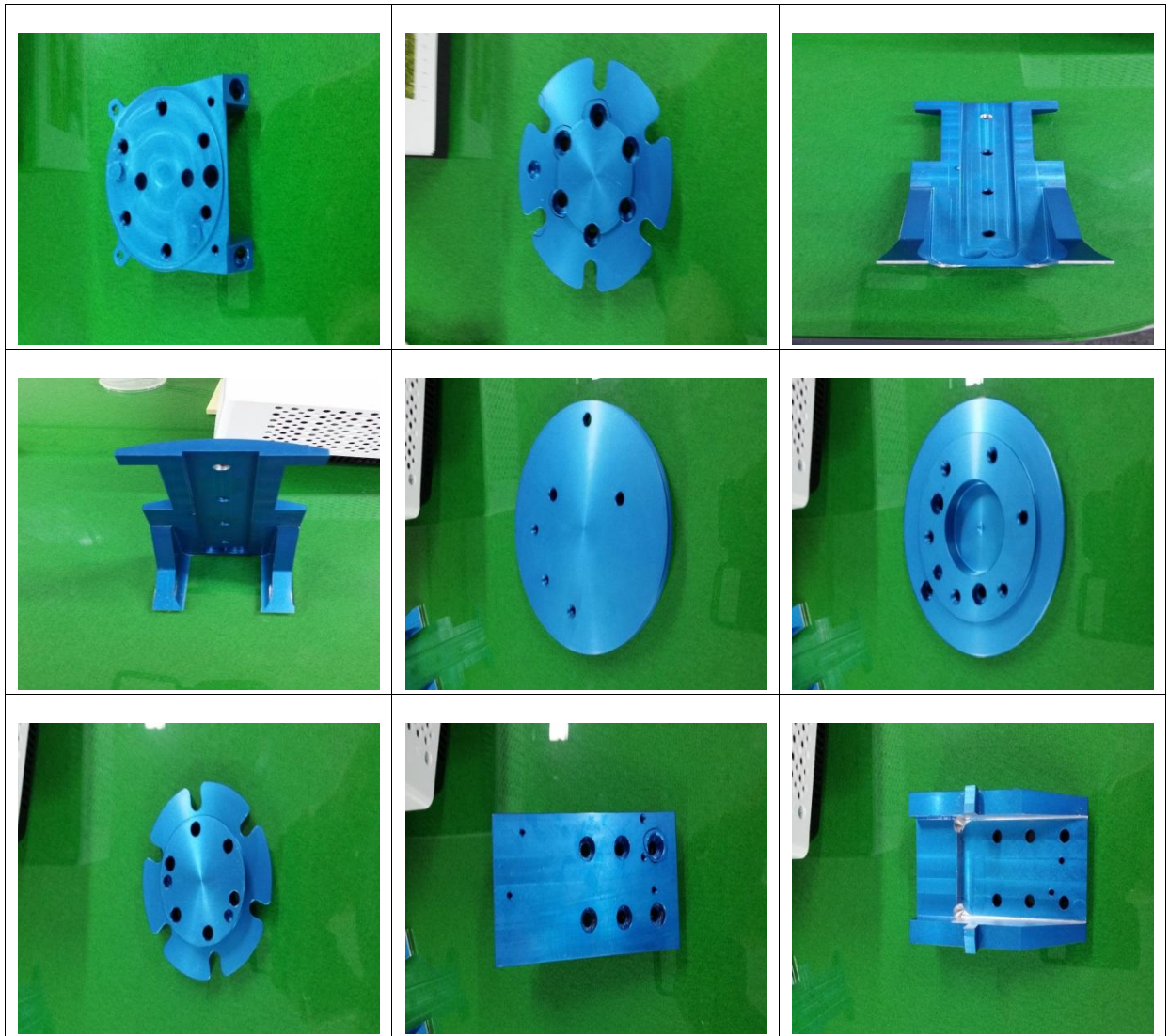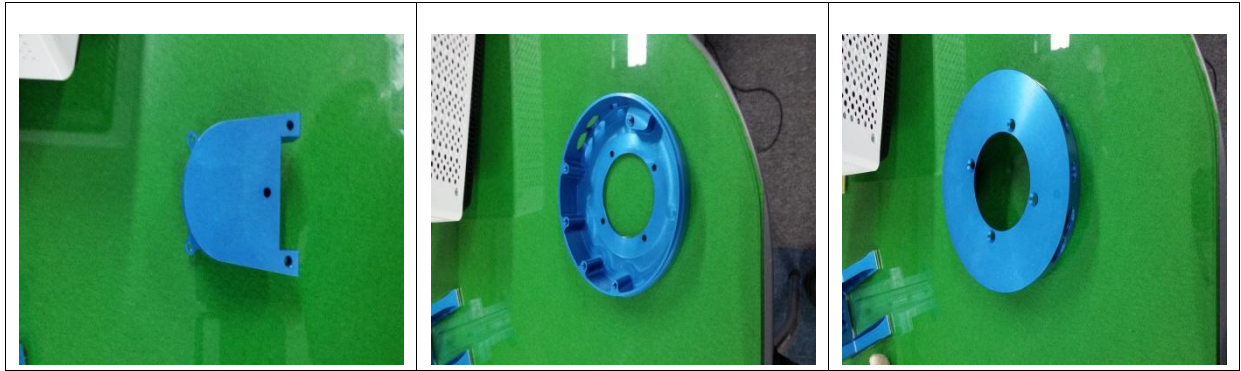
Fig. 21 Manufacturing of IDC device's components.
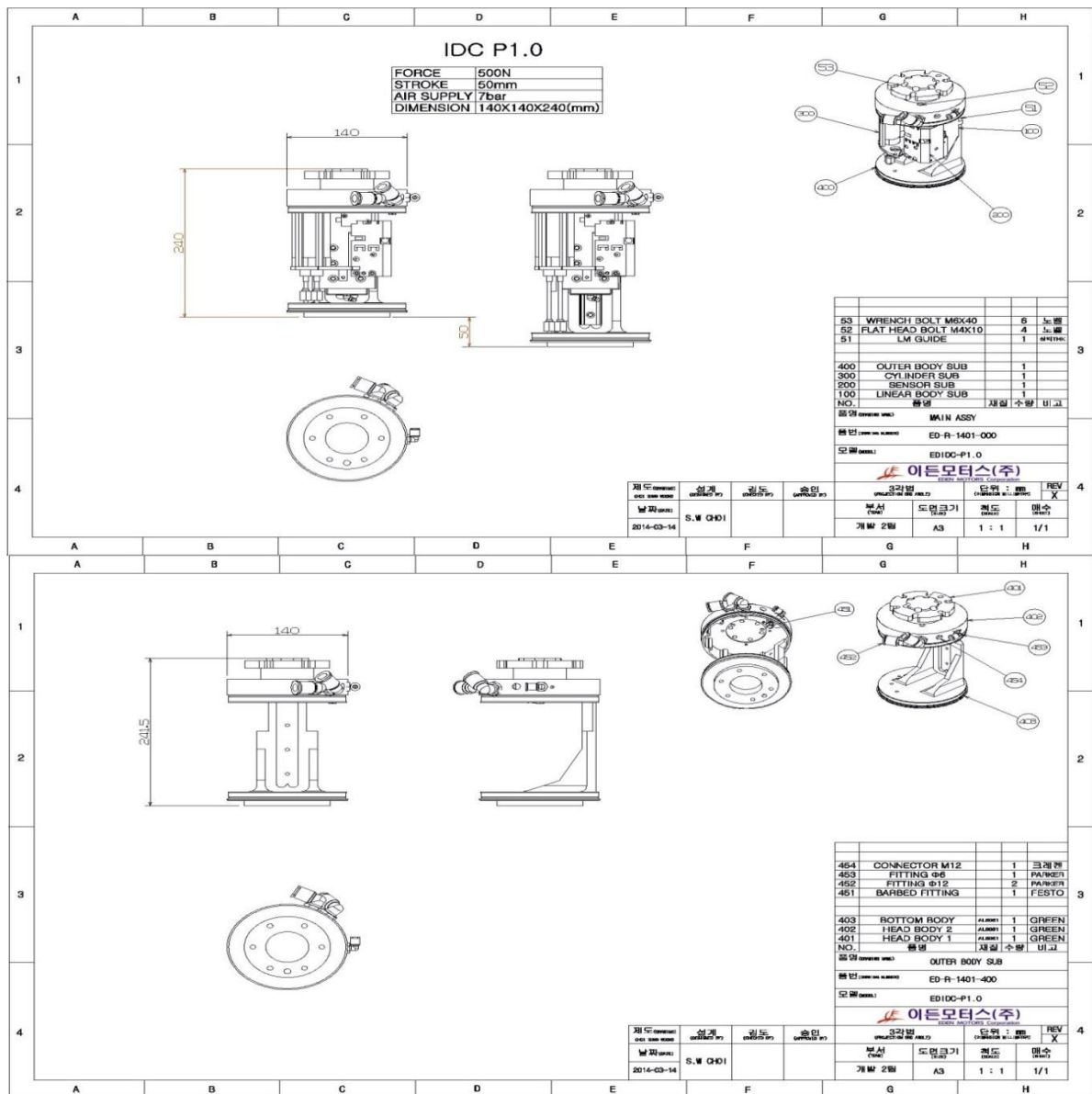
Fig. 22 Drawings of IDC design.

3.2   The pneumatic cylinders

The pneumatic cylinders are driven by air compressor, and are used to regulate the IDC device's pressure, stroke… These cylinders are products of FESTO. The magnetic cylinder type can sense the position information of the cylinder bores. The maximum stroke of the cylinder is 50 mm (2 in), and the cylinder outer diameter is 32 mm (1.25 in). Fig. 24 is a photograph of the cylinder attached to the product.

Fig. 23 Pneumatic cylinders.
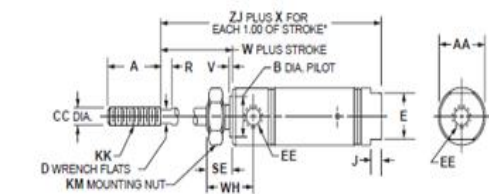
Bore size	SR	SRM	Std. stroke (in)	Max. stroke (in)	SS rod std
7/16"	•		1/2, 1, 1-1/2, 2, 3, 4	6	✔
9/16"	•	•	1/2, 1, 1-1/2, 2, 3, 4	6	✔
3/4"	•	•	1/2, 1, 1-1/2, 2, 3, 4	6	✔
7/8"	•		1/2, 1, 1-1/2, 2, 3, 4	6	✔
1-1/16"	•		1/2, 1, 1-1/2, 2, 3, 4	6	✔
1-1/4"	•	•	1, 2, 3, 4	6	✔
1-1/2"	•		1/2, 1, 2, 3, 4	6	✔
1-3/4"	•	•	1/2, 1, 1-1/2, 2, 2-1/2, 3, 4	6	

Bore size	A	AA	B	C	CC	D	E	EE	J	KK	KM	V	W	X	ZJ SR	SRM
7/16"	0.50	–	0.374	0.25	0.188	3/16	–	#10-32	0.19	#10-32 UNF	3/8-24	0.05	0.56	0.94	1.56	–
9/16"	0.50	–	0.437	0.25	0.188	3/16	–	#10-32	0.19	#10-32 UNF	7/16-20	0.06	0.62	1.62	1.78	2.03
3/4"	0.50	–	0.499	0.25	0.250	1/4	–	1/8 NPTF	0.19	1/4-28 UNF	1/2-20	0.09	0.69	1.69	1.75	2.00
7/8"	0.50	–	0.624	0.25	0.250	1/4	–	1/8 NPTF	0.19	1/4-28 UNF	5/8-18	0.09	0.75	1.56	2.09	–
1-1/16"	0.50	1.12	0.624	0.25	0.312	3/8	0.88	1/8 NPTF	0.19	5/16-24 UNF	5/8-18	0.09	0.75	1.56	2.19	2.44
1-1/4"	0.88	1.34	0.749	0.25	0.437	7/16	0.88	1/8 NPTF	0.25	7/16-20 UNF	3/4-16	0.09	0.88	1.81	2.66	2.78
1-1/2"	0.88	1.56	0.749	0.38	0.437	7/16	0.88	1/8 NPTF	0.25	7/16-20 UNF	3/4-16	0.09	1.00	1.69	2.56	2.81
1-3/4"	0.88	1.84	1.031	0.38	0.500	1/2	1.25	1/4 NPTF	0.25	1/2-20 UNF	1-14	0.09	1.12	2.0	3.03	3.15

* To determine lengths for half inch stroke increments, determine length for next highest whole number stroke and subtract one half inch.

Fig. 24 Specifications of pneumatic cylinders.

Typical specifications for industrial compressors are 7 to 9 bar. The pneumatic pressure is used in this study is designed on the basis of the most commonly used 7 bar. The cylinder design specification is shown in Equation 1.

Equation 1 Design specification of cylinders.

$$F = P \cdot A$$

$$A = \frac{F}{P} = \frac{500N}{7bar} = \frac{500N}{700000Pa(N/m^2)}$$

$$= 7.1428e^{-4}[m^2]$$

$$= 7.14[cm^2]$$

$$\cong 7.5[cm^2]$$

$$A = 7.5[cm^2]$$

$$A = \pi \cdot D^2$$

$$D = \sqrt{\frac{A}{\pi}} = \sqrt{\frac{7.5}{\pi}} = 1.5454[cm]$$

$$D \cong 15.5[mm]$$

The theoretical cylinder diameter in Equation 1 was derived as Ø15.5. Where the design safety factor is multiplied by 3, the cylinder diameter should be about Ø46 or more. Considering the constraints on the product space and the cost of the product, it is reasonable to use two cylinders of Ø23 or more.

Table 2 Cylinder specification catalog.

Bore size	A	AA	B	C	CC	D	E	EE	J	KK	KM	V	W	X	ZJ SR	SRM
7/16"	0.50	–	0.374	0.25	0.188	3/16	–	#10-32	0.19	#10-32 UNF	3/8-24	0.05	0.56	0.94	1.56	–
9/16"	0.50	–	0.437	0.25	0.188	3/16	–	#10-32	0.19	#10-32 UNF	7/16-20	0.06	0.62	1.62	1.78	2.03
3/4"	0.50	–	0.499	0.25	0.250	1/4	–	1/8 NPTF	0.19	1/4-28 UNF	1/2-20	0.09	0.69	1.69	1.75	2.00
7/8"	0.50	–	0.624	0.25	0.250	1/4	–	1/8 NPTF	0.19	1/4-28 UNF	5/8-18	0.09	0.75	1.56	2.09	–
1-1/16"	0.50	1.12	0.624	0.25	0.312	3/8	0.88	1/8 NPTF	0.19	5/16-24 UNF	5/8-18	0.09	0.75	1.56	2.19	2.44
1-1/4"	0.88	1.34	0.749	0.25	0.437	7/16	0.88	1/8 NPTF	0.25	7/16-20 UNF	3/4-16	0.09	0.88	1.81	2.66	2.78
1-1/2"	0.88	1.56	0.749	0.38	0.437	7/16	0.88	1/8 NPTF	0.25	7/16-20 UNF	3/4-16	0.09	1.00	1.69	2.56	2.81
1-3/4"	0.88	1.84	1.031	0.38	0.500	1/2	1.25	1/4 NPTF	0.25	1/2-20 UNF	1-14	0.09	1.12	2.0	3.03	3.15

* To determine lengths for half inch stroke increments, determine length for next highest whole number stroke and subtract one half inch.

The cylinder is selected as on Table 2 with bore size 1-1 / 16 "(27mm), but select 1-1 / 4" (31.75mm) product considering stroke. The 1-1/4" model satisfies both of design goal 500N and the stroke of 50mm.

3.3   Magnetic cylinder position sensor.

The magnetic cylinder position sensor can be mounted on the side of the magnetic cylinder as shown in Fig. 25 to detect the position of the cylinder bore. It is a SICK product, which is specialized in the sensor, and it has a sampling time of 1ms with an accuracy of 0.05mm. The specification table is shown in Fig. 25.

	MPS with analog output	MPS with IO-Link
Cylinder type	T-slot	
Cylinder types with adapter	Round body cylinders Cylinders with dove-tail slot SMC rails CDQ2 SMC rails ECDQ2	
Measuring range [1]	32 mm ... 256 mm (depending on type)	
Housing length	45 mm ... 269 mm (depending on type)	
Output function	Analog	IO-Link
Analog output (voltage)	0 V ... 10 V	–
Analog output (current)	4 mA ... 20 mA	–
Teach-in	✔ (depending on type)	✔
Enclosure rating [2]	IP 67	
Supply voltage	15 V DC ... 30 V DC	
Load resistance, max. [1]	500 Ω	
Min. load resistance [2]	2 kΩ	
Protection class	III	
Magnetic field sensitivity, typ.	3 mT	
Resolution typ. [3]	0.03 % FSR (≥ 0.05 mm)	
Linearity typ.	0.3 mm	
Repeat accuracy typ [3]	0.06 % FSR (≥ 0.1 mm)	
Sampling rate	1 ms	

Fig. 25 Magnetic cylinder position sensor.

3.4   Piezo-electric pressure regulating valve.

The pressure-regulating valve is used to supply the air into the pneumatic cylinder from an air compressor. It is a product of HOERBIGER Co., Ltd. The pressure control range is 0 ~ 8 bar, and the air pressure required for IDC is 7 bar. The flow rate is 350 l / min, the precision is 0.4 bar or less, the development target is 5 ~ 10 l / min, and ± 0.5 bar. The response time is 7 milliseconds. Fig. 26 shows the pressure control valve's specification.

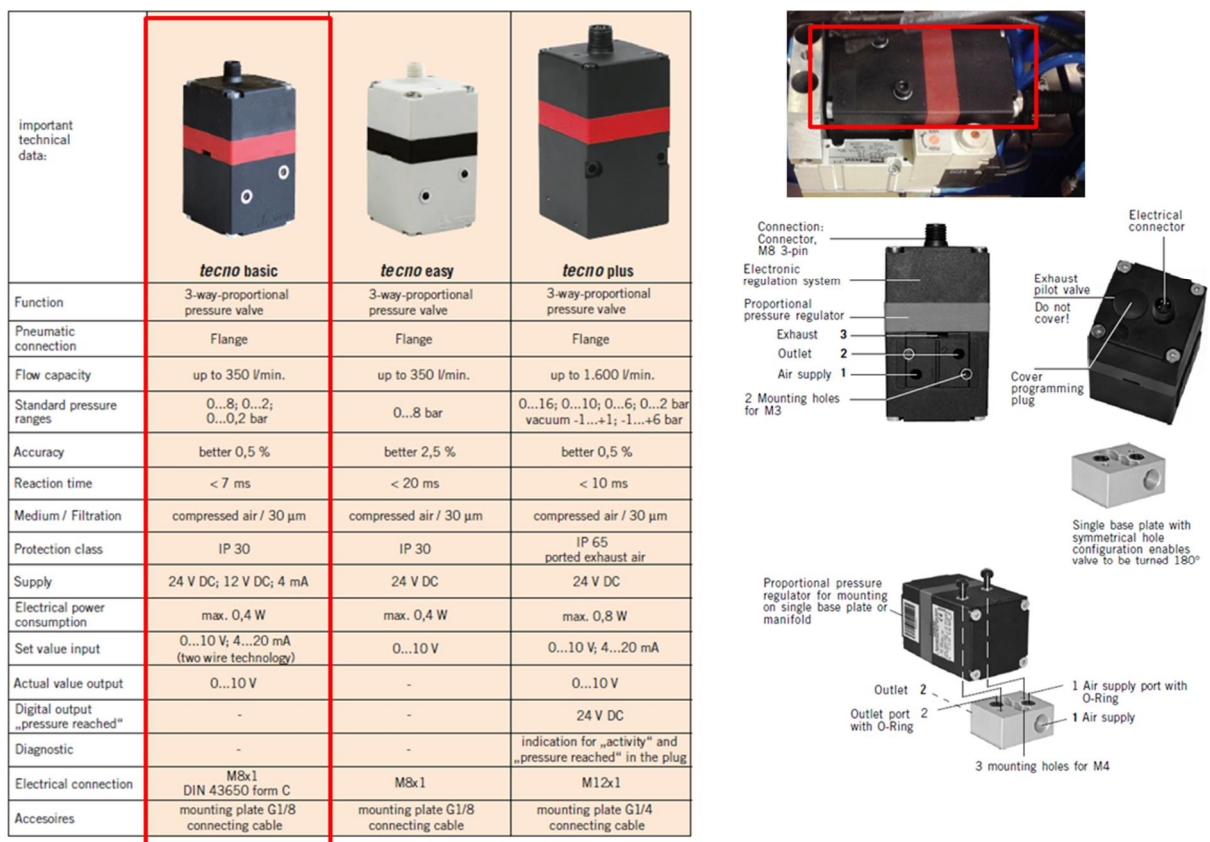| important technical data:	*tecno* basic	*tecno* easy	*tecno* plus
Function	3-way-proportional pressure valve	3-way-proportional pressure valve	3-way-proportional pressure valve
Pneumatic connection	Flange	Flange	Flange
Flow capacity	up to 350 l/min.	up to 350 l/min.	up to 1.600 l/min.
Standard pressure ranges	0...8; 0...2; 0...0,2 bar	0...8 bar	0...16; 0...10; 0...6; 0...2 bar vacuum -1...+1; -1...+6 bar
Accuracy	better 0,5 %	better 2,5 %	better 0,5 %
Reaction time	< 7 ms	< 20 ms	< 10 ms
Medium / Filtration	compressed air / 30 μm	compressed air / 30 μm	compressed air / 30 μm
Protection class	IP 30	IP 30	IP 65 ported exhaust air
Supply	24 V DC; 12 V DC; 4 mA	24 V DC	24 V DC
Electrical power consumption	max. 0,4 W	max. 0,4 W	max. 0,8 W
Set value input	0...10 V; 4...20 mA (two wire technology)	0...10 V	0...10 V; 4...20 mA
Actual value output	0...10 V	-	0...10 V
Digital output „pressure reached"	-	-	24 V DC
Diagnostic	-	-	indication for „activity" and „pressure reached" in the plug
Electrical connection	M8x1 DIN 43650 form C	M8x1	M12x1
Accesoires	mounting plate G1/8 connecting cable	mounting plate G1/8 connecting cable	mounting plate G1/4 connecting cable

Fig. 26 Specifications of the pressure regulating valve.

3.5   The directional solenoid valve.

The solenoid valve transmits the constant pressure air pressure through the pressure control valve to the rod-head port of the cylinder to operate the cylinder, and it is also

referred to as the direction control valve depending on the operation mode. Parker's A05PS25-1S solenoid valve is used, the operating pressure range is 1.5 to 7 bars, and the response time is 10 milliseconds. Fig. 27 below shows the solenoid valve specification table.

Specifications

Model No.		Unit	A05PS25	A05PD25	A05PD35	A05PE35	A05PO35
Fluid			Non-lubricated/lubricated air				
Port size			Rc 1/8				
Effective area		mm²	5.8		4.5		6.7
Cv value			0.32		0.25		0.37
Operating ambient temperature		℃	−5~				
Pressure range		MPa	0.15~0.7	0.1~0.7			
				−0.1~0.7 For exter			
Maximum frequency		cycle/min	600				
Response time	DC	ON	s	0.010	0.010			
		OFF	s	0.010 (0.016)	—			
Pilot air exhaust			Captured exhaust				
Manual override			Screwdriver-operated locking button				
Mounting position			Free				
Shock resistance, vibration resistance		m/s²	150/30				
Mass	Without sub-base	g	52	67		69	
	With sub-base	g	108	126		128	

Fig. 27 Specifications of the solenoid valve.

3.6　Valve System Plate

The valve system plate is designed as the conduit of between the pressure valve and solenoid valve for transferring the air through each other. Fig. 28 below shows the disassembly of the valve plate and solenoid valve, and the detail of plate port. Unlike other parts, the valve plate is judged to be manufactured to the specifications. It is manufactured to conform to the solenoid valve and pressure control valve specifications as prototyping.

Fig. 28 Valve system plate.

3.7   Linear Motion (LM) Guide

The LM guide serves to allow the IDC to expand and contract when the cylinder is in a shrink-expand operation. All other components are assembled onto the LM Guide. Fig. 29 shows LM Guide specifications.

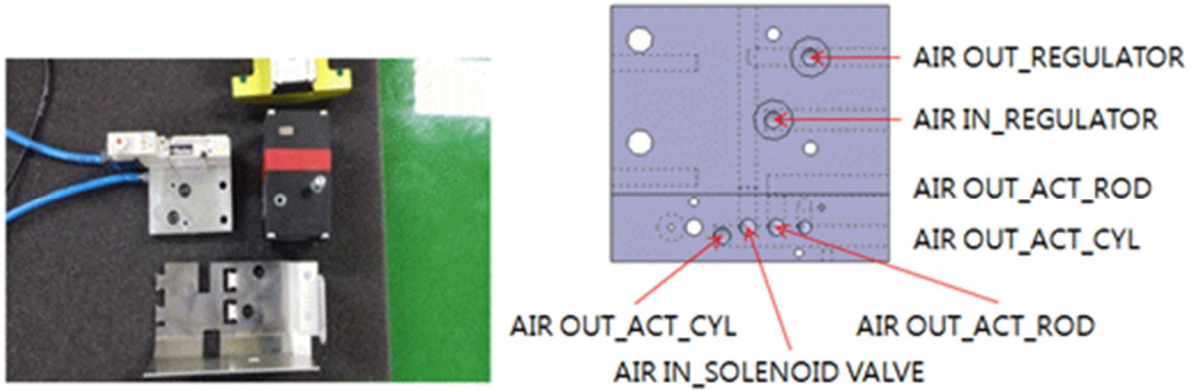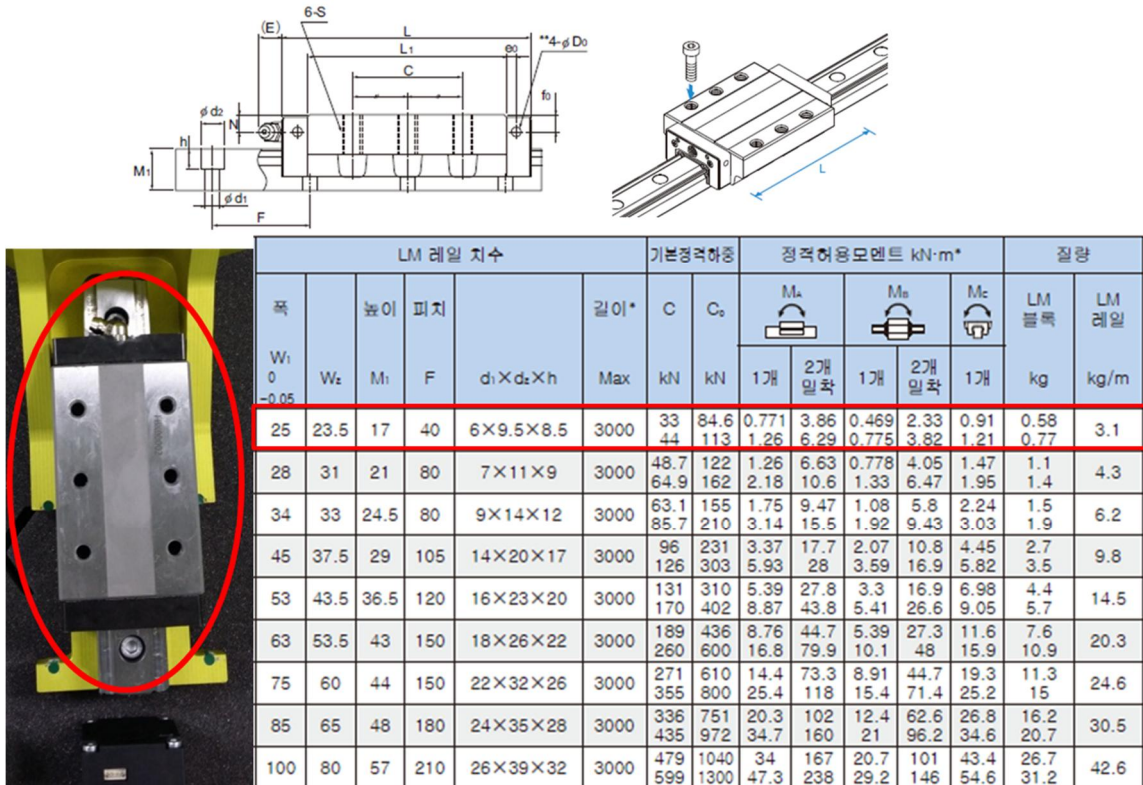| LM 레일 치수						기본정격하중		정적허용모멘트 kN·m*					질량	
폭		높이	피치		길이*	C	C₀	M_A		M_B		M_C	LM 블록	LM 레일
W_1 0 -0.05	W_2	M_1	F	$d_1 \times d_2 \times h$	Max	kN	kN	1개	2개 밀착	1개	2개 밀착	1개	kg	kg/m
25	23.5	17	40	6×9.5×8.5	3000	33 / 44	84.6 / 113	0.771 / 1.26	3.86 / 6.29	0.469 / 0.775	2.33 / 3.82	0.91 / 1.21	0.58 / 0.77	3.1
28	31	21	80	7×11×9	3000	48.7 / 64.9	122 / 162	1.26 / 2.18	6.63 / 10.6	0.778 / 1.33	4.05 / 6.47	1.47 / 1.95	1.1 / 1.4	4.3
34	33	24.5	80	9×14×12	3000	63.1 / 85.7	155 / 210	1.75 / 3.14	9.47 / 15.5	1.08 / 1.92	5.8 / 9.43	2.24 / 3.03	1.5 / 1.9	6.2
45	37.5	29	105	14×20×17	3000	96 / 126	231 / 303	3.37 / 5.93	17.7 / 28	2.07 / 3.59	10.8 / 16.9	4.45 / 5.82	2.7 / 3.5	9.8
53	43.5	36.5	120	16×23×20	3000	131 / 170	310 / 402	5.39 / 8.87	27.8 / 43.8	3.3 / 5.41	16.9 / 26.6	6.98 / 9.05	4.4 / 5.7	14.5
63	53.5	43	150	18×26×22	3000	189 / 260	436 / 600	8.76 / 16.8	44.7 / 79.9	5.39 / 10.1	27.3 / 48	11.6 / 15.9	7.6 / 10.9	20.3
75	60	44	150	22×32×26	3000	271 / 355	610 / 800	14.4 / 25.4	73.3 / 118	8.91 / 15.4	44.7 / 71.4	19.3 / 25.2	11.3 / 15	24.6
85	65	48	180	24×35×28	3000	336 / 435	751 / 972	20.3 / 34.7	102 / 160	12.4 / 21	62.6 / 96.2	26.8 / 34.6	16.2 / 20.7	30.5
100	80	57	210	26×39×32	3000	479 / 599	1040 / 1300	34 / 47.3	167 / 238	20.7 / 29.2	101 / 146	43.4 / 54.6	26.7 / 31.2	42.6

Fig. 29 Specification of Linear Motion Guide

3.8   Inclination sensor

The Inclination sensor is mounted on a fixed part of IDC device to determine the working angle of the deburring tool. It is useful to calculate the actual force.

- Long-term stabilities up to ±0,067% FS / 0,036°/ 0,67mg (10 years)
- Repeatability < 0,01%FS, 0,01° / 0,18mg
- Resolutions up to ± 0.0015% / 0,00075° / 7µg (bei 1Hz)
- Temperature dependencies up to ±0,002°/°C
- shock resistance of the pendulum min. 50'000g

Parameter	Conditions	KAS901-04	Unit
Measuring range [4]		+/- 1,7 +/- 90	G °
Repeatability at 0° (horizontal position) [1]	at 0...40℃, 20℃ typ	4 0,2	mg °
Resolution at 0°/ 1g	DC .. 1Hz	0,2 0,01	mg °
typ. Offset temperature dependency	20...60℃	0.6	mg/°
long term stability [6]	10 years [6]	approx. 1,5	mg
Measuring direction		x-axis	
Cross axis sensitivity [2]		4	%
damping	-3 dB	50	Hz [5]
Operating temperature range		-30[7] .. +85	℃
Shock resistance (Chip)		20'000	g
Output signal V_{out} Offset = V_{out} in 0°/1gposition Sensitivity		0,5 .. 4,5 2,5 4	V V V/g
Power supply [3]		7... 36	VDC

Fig. 30 Specification of inclination sensor.

IV.   The JIG of the workpiece.

The fixed JIG is fabricated as Fig. 31 for removing the gates and burrs of products. Due to scratch-resistant fabrication products, JIG blocks and fixed clamp JIG were made of PE and MC material.
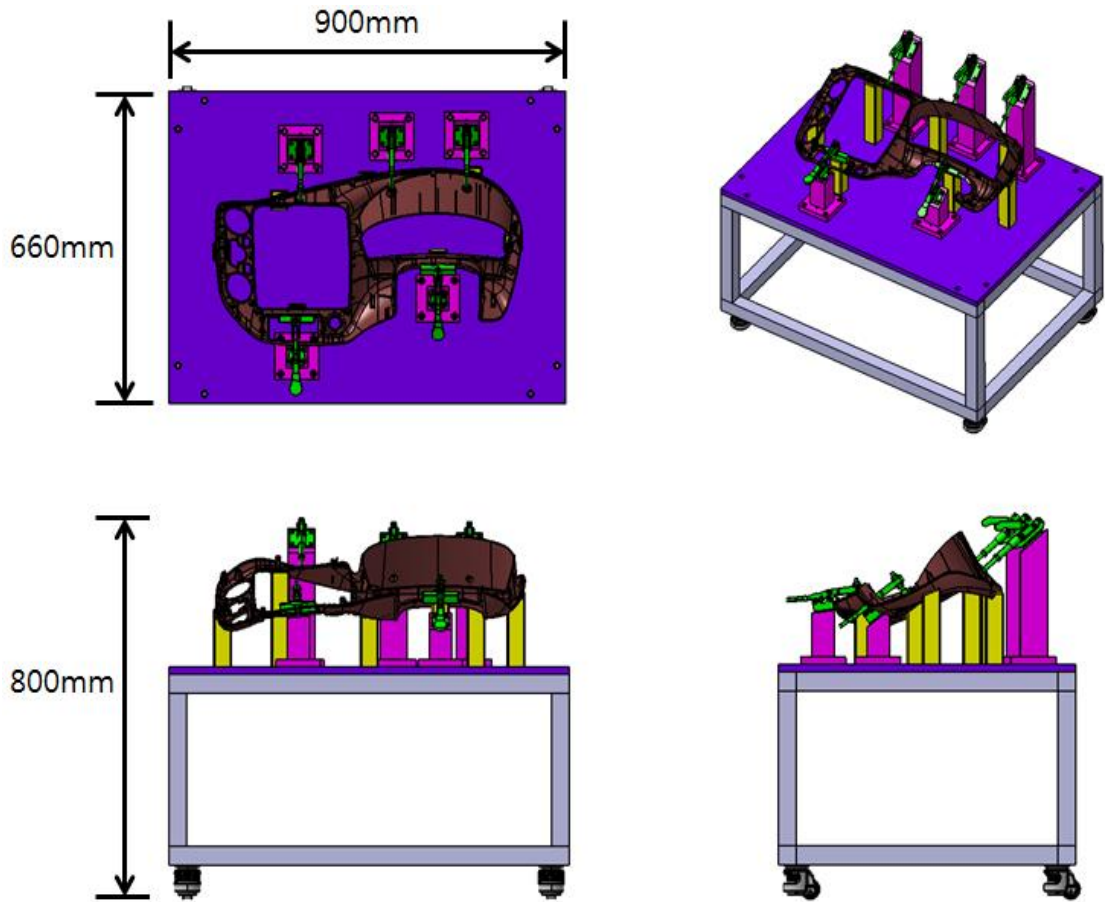
Fig. 31 Outline of product fixed JIG.

In order to fix the workpiece to the JIG, place the workpiece on the JIG block and fix the workpiece with a clamp at each point.
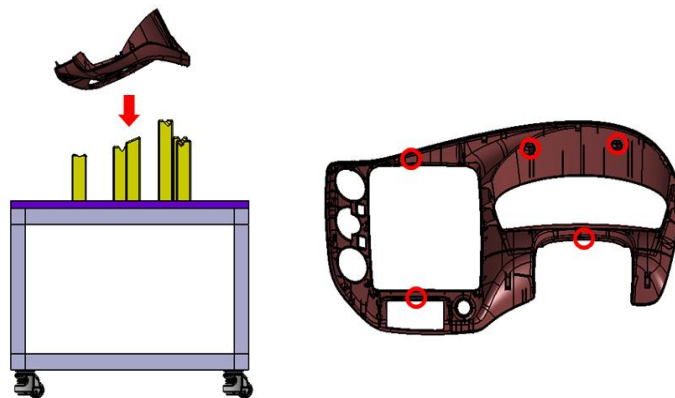

Fig. 32 Fixing JIG mechanism for the workpiece.

As a result of the first prototype test of the fixing JIG, scratches were generated at the corner of the fixing JIG, and the product was partially fixed and the product was shaken. The second fixing JIG was fabricated by complementing the above two problems as shown in Fig. 33.
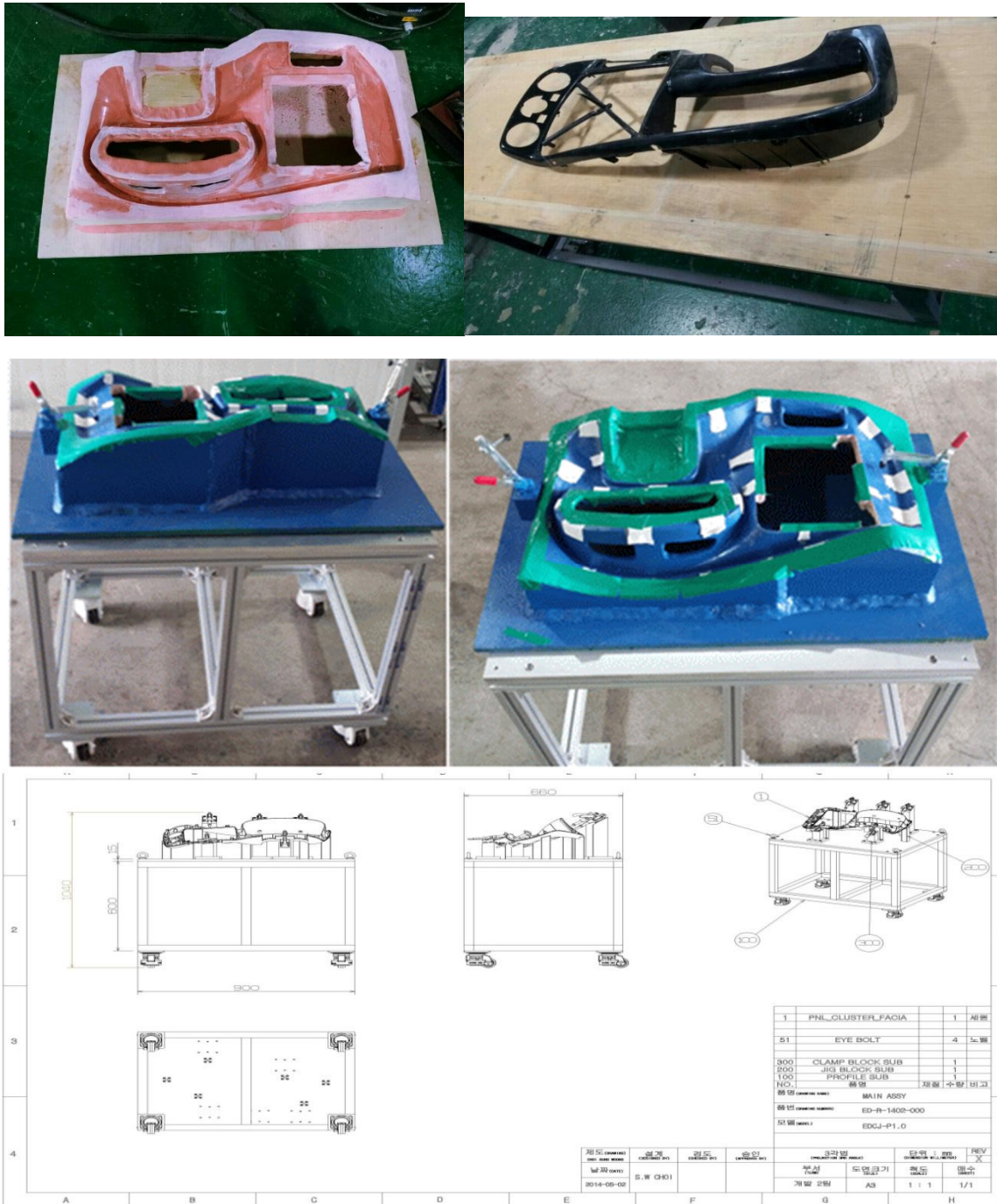

Fig. 33 Fabrication of the second prototype of JIG.

As a result of the test of the second fixing JIG, the clamps were fixed by two clamps on the left and right sides, but the surface of the JIG was not uniform and scratches occurred. Although the scratch phenomenon has been eliminated by using a cloth as a temporary measure, the problem will be solved through the contact with the product in the production of the third prototype.

V.   Robot simulation and simulation optimization

Robot Teaching is divided into one-line and off-line. One-line teaches by using pendant of the robot in the field, and off-line teaching is done before production of equipment or robot. Before installing and commissioning, it is necessary to create a space close to actual 3D by using a computer program, teaching the robot on the program, commissioning the program to the robot in the field, download it, and supporting the site.

Before making in fixed JIG manufacturing and process development using robots to reduce the number of mistakes and to improve the accuracy of the process development. The scope of the 3D simulation, that we want to develop in this development, is the process that can be done in manufacturing by pre-simulation by attaching IDC, tool changer and cutting tool to robots.

- Creation of simulation environment for robot automation system and modeling of robot simulation.

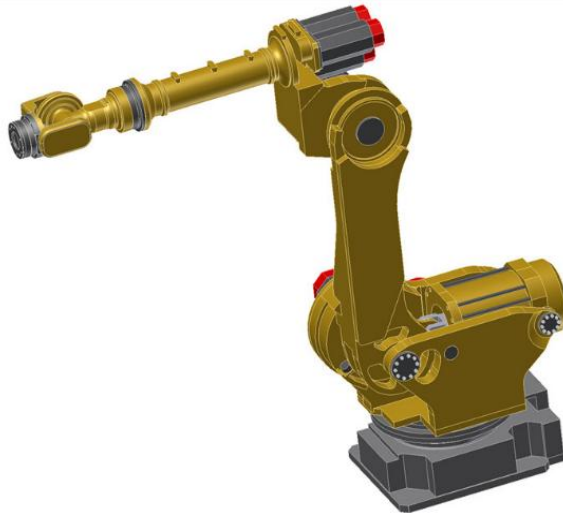- Robot simulation using MATLAB and ANSYS.

Fig. 34 The 3D model of the robot.

Simulation of robots using 3D modeling work is done by MATLAB/Simmechanics.
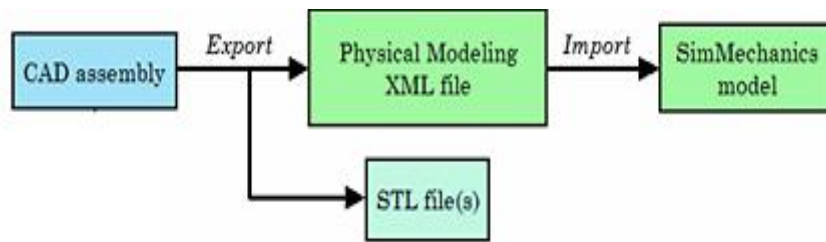

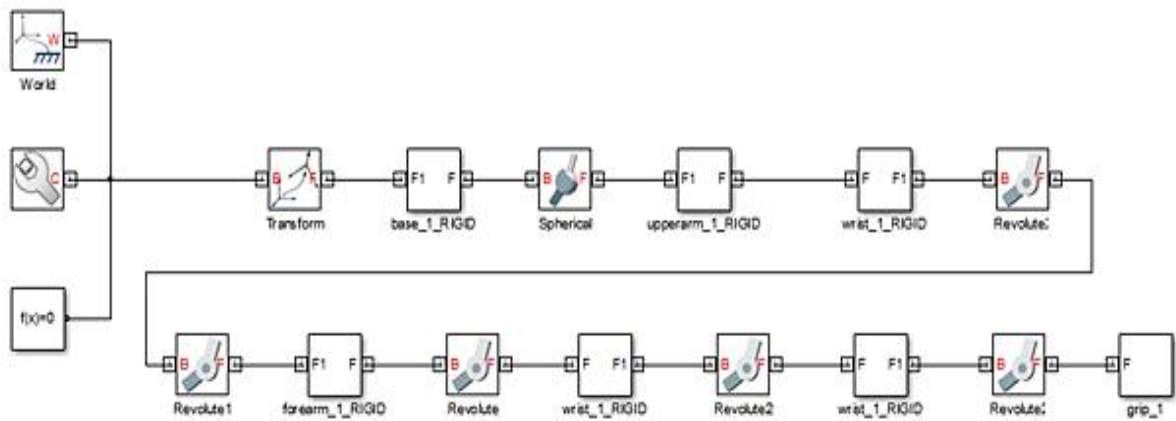Fig. 35 Simmechanics model generation method using CAD files.

Fig. 36 Simmechanics model of the deburring robot.

50

Fig. 37 Example of deburring robot modeling.

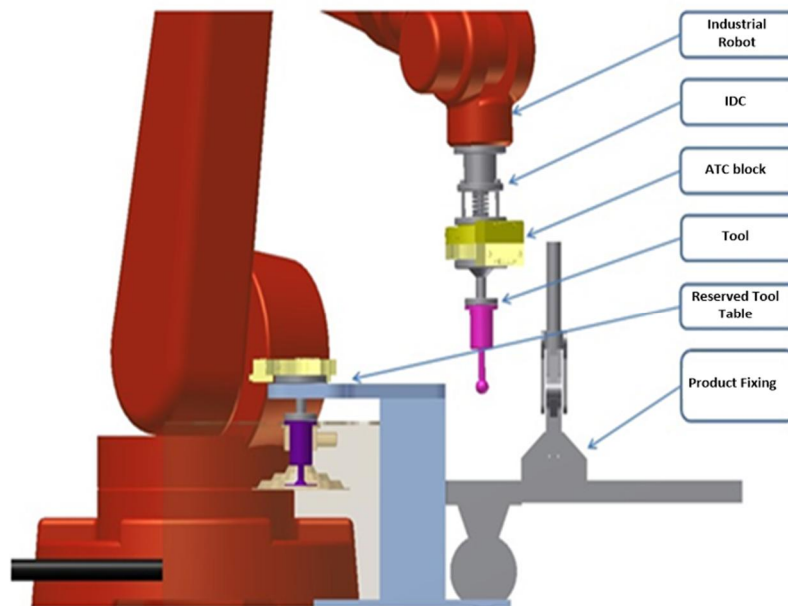VI.   Application of prototype mass production.

Fig. 38 Deburring robot system.

At the stage of mass production technology development, the aim is to improve the performance and quality of prototype products based on the products and data developed during the first and second years. In order to improve durability, which is one of the most important items in the mass production for the compatibility of IDC, fixed jig and dedicated tool manufactured by the prototype, it is judged whether there is any interference between parts, parts, materials, and materials, Thereby enabling

51

stable process production. After that, we focus on process interlocking by clarifying and minimizing the process start range so that C / T can be matched with the in-plant process that is currently being mass-produced.
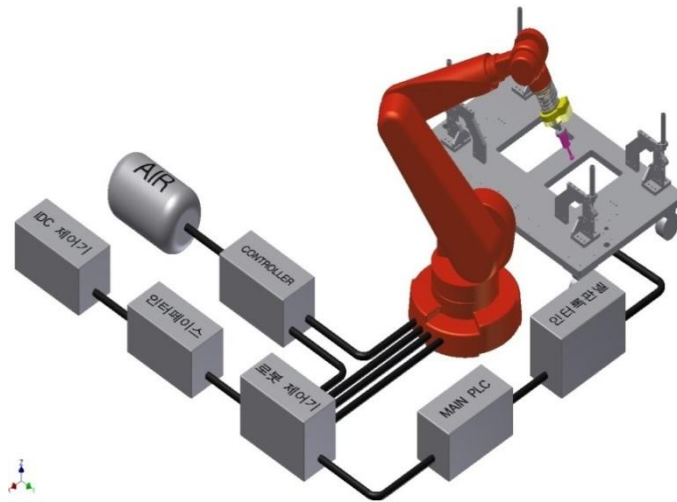

Fig. 39 3D Conceptual Diagram of Deburring Automation System.

Optimization of C/T is the first step in optimizing the process configuration in accordance with the entire process C/T in the input process of the participating companies and the demanding enterprise. In consideration of the worker's movement line, the process can be improved by configuring the other process and the worker to be in charge of the common line.

VII.   Concluding Remarks

The research project was carried out by investigating the related patents, product benchmarking, and some similar products. The mechanical mechanism and algorithm are studied for designing the general structure and choosing the main components. The IDC and ATC devices were fabricated for controlling the deburring robot system to reducing the impact between the deburring tool and workpiece, compensating the tolerance of workpiece surface. The deburring automation system aims to produce the number of uniform products, to reduce the production cost, improving the performance of products.

CHAPTER III MODELING OF

INTELLIGENT DEBURRING CONTROL

(IDC) DEVICE

I.   Introduction and Overview

In the recent years, the robot arm is used widely in automotive industry for surface processing. In general, a normal manipulator needs to be controlled the path planning and the position. In the surface processing, beyond controlling path planning and position of end-effector, the impact force, which acts on the surface of the work-piece, needs to be regulated. So, the IDC mechanism is designed for monitoring the contact between surface and tool, and controlling this contact force to improve the surface quality of products.

Fig. 40 Force Measurement Test using IDC Device.

The surface processing is significant for machined parts, especially in automotive component de-burring. The formation of unwanted burrs is common to all machining, forming and casting processes. Robotic de-burring systems, where the cutting tool is regulated by the robot arm, are capable of de-burring at faster rates with higher chamfer quality than possible manually.

Actually, the automotive industries develop in the worldwide, along with the advances in technology, customer demands of interior and exterior instruments are also increased. Especially, the performances of components surface are concentrated. So the competitions are coming up strongly. The pneumatic system with two of double acting pneumatic cylinders is mounted on robot arm was applied for improving the component surface performances in grinding or deburring process by maintaining contact force. Pneumatic cylinders are commonly applied in the manufacturing industry as robotics, automation system for reasons related to their good power/weight ratio, easy maintenance and assembly operations, clean operating conditions and low cost. In addition, modern robot control algorithms require the ability to control directly the actuator output force and torque for compliant motions.

A mathematical model of pneumatic servo actuator based on the linearized flow rate constant of the pneumatic cylinder was mentioned [67] by Liu and Bobrow. Bobrow and Jabbari [68] discussed a dynamic model of the pneumatic actuator has been derived for force and position control. McDonell and Bobrow [69] presented an adaptive controller for simultaneous parameter identification and tracking feedforward control of one degree of freedom pneumatic actuator. Arun and Radke [70] reduced the order of sliding mode position controller by using two-way on/off solenoid valve. Ben-Dov and Salcudean [71] developed a force-controlled pneumatic actuator included the dynamics model and compressible air flow characteristics of the valve design. Al-Ibrahim and Otis [72] recommended the experiment method for charging and discharging processes of air inside an actuating cylinder. In 2000, Richer and Hurmuzlu [73] designed the mathematical model and experiments to identify characteristics of the pneumatic system with proportional spool valve. Carneiro and Almeida [74] used reduced-order models to describe the pressure prediction effected by temperature and heat transfer.

In this work, we build a mathematical model and launch in MATLAB/Simulink. The model includes a polytropic model for temperature evolution of cylinder in an

isothermal process, first-order modeling of the piezo-electric pressure-regulating valve and the airflow rate in the valve by comparing the supply pressure and cylinder chamber pressure. We do the experiment in stroke range of 50 mm and 50 kg actuating force for investigating effects of the pneumatic system in extension process of IDC device, in which the double of pneumatic cylinders is controlled by the valve system consisting of on/off solenoid valve and pressure regulating valve.

II.   Description of IDC Device

2.1   Pneumatic System of IDC Device

The pneumatic system consists of the components: the double pneumatic cylinders with 50 mm stroke, a magnetic position sensor for monitoring the movement of piston, an inclination sensor for measuring working angle of deburring tool, a pressure regulating valve (Hoerbiger, Pre-U model) integrated with an on/off solenoid 5/2 valve for switching air flow direction.
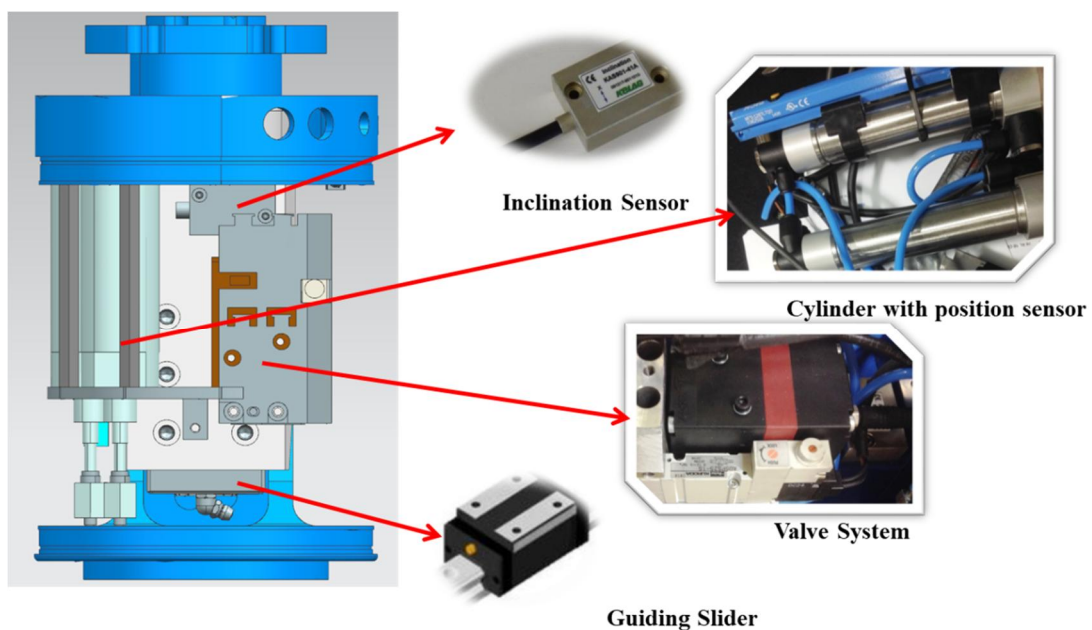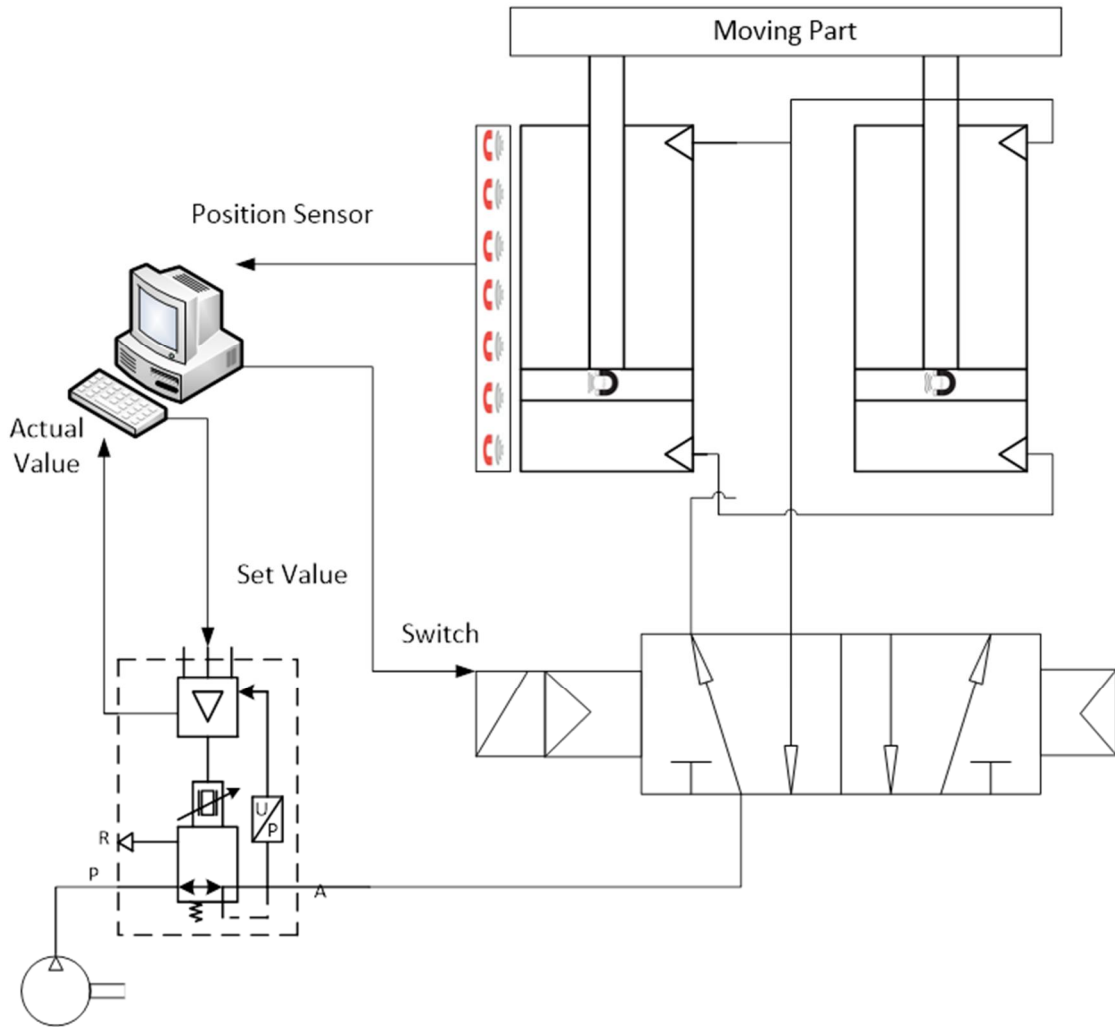

Fig. 41 Structure of IDC device

Fig. 42 Pneumatic Circuit Diagram of IDC device.

For supporting the pneumatic system, there are some components as sliding part of THK, connecting tube, air supply system.

This pneumatic system aims to control contact force by regulating the inlet pressure of cylinder chambers. The position sensor aims to measure the stroke of piston and acceleration sensor aims to measure the change rate of acting force in instantly.

The cylinder chamber inlet pressure is regulated via a piezo-electric pressure regulating valve (Hoerbiger, Pre-U model).
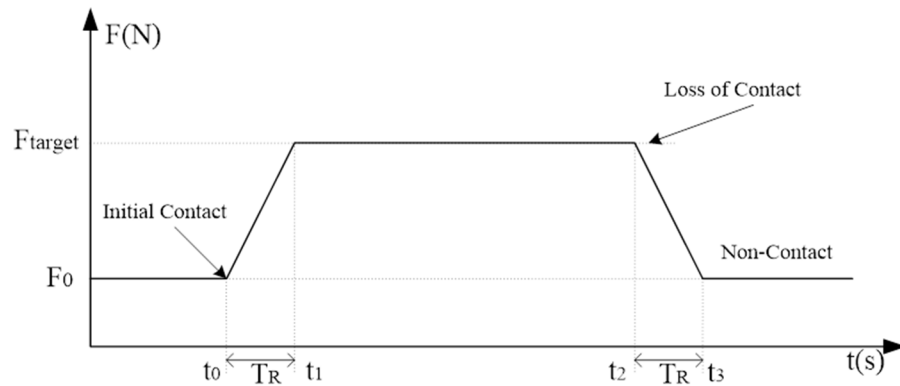
2.2   Operation Principle of IDC Device

Fig. 43 Force profile of IDC device.

The contact between the tool and the work-piece is monitored by using sensing device. If the contact is detected, the mechanism will be used to control the acting force (acts to regulating element (pneumatic cylinder)) to reach target force – predefined force profile. This force will be maintained until loss of contact, the acting force will get return the minimum force F_0 in time interval T_R. The cycle is able to be repeated depending on the contact between the tool and the work-piece.

T_R (t_0-t_1, t_2-t_3): time interval, the time needed to change the force from F_0 to F_{target} or inverse.

t_1-t_2: the contact time.

t_0< or >t_3: have no contact.

These apparatus uses the pneumatic system to generate supplied force to pneumatic cylinders to react impact force between tool and work-piece.

The original principle of IDC Device is designed as a suspension system with variable stiffness. The variable stiffness is generated by regulating the input pressure. When the input pressure is changed, the acting force (also variable stiffness) is changed respectively.

58

III.   Kinematic Motion of IDC simulated by SimMechanics

This section describes the downward or upward movements of IDC tool flange along with sliding part. At first, the IDC Device's 3D model is designed by SolidWorks or CATIA… and using SimMechanics of Matlab/Simulink for simulating the simple kinematic operation of IDC Device.

3.1   CAD Modeling

The IDC Device is a system consisting of 2 cylinders; valve system: regulation valve, directional valve, manifold; sliding device; position sensor, acceleration sensor; and rigid bodies.

The motion of IDC is translational displacement following the vertical axis of cylinders and sliding mechanism. So, the IDC is separated into 2 parts: IDC_upper_part and IDC_bottom_part as below:
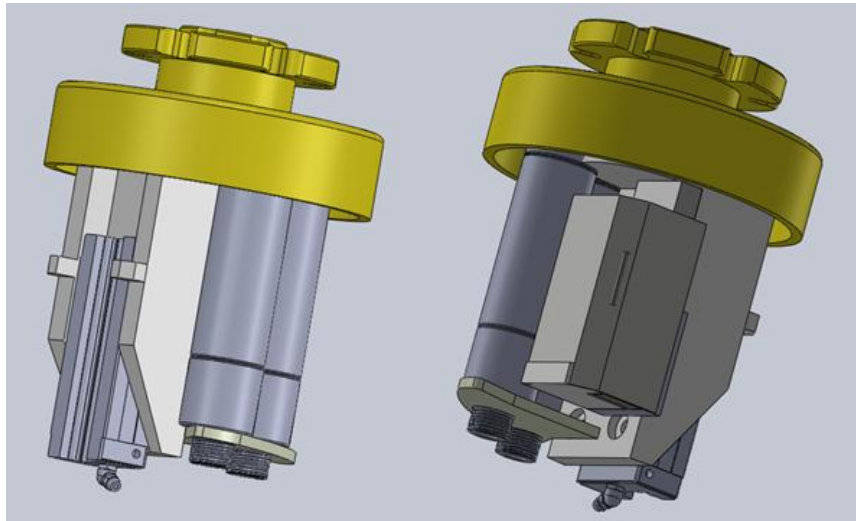

Fig. 44 IDC_upper_part consisting of cylinder tubes, the bearing of the sliding mechanism, valve system, sensors.
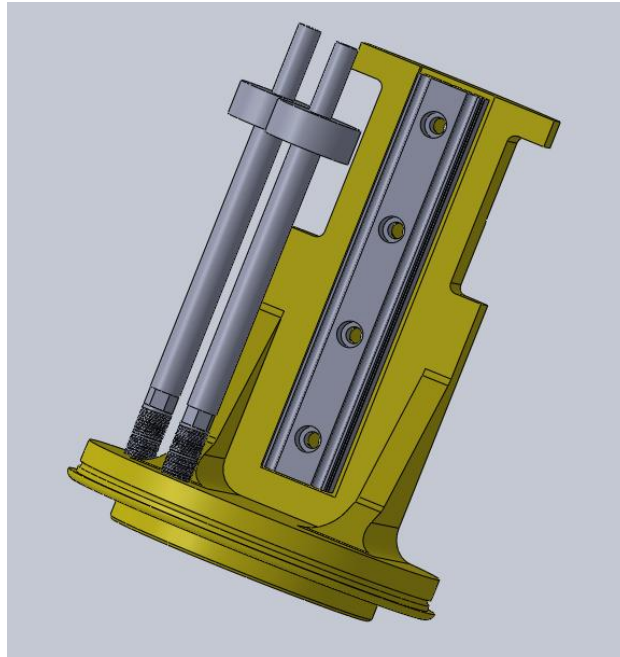
Fig. 45 IDC_bottom_part.

3.2   Importing the SolidWorks CAD Model to SimMechanics Model

Exporting CAD model to XML model

Importing XML to SimMechanics Model

When the 3D model is exported into an XML file, the SimMechanics use these files to import the Model. The process is described in Fig. 46.

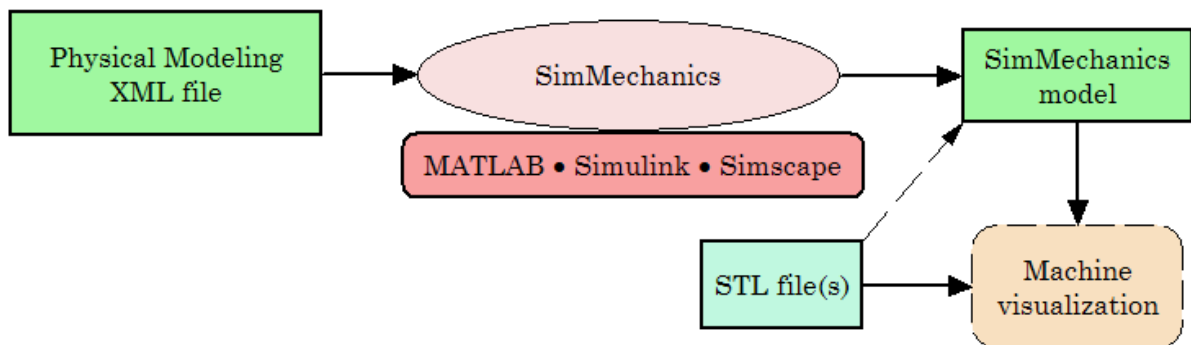Fig. 46 Diagram for importing XML to SimMechanics Model

3.3   Building SimMechanics-Matlab/Simulink Model

The model has 2 rigid bodies:

IDC_upper_part (yellow)
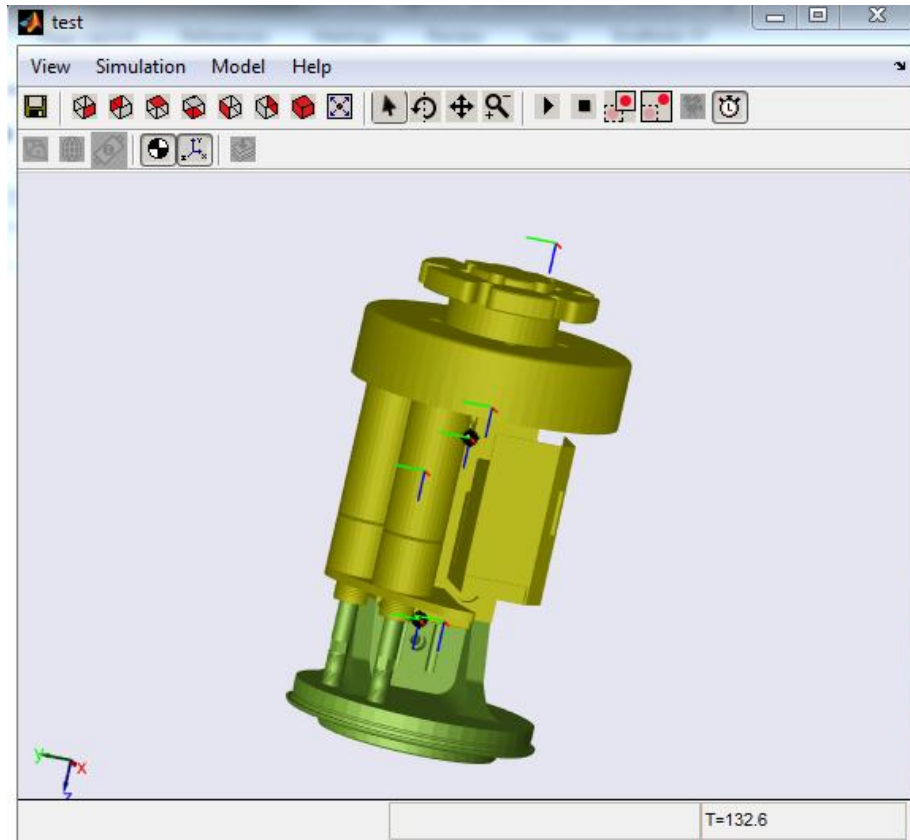
IDC_bottom_part (green)

Fig. 47 Schematic of a visualized system for IDC device.

Because the IDC only obeys vertical translational displacement, thus the prismatic joint is used for connecting between IDC_upper_part and IDC_bottom_part.

61
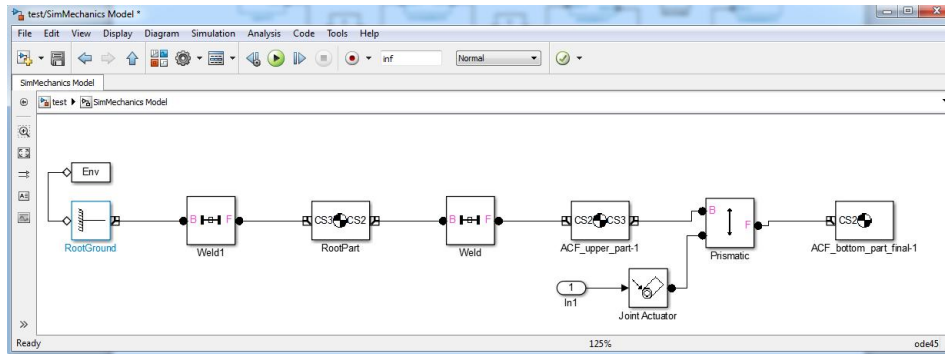
Fig. 48 SimMechanics Model of IDC device.

The translational displacement is generated by motion actuation under affected by position relation, velocity, and acceleration.

3.4 Testing the motion of IDC basing on SimMechanics and MATLAB/Simulink
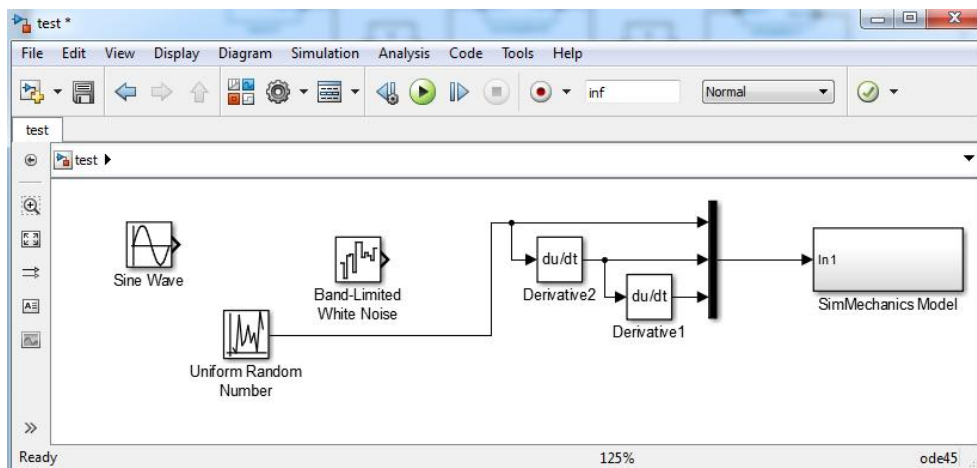
Fig. 49 Matlab/Simulink Simulation of IDC motion.

As mentioned above, the input of SimMechanics model is translational motion. In this simulation, a pseudo-motion signal is built with constraints as the input of SimMechanics model. The motion is displayed in the graphic window as Fig. 47.

On the other hand, the input signal will be generated by Pneumatic System Simulation Model. This model is built based on mathematical modeling of the pneumatic system,

mainly consisting of pneumatic cylinder motion equation, modeling of cylinder chamber and valve system.

The SimMechanics model aims to display the observable motion.

The input signal of SimMechanics model is the output of Pneumatic System Simulation Model. This signal is controllable.

The main problem of the simulation of IDC motion is focused on modeling of IDC full system.

To carry out the testing of IDC signal connecting to PC through cable and Arduino I/O module, a program is built to detect displacement of IDC through position sensor and an acceleration sensor, the pressure of the regulation valve. Basing on experiment result, we compare the simulation result and experiment and modify the simulation program conveniently.

IV. Simulation Modeling, Experimental Investigation for IDC Device's Pneumatic System

4.1 Modeling of the Pneumatic System
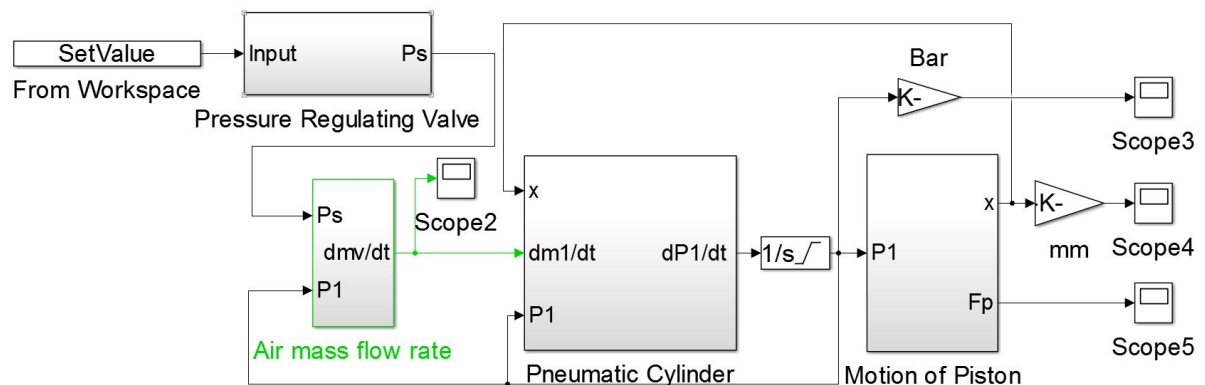
Fig. 50 Simulation diagram of the pneumatic system

The diagram describes the relationship between the motion of the piston, cylinder chamber pressure, flow rate, and the supply pressure of pressure valve.

4.2   Motion of piston

The dynamic equation of pneumatic cylinders system [75]:

$$F_{act} = M\ddot{x} = (p_1 A_1 - p_2 A_2) - Mg \qquad (2.1)$$

Where

x: the position of the piston.

M: total mass of piston and load.

p_1, p_2, A_1, A_2: absolute pressures, effective areas of chamber 1 and 2.

g: gravitational acceleration.

Fig. 51 Block of piston motion

4.3   The pressure of cylinder chambers

As early researches, the thermodynamic model is considered based on three equations of ideal gas law, continuity equation of mass flow and the energy equation.

The ideal gas law of adiabatic process

$$P = \rho RT \tag{2.2}$$

The mass flow rate is determined by the continuity equation
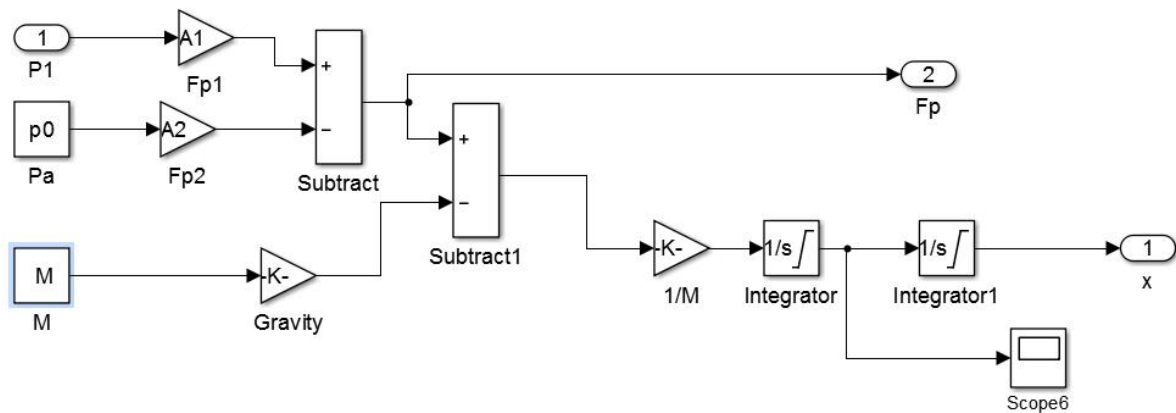
$$m = \rho V \tag{2.3}$$

So, relation P, V, m is:

$$PV = mRT \tag{2.4}$$

On condition of the process occurs without transfer of heat and temperature through all of the system is remained constant. When the piston moves, the mass flow rate, volume, and pressure is varied in the cylinder chamber. Differentiating the equation (2.3):

$$\dot{P}V + \dot{V}P = \dot{m}RT \tag{2.5}$$

Hence,

$$\dot{P}_1 = \frac{RT}{V_i}(\dot{m}_{in} - \dot{m}_{out}) - \frac{P_i}{V_i}\dot{V}_1 \tag{2.6}$$

Where

   R: ideal gas constant.

   T: temperature.

   $\dot{m} = \dot{m}_{in} - \dot{m}_{out}$

   $V_1 = V_0 + A_1 x$

   $V_2 = V_0 + A_2(L - x)$

   i: chamber i of the cylinder.

V_0: inactive volume of cushion chamber.

L: a stroke of the piston.

In this equation, $\dot{m}_{in}$ is outlet flow rate of pressure valve, and $\dot{m}_{out}$ is exhausted air flow rate.

So, an example of chamber 1

$$\dot{P}_1 = \frac{RT}{V_0+A_1x}\left(\dot{m}_p - \frac{\dot{P}_2(V_0+A_2(L-x))-P_2A_2\dot{x}}{RT}\right) - \frac{P_1\dot{x}A_1}{V_0+A_1x} \qquad (2.7)$$
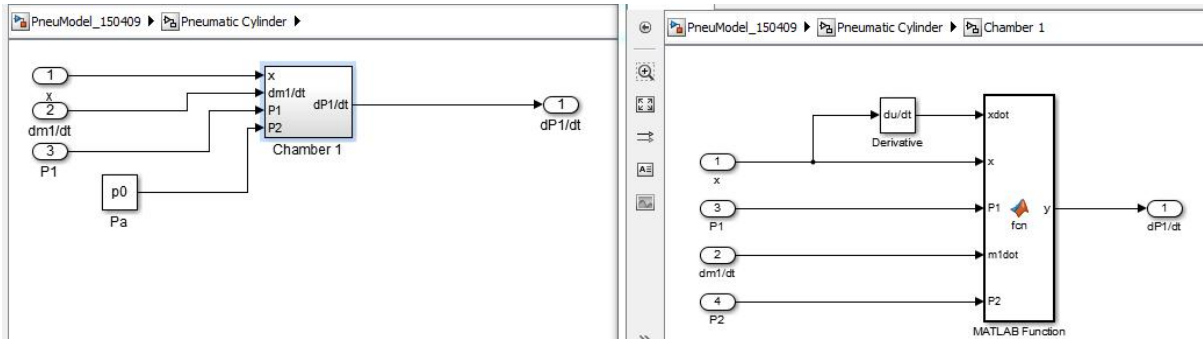
Fig. 52 Block of pneumatic cylinders

Equation (2.7) is the key equation of problem when the displacement is maintained constantly that means the pressure of the chamber is depended on the flow rate of pressure valve. For controlling the constant force, the flow rate must be regulated as constant.

4.4   Piezo-electric pressure regulating valve

The Pre-U pressure regulating valve consists of an internal-regulator inside. This regulator aims to assure the pressure supplied to pneumatic system adopting the desired set-value.

This valve is proposed by using first-order model [76].

$$\frac{C(s)}{R(s)} = \frac{K}{\tau s+1} \qquad (2.8)$$

66

Where K and τ are first order system parameters.

These parameters are calibrated based on simulation process and will be compared with next experiments. In the current experiment, the response pressure is delay about a half second with respect to the input pressure.

Fig. 53 Block of the piezo-electric pressure regulating valve
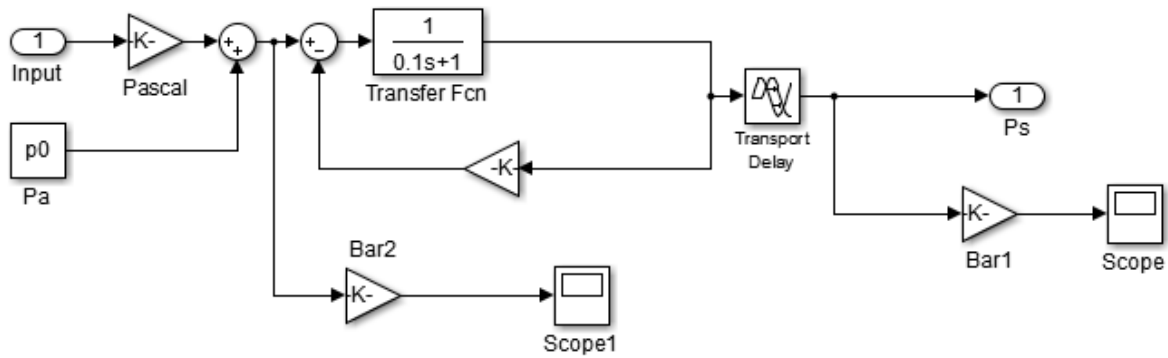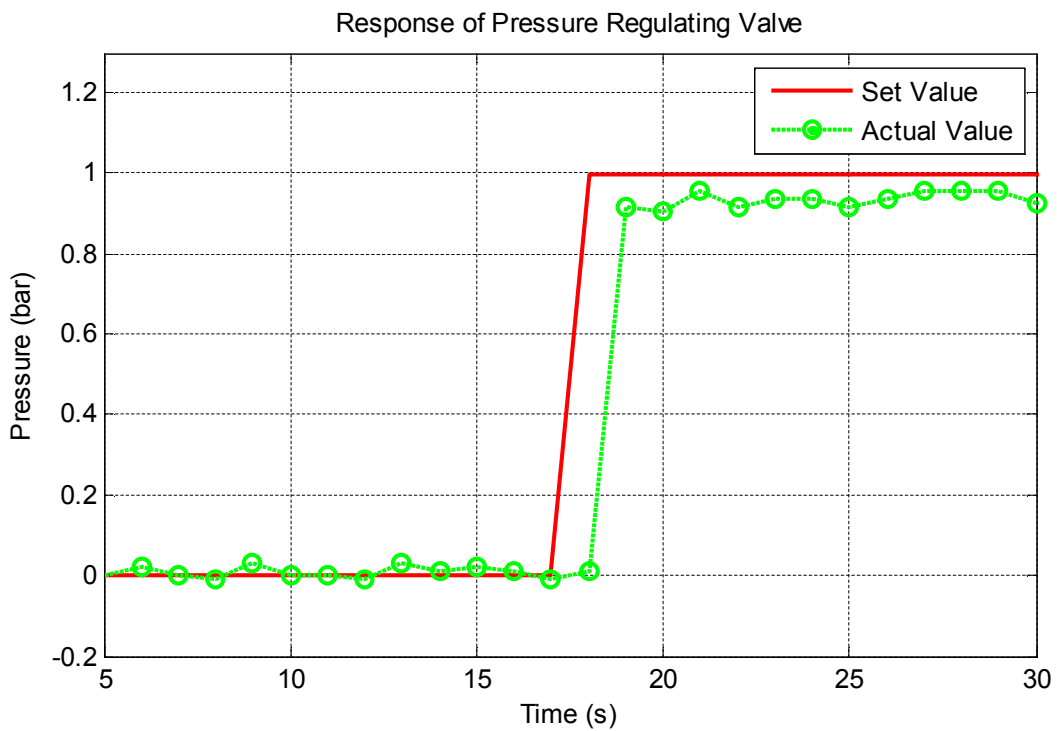

Fig. 54 The response of piezo-electric pressure regulating valve

67

4.5   Flow Rate of Pressure Valve

As abovementioned, with the inlet pressure of cylinder is P_1 and supply pressure P_s is an outlet of pressure valve [77]. The thermodynamic model is obtained from inlet flow rate and the change of cylinder volume. The inlet flow rate is also the flow rate of pressure valve, expressed as follows:

$$\dot{m}_p = \frac{A_s C_s P_s}{\sqrt{RT}} f_r \left(\frac{P_1}{P_s} \right) \tag{2.9}$$

Where, A_s is orifice area of valve and C_s is flow rate coefficient (0.95). And piecewise flow function f_r is:

$$f_r(u) = \begin{cases} \sqrt{\frac{2\gamma}{\gamma-1}\left(u^{\frac{2}{\gamma}} - u^{\frac{\gamma+1}{\gamma}} \right)} & \text{if } u \geq r_c \\ \sqrt{\gamma \left(\frac{2}{\gamma+1} \right)^{\frac{\gamma+1}{\gamma-1}}} & \text{if } u < r_c \end{cases} \tag{2.10}$$

The critical pressure ratio r_c is given:

$$r_c = \left(\frac{2}{\gamma+1} \right)^{\frac{\gamma}{\gamma-1}} \tag{2.11}$$

Where γ is the ratio of specific heats of an ideal gas.

4.6   Experimental Apparatus

In the deburring processing, the robot arm usually works along the vertical direction, the work-piece is put on the horizontal platform, so the IDC Device works along the downward direction. The experimental apparatus is shown in Fig. 55, the IDC Device is mounted on aluminum profiles for testing downward movement, includes the IDC device, a load cell for measuring acting force, I/O Module. And the I/O Module consisting of I/O block and Arduino MEGA 2560, communicated between a

pneumatic system and computer by Matlab/Simulink with Arduino Hardware Support Packages. The air is supplied by a compressor 8.0 bar 2.5 HP.
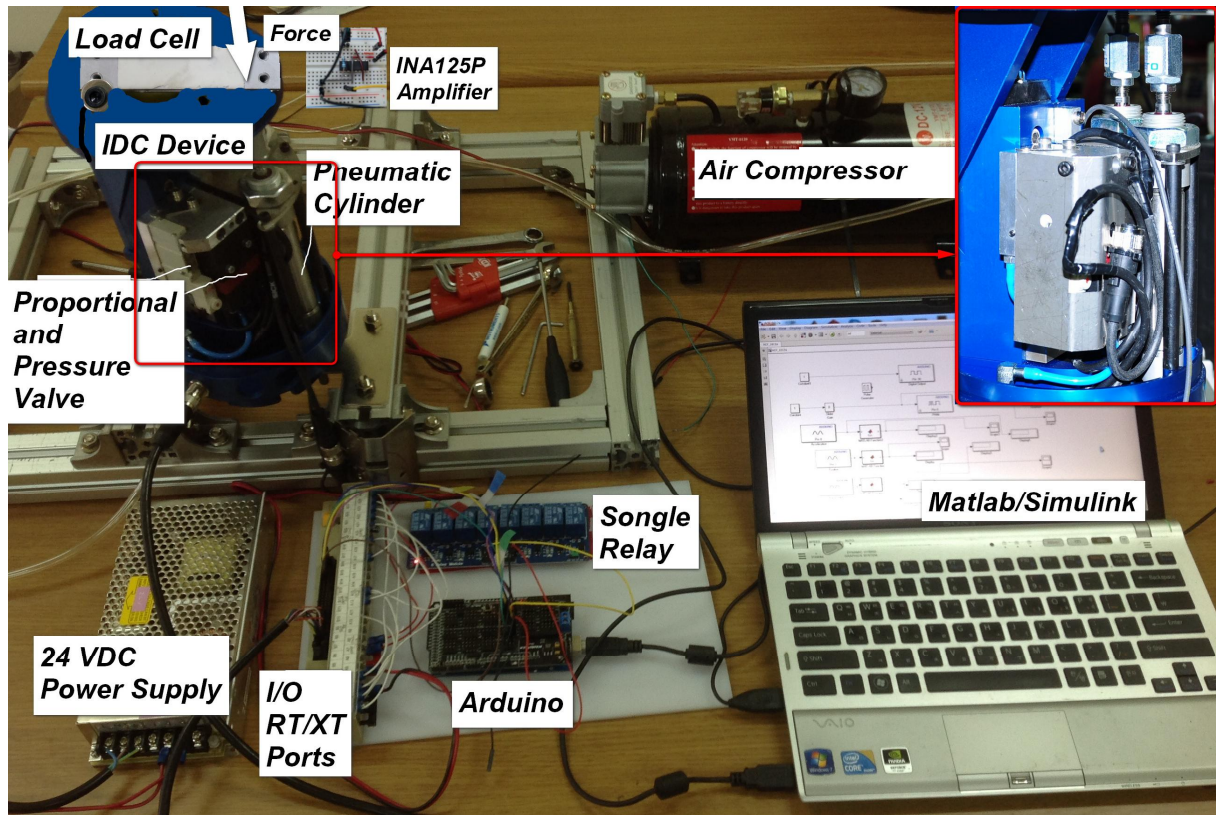
Fig. 55 Experimental Apparatus for Pneumatic System

As above-shown, for controlling the upward or downward of double acting cylinders, the 2 positions 5 ways on/off solenoid valve is used. And the on/off state of the solenoid valve is switched by a Songle relay. The stroke of the piston is measured by a magnetic position sensor, the acceleration sensor is used for measuring the orthogonal acceleration of IDC device as a contact state. The piezo-electric pressure valve is controlled by turning set value and feedbacks the actual value to PC. The set value is 0-10 VDC (0-8 VDC for IDC), is set by a 0-5V PWM module of Arduino and a first-order RC circuit. The actual value is connected to Arduino by a linear voltage conversion circuit for converting 0-10 VDC (1.25-6.25 VDC for IDC) to 1-5 VDC. The load cell 50 kg capacity, 2.0 mV/V output rate is connected the Arduino through an INA125P amplifier and 100 Ohm resistance (121 Ohm as an assumption). The

69

Arduino is connected to Matlab/Simulink for receiving and transmitting signals. The calibration process is shown in the appendix section. All data are imported into the workspace.
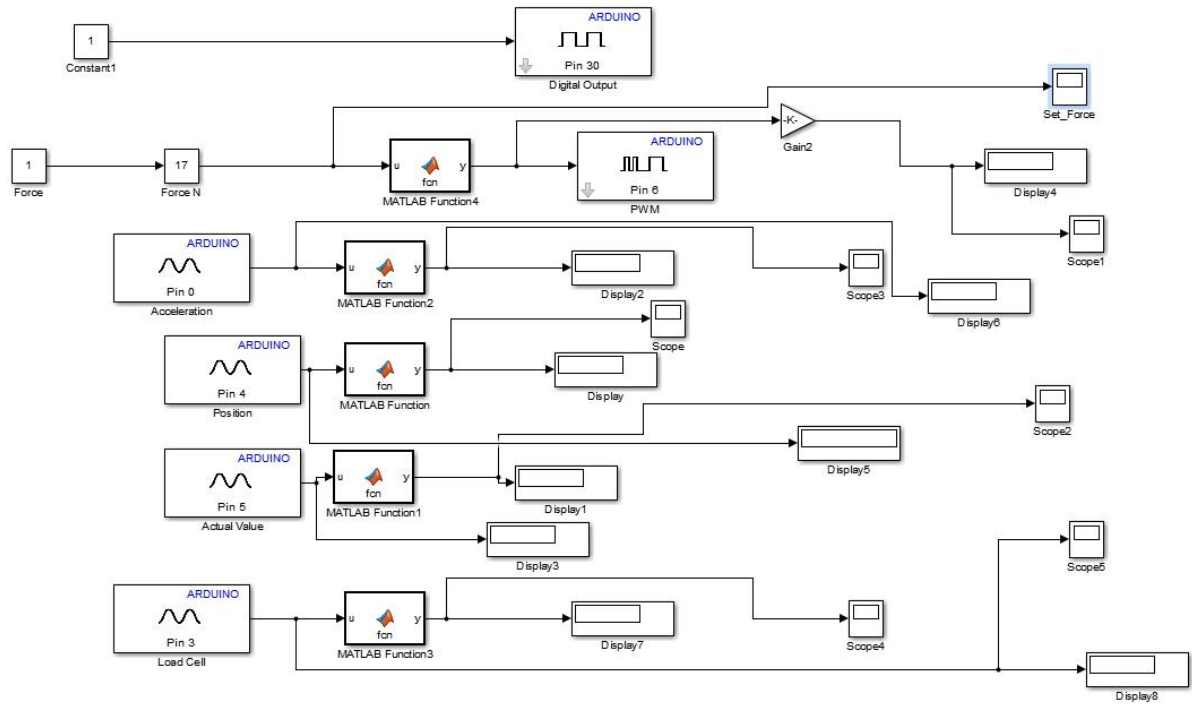
Fig. 56 Simulink program for receiving and transmitting the signals for IDC Device

After calibrating load cell parameters using Origin 8.0, the experiment obtained results as below:
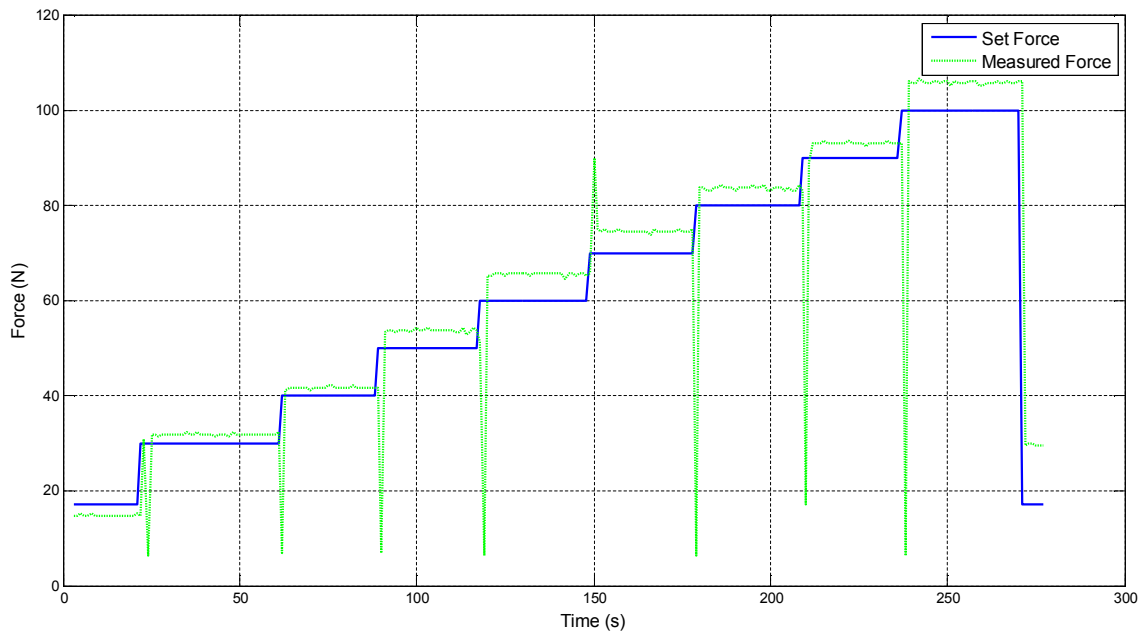
Fig. 57 Set Force and Measured Force of IDC Device
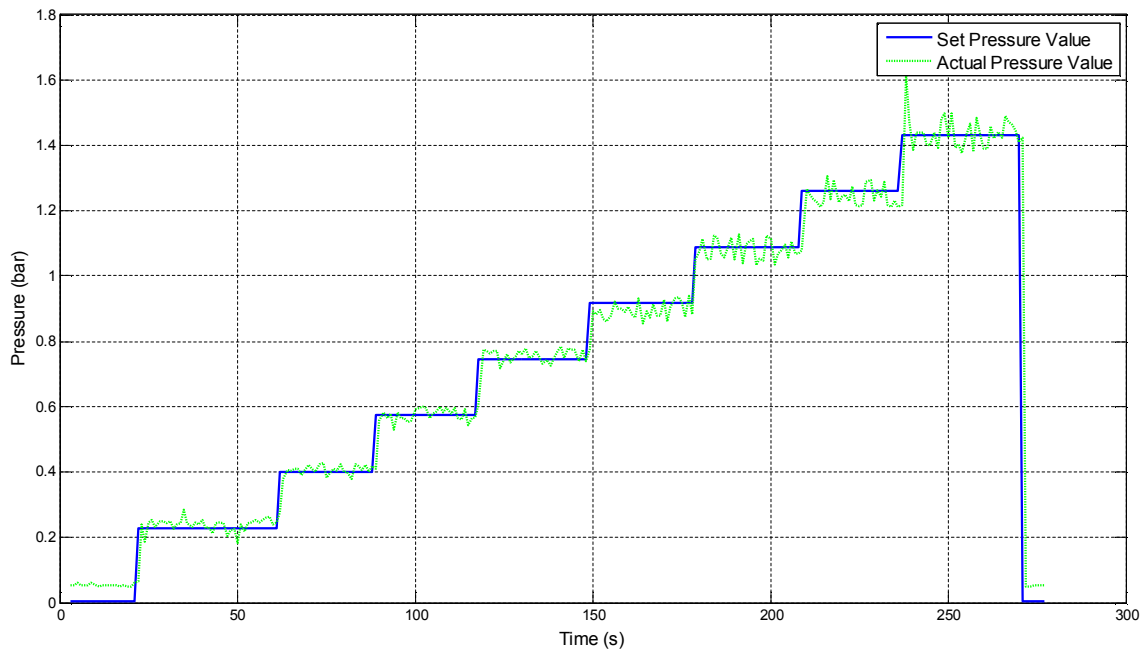
Fig. 58 Pressure responses of the pressure regulating valve

71
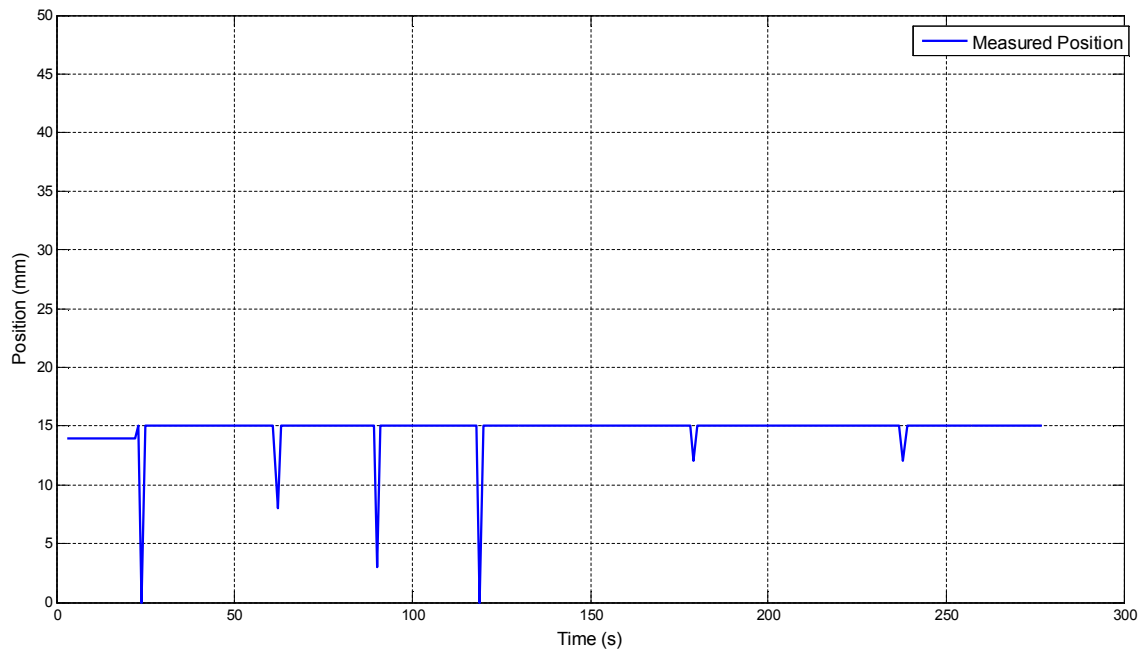
Fig. 59 Stroke of piston

4.7   Simulation and Experimental Results

As abovementioned, the modeling of the pneumatic system describes the linkages of the force, displacement of the piston, the pressure of cylinder chambers, supply pressure and flow rate of pressure valve in mathematical relations. These relations are carried out by each MATLAB/Simulink block respectively. In addition, the experimental parameters are also restored on the workspace of MATLAB. In this simulation, the identical input signal of real apparatus is applied to the simulation model and making the comparison between the simulation modeling and experiment apparatus.

As known, the double acting cylinder can move extension and contraction, but this simulation just considers the extension of the piston with respect to acting force, chamber pressure and parameters of the pressure regulating valve.

The general simulation model is shown in Fig. 50, the input signal of pressure valve is imported via the set value of the testing model. The set value is generated in two cases,

72

case 1: a step-like signal for estimating the response of acting force and the effect of supply pressure in a single period, and case 2: a stairstep with 3 levels for testing the alternative response of acting force.

This simulation aims to evaluate the math modeling with respect to experiment processing.

4.8   Case 1: Response of Step-like Input Pressure

This case aims to describe the response of acting force on the surface when input pressure is constant.

The first step, the experiment is carried out for collecting the input and response signals of the pressure regulating valve as a step-like signal and import these values into the simulation program. The responses of simulation and experiment are deflected. This deflection is existed by the difference of Arduino delay and Simulink delay setting. As shown below, the case 1 mentions the simple operation of the system when the 1.8 bar input pressure is supplied. The set value is established for triggering regulation valve, the actual value is output signal of the regulation valve, the magnetic position sensor detects a stroke of the magnetic piston and acting force is measured by load cell 50 kg 2.0 mV/V.

Fig. 60 The pressure of regulation valve with step input
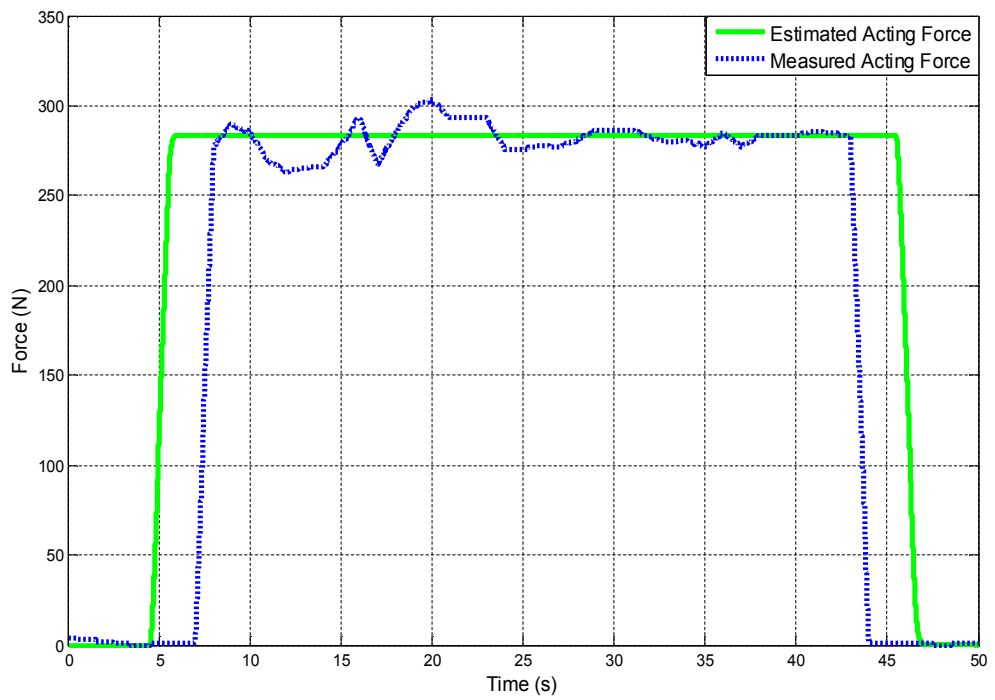
Fig. 61 The acting force of cylinder with step input
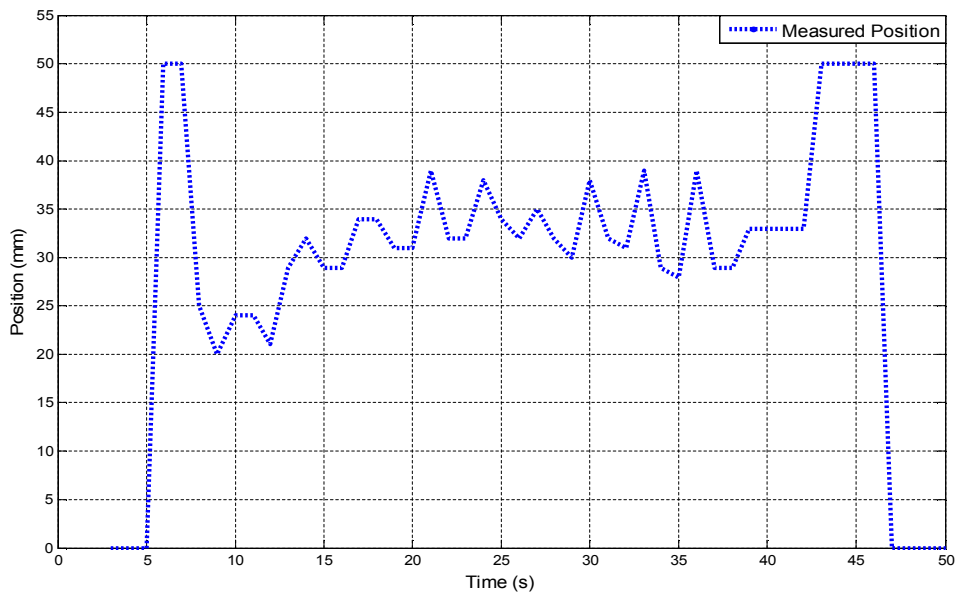
Fig. 62 Stroke of the piston with step input

When pressure input is constant, the acting contact force is also constant. The deviation of piston displacement between simulation and the real cylinder is occurred because of delay signal when using Arduino I/O Module.

4.9   Case 2: Response of System with Stairstep Signal

The principle of IDC device is the control of the constant acting force when the robot arm works on the work-piece surface. To maintain such acting force, a pressure valve with built-in electronic control board is used for regulating the input pressure of the pneumatic cylinder.

The desired value of pressure is set as stairstep signal and its actual response is shown in Fig. 63.
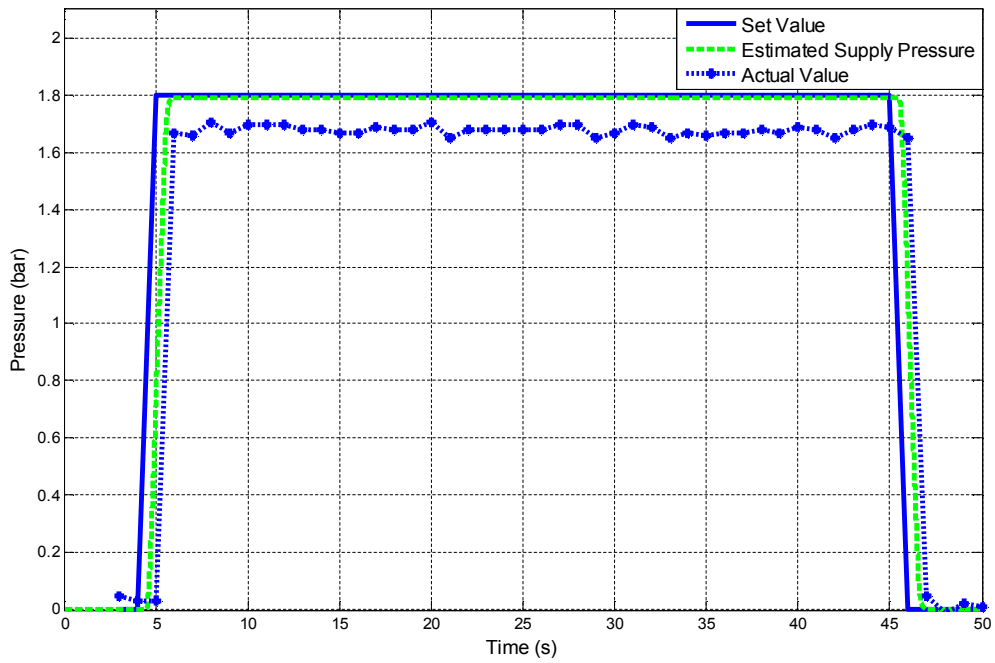
75
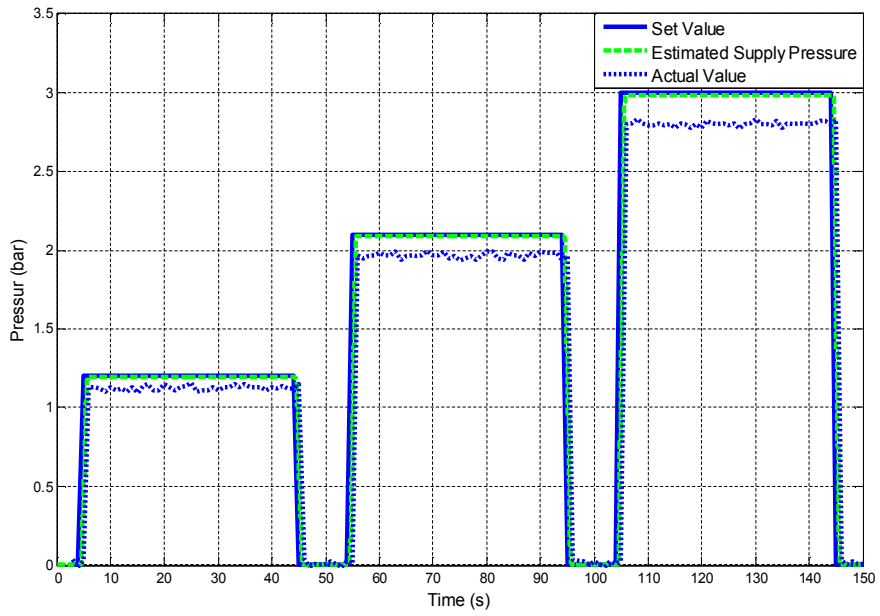
Fig. 63 The pressure of regulation valve with stairstep input.
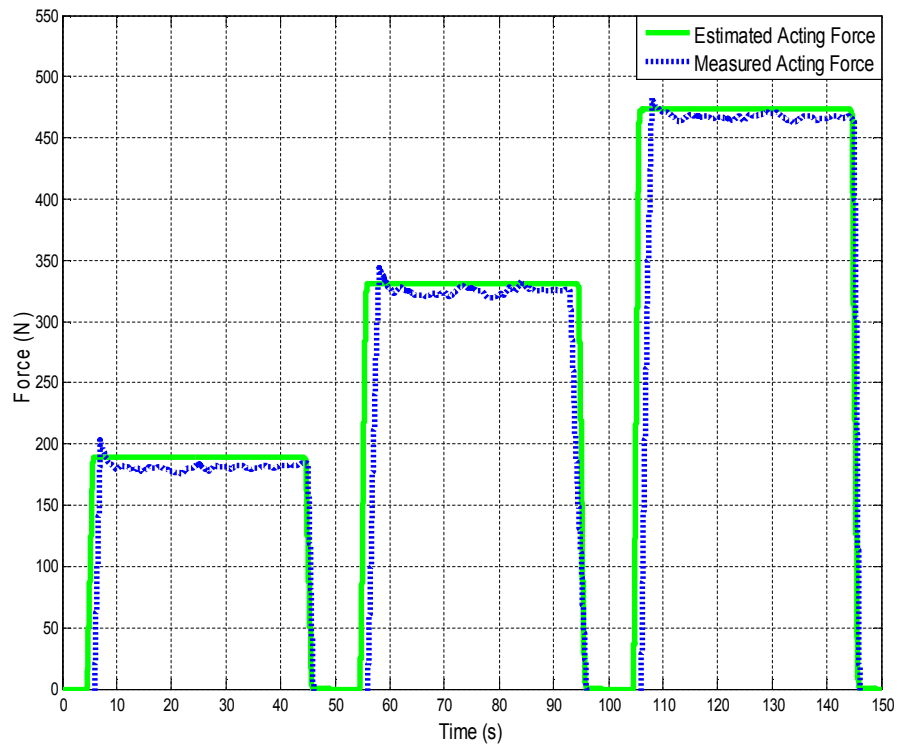
Fig. 64 The acting force of cylinder with stairstep input.
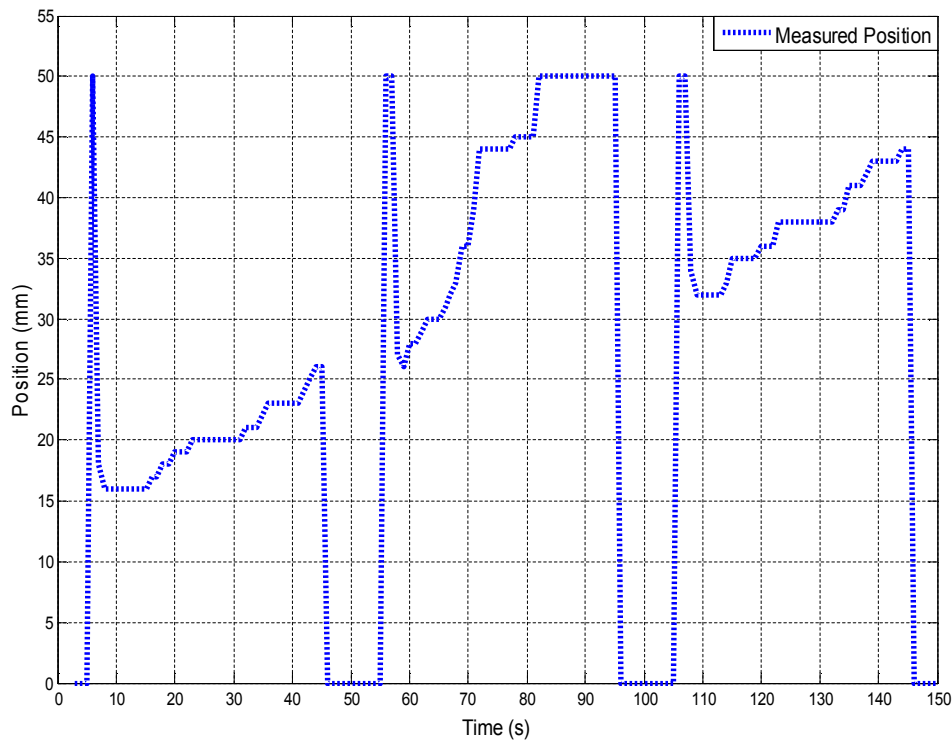
Fig. 65 Stroke of the piston with stairstep input.

The acting force also responds as stairstep signal respect to supply pressure at about 1.2, 2.1 and 3.0 bar respectively, such response ratio is almost regular. The average measured value of load cell is suitable with the response of estimated acting force. However disadvantage that the measured data are not as good as expected, the results are variant form because the measured signals are affected by the noises of load cell connections and the manual reactions.

In this chapter we considered a mathematical modeling of the pneumatic system included double acting pneumatic cylinder, pressure regulating valve and on/off solenoid valve. The position is measured by a magnetic position sensor, and the acting force is measured by additional load cell connected to Arduino through an INA125P amplifier of Texas Instruments. This model uses the thermodynamics and air flow rate through pressure valve combined with modified feedback linearization in MATLAB/Simulink. The results of the simulation are compared to the experiment

results with step-like and stairstep input signal for acting force response. And then for the more checking response of such system modeling with variable external force and constant desired acting force, the results show acting force is kept constant and the position is varied when acting a manual force. Through that, we can control the constant contact force by regulating the input pressure respectively. So that without chamber pressure sensor, this model can be used to estimate the acting force. For more accurate observation, the noises of load cell force sensor should be treated. Basing on above simulations, such model can be used to develop performance force control algorithm for applications in robotics and automation.

CHAPTER IV FORCE CONTROL FOR

DEBURRING ROBOT USING POSITION

ERROR-BASED IMPEDANCE

CONTROL MODEL

As known, the study on the interaction between the robot and its environment has an important role for industrial tasks using the robotic application. In this topic, the interaction is studied for surface processing. These applications require the contact between the robot tool and the environment or the tool must penetrate into the environment.
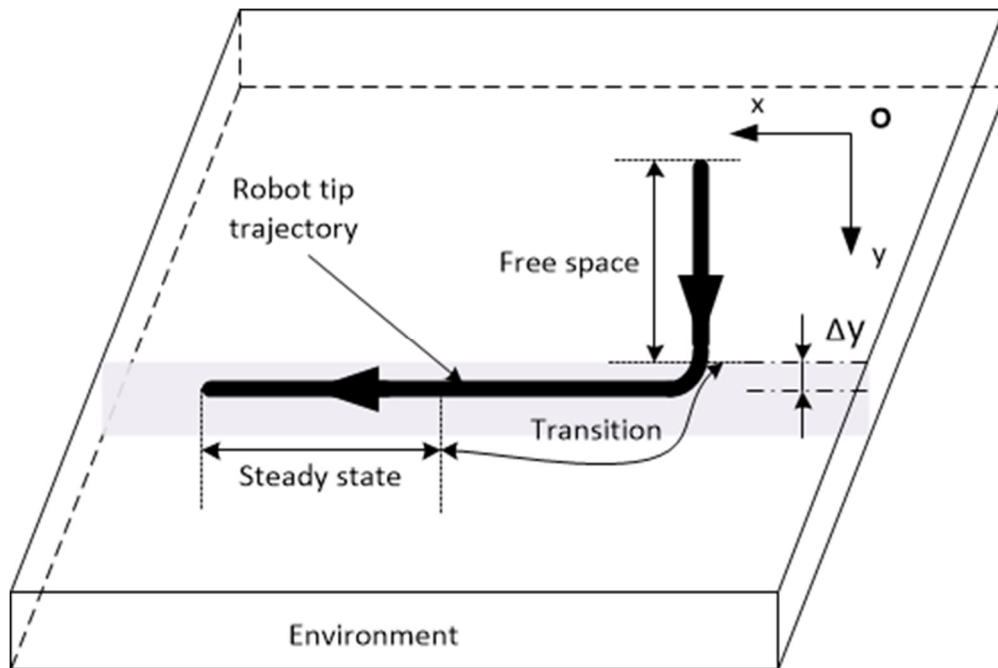
Fig. 66 Motion mechanism of the deburring robot.

The penetration motion of robot consists of free space motion, the transition of motion and contact motion [78]. The trajectories of robot's end-effector are analyzed in three states such as free space motion, transient motion from the free space state to the steady state. The transient motion also could be generated when the tool contact with the burrs on the workpiece. Moreover, each workpiece it possesses a specific material, so it required the pertinent contact force for the different type of product which is decided by its manufacturer. The problem is issued that how to control the pertinent contact force by using the motion of robot [79]. As aforementioned, the pertinent force is also affected by the transient and contact motion of the robot. In this chapter, the transient motion and transient force, the unification of force and motion, and the impedance control for pertinent force control are studied.
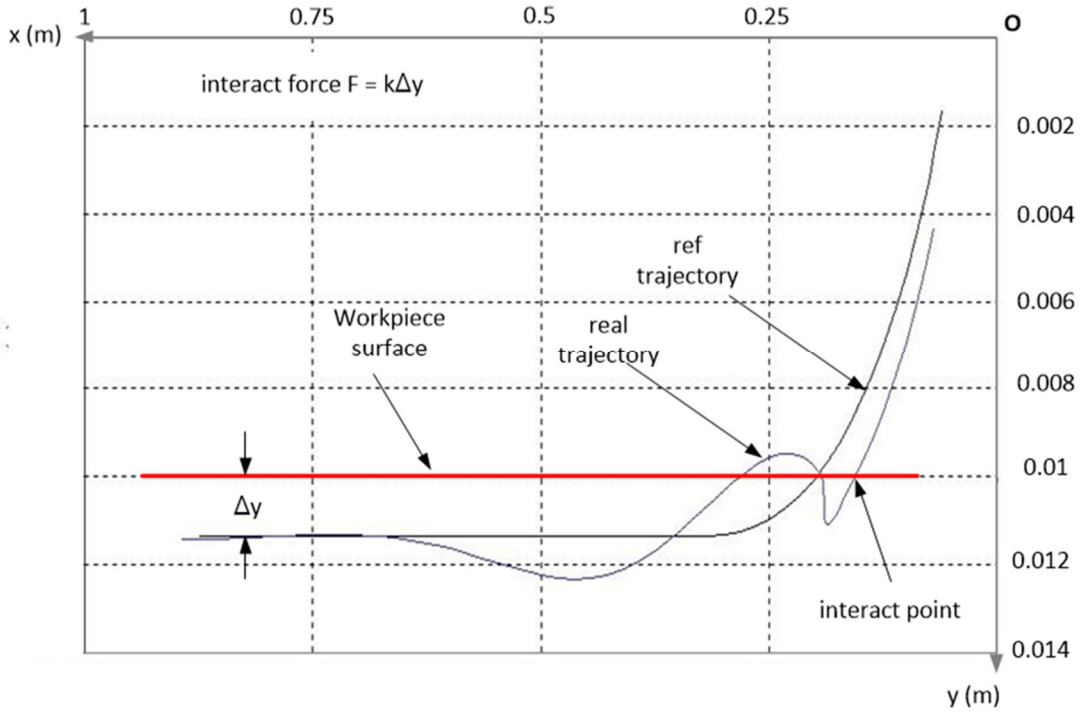
Fig. 67 Estimation of robot's motion in the XY coordinate

I.   Transient processes of motion and force.

To describe the transient process of robot motion, the penetration $\eta(t)$ is defined as the deviation between the workpiece surface position $z(t)$ and programmed motion of robot end-effector $z_p(t)$. The characteristics of transient motion [80] are determined by the continuous function P as:

$$\ddot{\eta} = P(\eta, \dot{\eta}) \tag{3.1}$$

 The such function is defined to get stability of robot motion with the initial position and velocity of the inherent robot. The P function is a function of vectors of motion deviation and deviation rate with respective constant matrices Γ_1 and Γ_2, so the motion deviation differential equation are:

$$\ddot{\eta} = \Gamma_1 \dot{\eta} + \Gamma_2 \eta \tag{3.2}$$

The equation (3.2) can be transformed to the system of second order:

81

$$\dot{w} = \Gamma_\eta w \tag{3.3}$$

Where $w = \begin{bmatrix} \eta \\ \dot{\eta} \end{bmatrix}, \Gamma_\eta = \begin{bmatrix} 0_2 & I_2 \\ \Gamma_2 & \Gamma_1 \end{bmatrix}$.

The main target is that the actuation force is expected to be stable so the robot motion is expected to be stable simultaneously. Analogously, the force deviation is symboled as μ(t) [81] which is described as equation (3.4).

$$\ddot{\mu} = Q(\mu, \dot{\mu}), \mu(t) = F(t) - F_p(t) \tag{3.4}$$

Where μ is force deviation between measured force F and programmed force F_p. The function Q is a continuous function which is derived from transient motion and dynamic modeling of robot.

In which, the force is considered as the function of robot motion:

$$F(t) = f(z(t), \dot{z}(t), \ddot{z}(t)) \tag{3.5}$$

The actual force F(t) which robot acts on the environment or reaction of the environment to the robot with the initial conditions at $z(t_0) = z_0$ and $\dot{z}(t_0) = \dot{z}_0$.

When the robot contacts to the environment, the robot motion will be controlled to be stable long desired trajectory z_p and the interaction force reaches the desired force $F_p(t)$, in which the $F_p(t)$ satisfies:

$$F_p(t) = f(z_p(t), \dot{z}_p(t), \ddot{z}_p(t)) \tag{3.6}$$

The control target of the interaction control is to maintain the actual force and robot motion simultaneously satisfy the stability:

$$z(t) \rightarrow z_p(t) \ as \ t \rightarrow \infty, F(t) \rightarrow F_p(t) \ as \ t \rightarrow \infty \tag{3.7}$$

II. Unified approach for synthesizing the stability of robot motion and actual

force

In general, the control law is synthesized by stabilizing the robot motion and interaction force simultaneously. The control law possesses exponential stability of closed-loop systems and ensures the preset quality of transient processes of motion and interaction force. This section uses the exponential stability theorem [82] for both motion and contact force. Force adapting such stability, the initial conditions and transient processes of motion and force need to be set to correspond with control laws. The control law, derived from dynamic modeling and stabilizing synthesis of transient processes, is applied for the robot closed-loop dynamic model:

$$\tau = H(z)\left[\ddot{z}_p + P(\eta, \dot{\eta})\right] + h(z, \dot{z}) - J^T(z)F \tag{3.8}$$

2.1 Dynamic Modeling of Robot Interacting with Dynamic Environment

The dynamic model of the robot [83] is expressed:

$$H(z)\ddot{z} + h(z, \dot{z}) = \tau + J^T(z)F \tag{3.9}$$

Where

H(z): the matrix of inertia moments of the robot mechanism

$h(z, \dot{z})$: the nonlinear function of centrifugal, Coriolis and gravitational moments

τ: the vector of the input control.

J^T(z): Jacobian matrix.

F: the actual force.

Assuming that the matrix $H(z)$ is invertible, the dynamic equation can be rewritten in the form of higher order differential equation:

$$\ddot{z} = H^{-1}(z)[-h(z, \dot{z}) + \tau + J^{T}(z)F] \tag{3.10}$$

Or

$$\ddot{z} = \Phi(z, \dot{z}, \tau, F) \tag{3.11}$$

Which satisfies the initial conditions $z(t_0) = z_0$ and $\dot{z}(t_0) = \dot{z}_0$.

If the control law is defined by a function of robot motion and interaction force, the dynamic model of the robot can be solved with the control law τ:

$$\tau = U(z, \dot{z}, \ddot{z}, F) \tag{3.12}$$

Where

$$U = H(z)\ddot{z} + h(z, \dot{z}) - J^{T}(z)F$$

2.2 Dynamic Modeling of Environment

In the case of contact task, the motion of the robot is constrained by workpiece surface. In which, the precision of motion is required rather than the accuracy of the contact force. Actually, the reaction force is influenced not only by the robot's motion, but also by the cause of the workpiece specification. So the dynamic environment modeling is considered through the position, velocity and acceleration of robot and the reaction of the environment [84].

$$[M(z)\ddot{z} + L(z, \dot{z})] = S^{T}(z)F \tag{3.13}$$

Where

$M(z)$: mass matrix.

$L(z, \dot{z})$: dynamic function.

S(z): Jacobian matrix.

So, the force is described as a continuous function of position, velocity, and acceleration of robot motion [85]:

$$F = f(z, \dot{z}, \ddot{z}) \tag{3.14}$$

In the contact processes, the stability of actual force and stability of robot motion are coherent in the unified force/position approach. In this method, the motion deviations and force errors are:

$$\eta(t) = z(t) - z_p(t) \tag{3.15}$$

$$\mu(t) = f\left(\eta + z_p, \dot{\eta} + \dot{z}_p, \ddot{z}_p + P(\eta, \dot{\eta})\right) - f(z_p, \dot{z}_p, \ddot{z}_p) \tag{3.16}$$

When applying such method for the surface processing, the product performance is qualified when the actual force is stable and the robot motion is stable too. In   which, the variation of interaction force μ(t) depends on the function f which determines the model of environment dynamics basing on transient process characteristics of motion P, motion deviation $\eta, \dot{\eta}$ and predefined trajectory $z, \dot{z}$. Due to the property of the robot's function P, which ensures the asymptotic stability of the system as a whole with respect to motion deviation and speed deviation [86], we can obtain:

$$\eta(t) \xrightarrow{t \to \infty} 0 \text{ and } \dot{\eta}(t) \xrightarrow{t \to \infty} 0 \tag{3.17}$$

And, because P is continuous function and P(0,0) = 0, it leads to:

$$\ddot{\eta}(t) \xrightarrow{t \to \infty} 0 \tag{3.18}$$

The dynamic environment model is defined by continuous function f, so:

$$\mu(t) \xrightarrow{t \to \infty} 0 \tag{3.19}$$

Thus, the control goal is achieved when the robot motion approaches to the desired motion and simultaneously the reaction force approaches the desired force between the robot and workpiece.

III.   Application of Unified Approach for the 2-DOF sliding joint manipulator
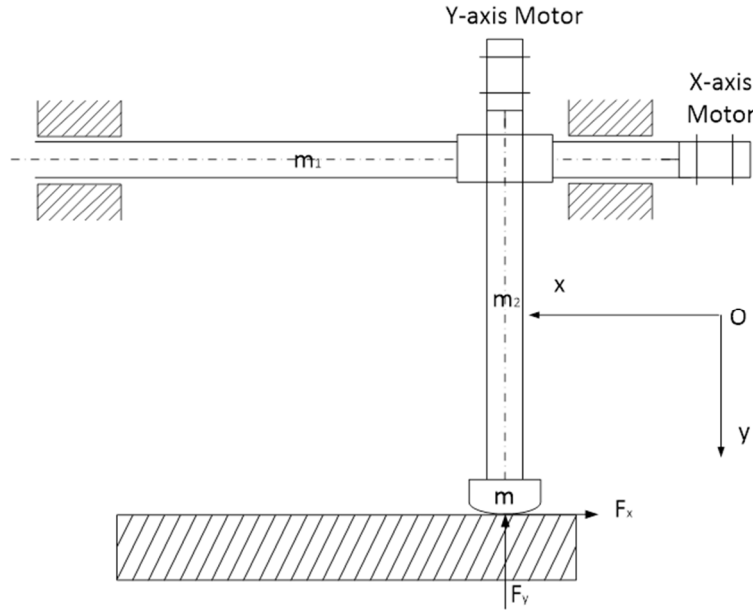
Fig. 68 The deburring robot works on the planar workpiece.

In the application of interaction control method, the 2-DOF sliding linear modules, the one axis moves the processing tool vertically and another one moves the workpiece horizontally. Supposing m_1 and m_2 are an inertial mass of the horizontal x-axis and the vertical y-axis. The experimental robot dynamics modeling [87] is described:

$$(m_1 + m_2)\ddot{x} = \tau_x - F_x \tag{3.20}$$

$$m_2\ddot{y} = \tau_y - F_y \tag{3.21}$$

The continuous function of vertical interaction force F_y is a sum of the inertial, friction and elastic terms in y-axis:

$$F_y = m_y \ddot{y} + h_y \dot{y} + K_y y \tag{3.22}$$

Along x-axis, F_x is the sum of inertial, friction terms:

$$F_x = m_x \ddot{x} + h_x \dot{x} + \nu F_y sign(\dot{x}) \tag{3.23}$$

For maintaining the constant interaction force, the desired interaction force along the y-axis is set as constant.

$$F_{y_p}(t) = F_y^0 = F^0 = const$$

And the x-axis linear module is driven with constant velocity $\dot{x}_p(t) = V_0$, $x_p(t) = V_0 t$.

Therefore the complement force F_x and motion y(t) are obtained: $F_{x_p}(t) = h_x V_0 + \nu F^0$ and $y_p(t) = F_0/K_y$.

The closed-loop based on control law:

$$\ddot{\eta}_x + 2\zeta_x \omega_x \dot{\eta}_x + \omega_x^2 \eta_x = 0 \tag{3.24}$$

$$\ddot{\eta}_y + 2\zeta_y \omega_y \dot{\eta}_y + \omega_y^2 \eta_y = 0 \tag{3.25}$$

In which, η_x, η_y are motion deviation between the real motion and programmed motion along x-axis, y-axis respectively. To examine the response of interaction control of motion and actuation force we analyze the stabilization of deviation of motion and actuation force in (3.24-25).

To analyze the stabilization of such deviations, we use Laplace transform to transform from the time domain to s-space.

The equation (3.24) can be rewritten as below, the same case for equation (3.25).

$$H(s) = \frac{\eta_x(0)s + (\dot{\eta}_x(0) + 2\zeta_x \omega_x \eta(0))}{s^2 + 2\zeta_x \omega_x s + \omega_x^2} \tag{3.26}$$

So the system has two poles and one zero. The root locus method is used to analyze the basic characteristics of the transient response of a closed-loop system is closely related to the location of poles and zeros. The trivial solution of zero is $s_0 = -2\zeta_x\omega_x - \frac{\dot{\eta}_x(0)}{\eta_x(0)}$ and solutions of poles are $s_{1,2} = -\zeta_x\omega_x \pm \omega_x\sqrt{\zeta_x^2 - 1}$. The problem is now considered as a simple second-order system. Assuming that the frequency ω_x is positive constant, on the imaginary and real of complex number coordinate frames, the locus of zeros is the line on the horizontal axis. The locus of poles is displayed as Fig. 69. The ramping ratio ζ is varied from -∞ to +∞. The radius of center circle depends on value of frequency ω. The response of system is stable when the root locus lies on left side of imaginary axis, so the ramping ratio should be chosen is from zero to positive infinity, the system response is in the transient process.
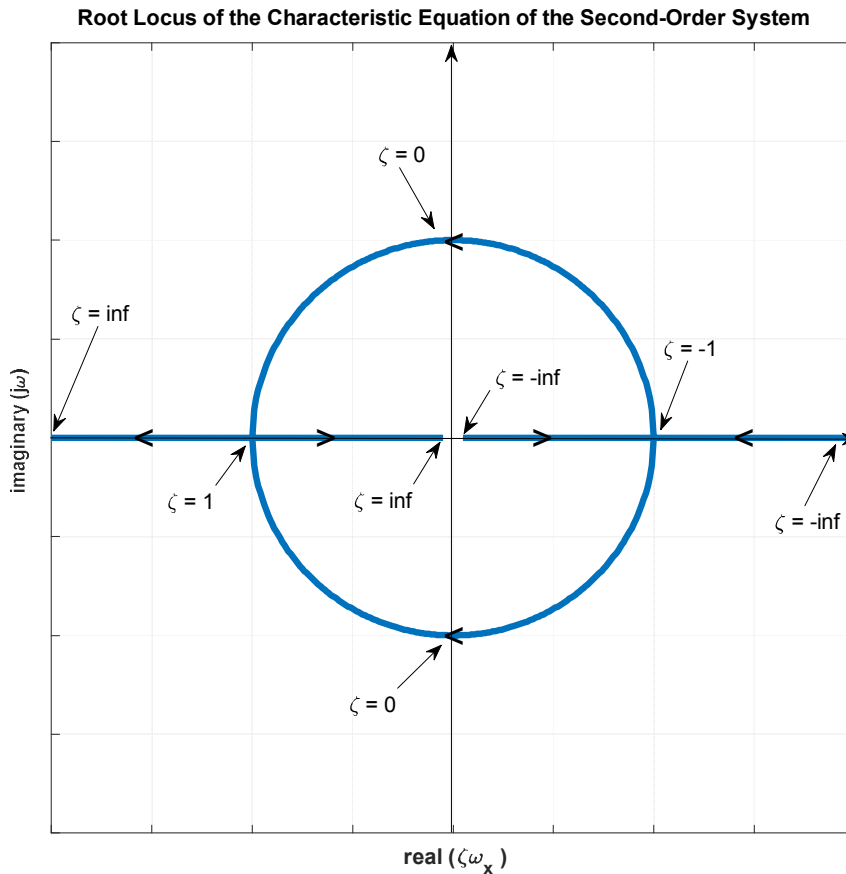
Fig. 69 Root Locus of poles.

Through some tests, the responses are acceptable if the damping ratio is in zero and one, the steady state is reached earlier following the variation of frequency ω.

 The closed-loop root locus of such controller with $\zeta = 0.7, \omega = 2$:
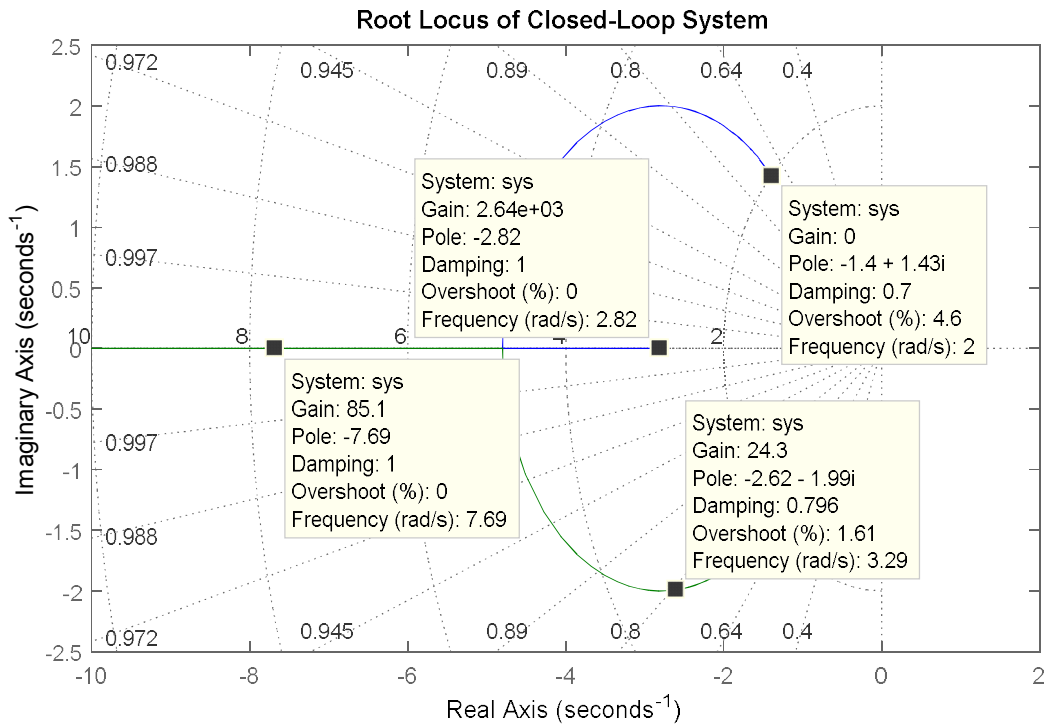
Fig. 70 Root Locus of assumed motion

Basing on the above root locus, we can do tuning the damping ratio and frequency to get the best responses for desired interaction control design [3].

As for our test, the simulation responses of proposed mechanism [88] are shown in Fig. 71:

(a)

(b)

(c)

(d)

(e)

(f)
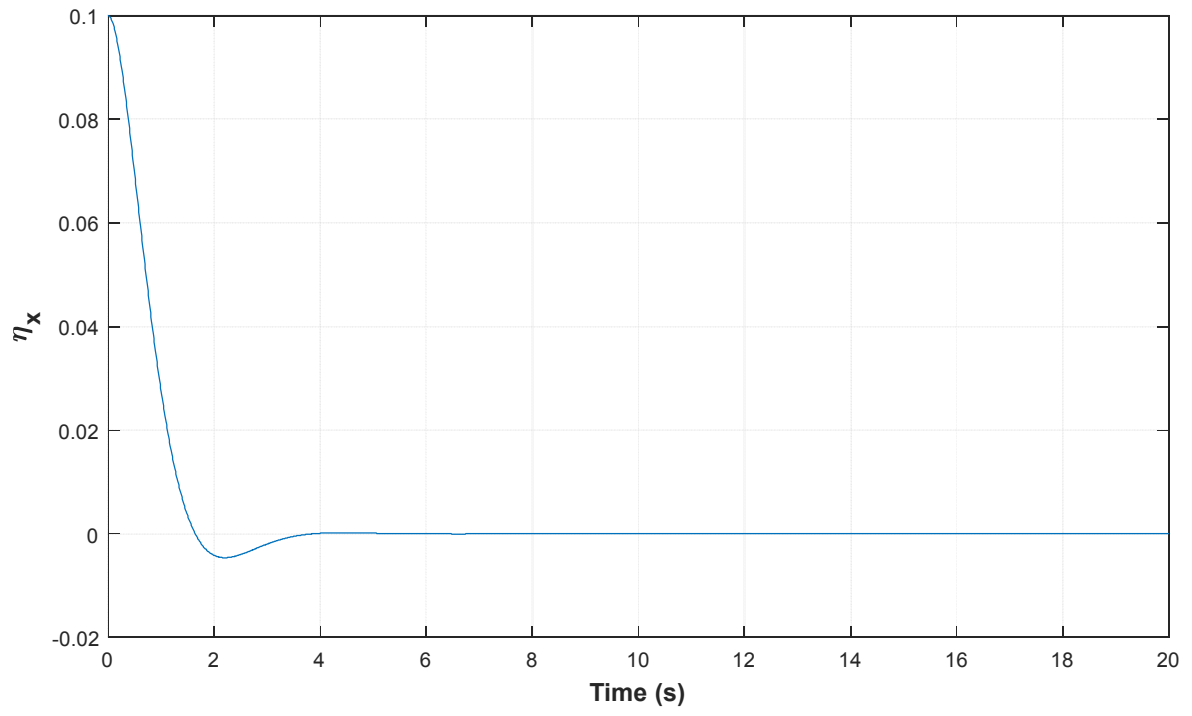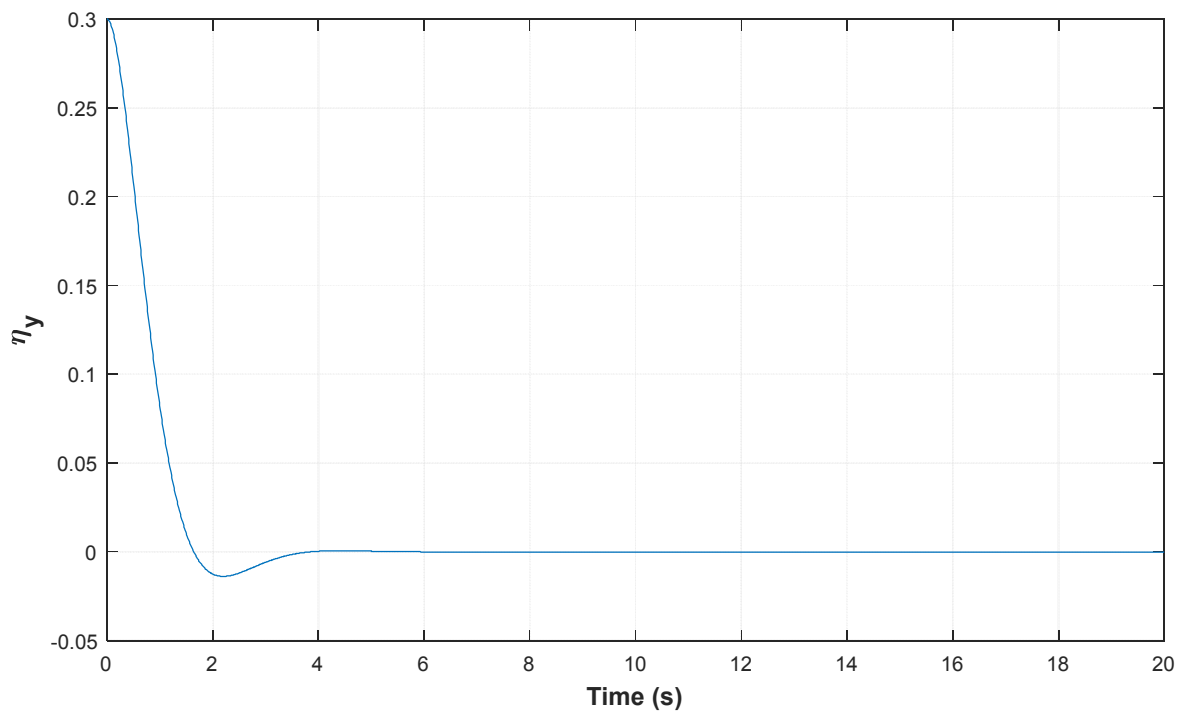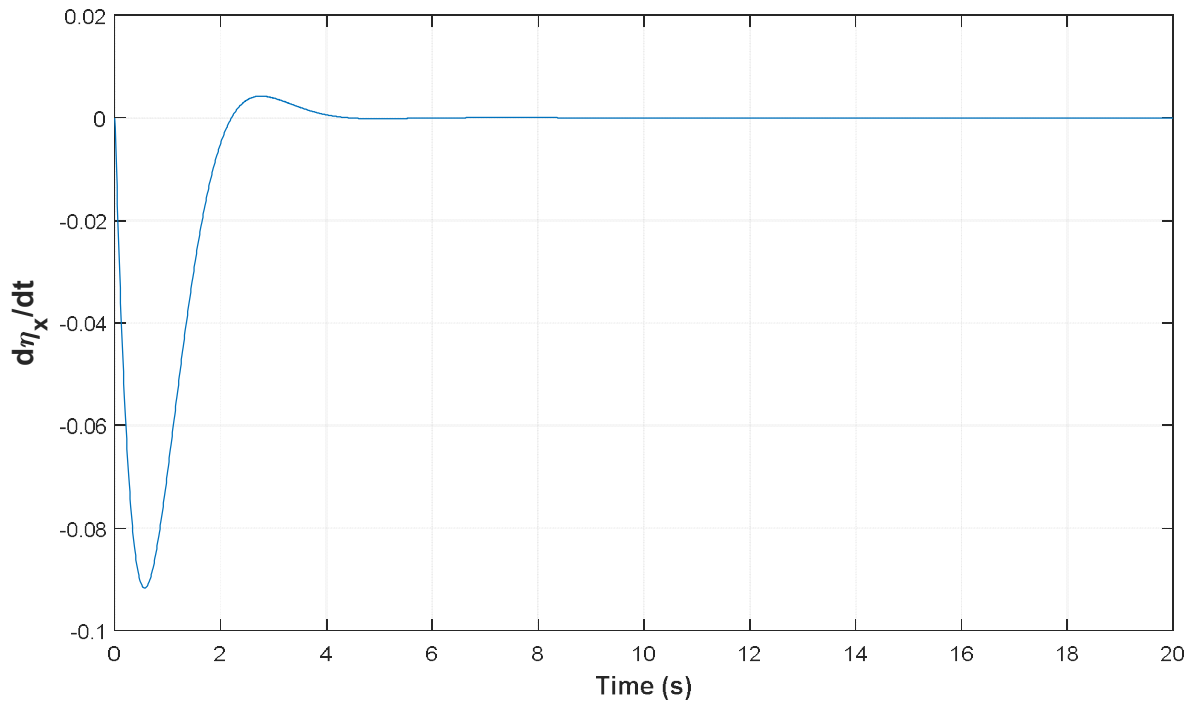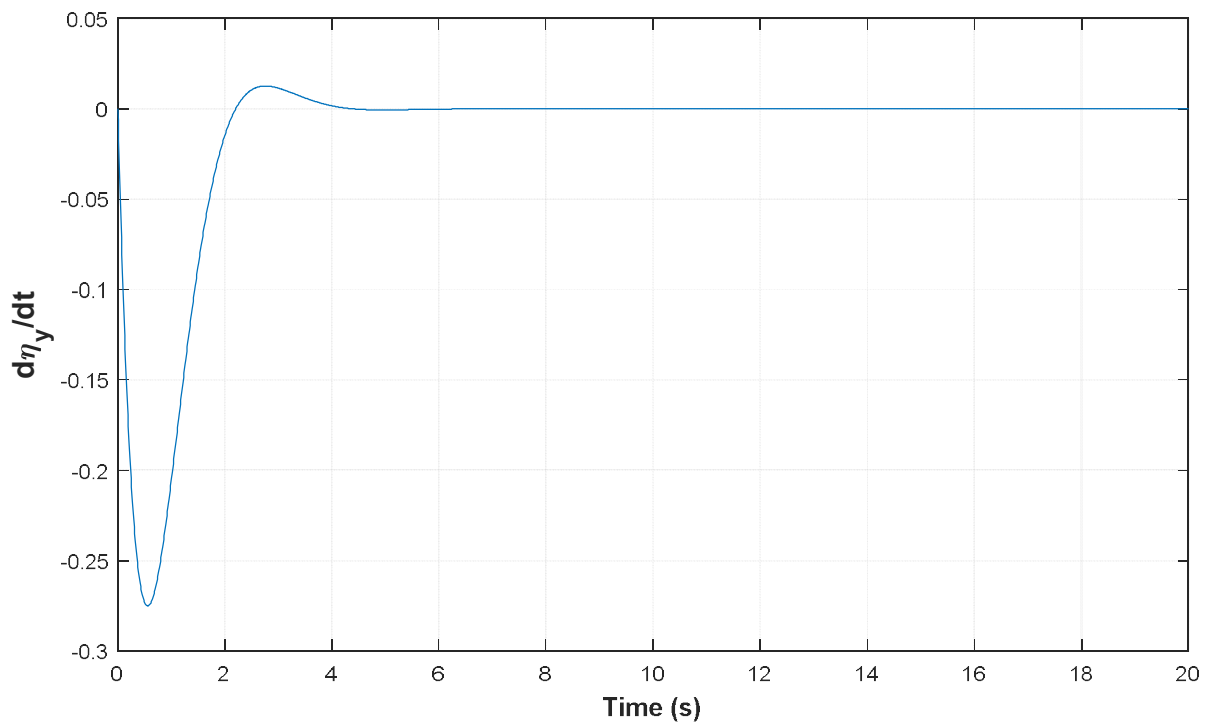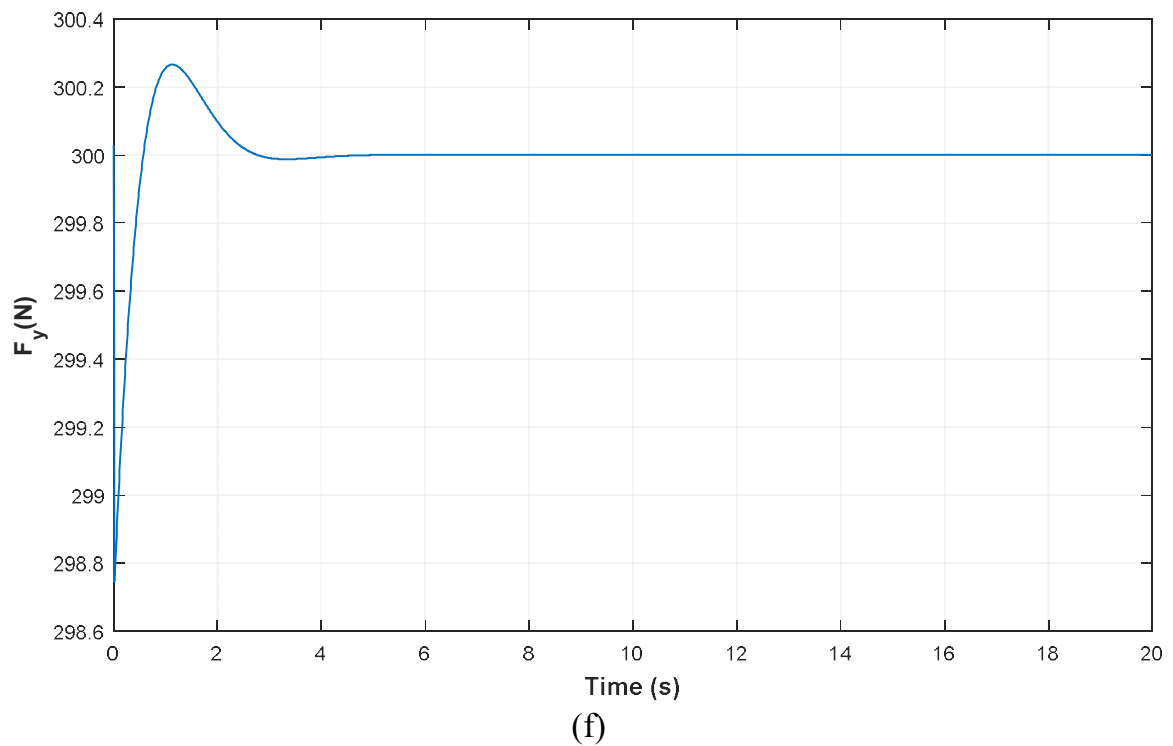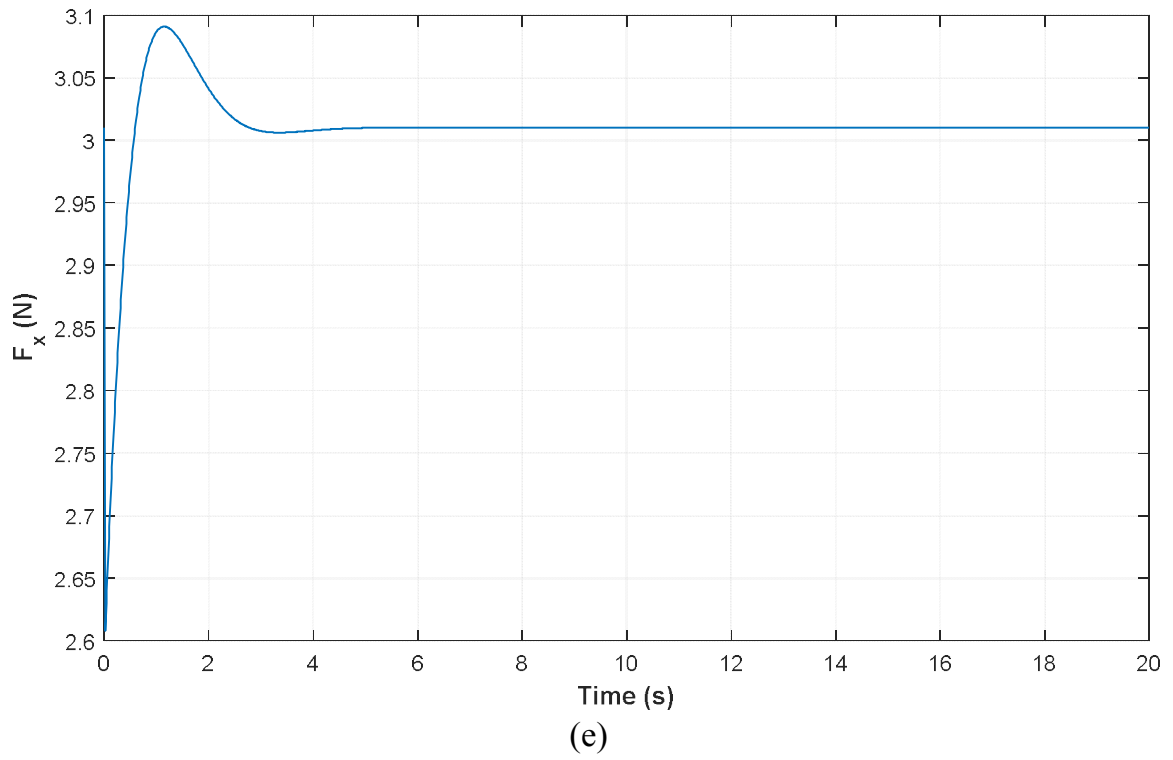
Fig. 71 Tracking of nominal force and motion. (a, b – position deviations in x, y axes); (c, d – velocity deviations in x, y axes); (e, f – reaction forces in x, y axes)

The simulation shows the responses of motion deviations η_x, η_y and acting force F_y, complement force F_x. Using this response along with dynamics model of the system, we generate the input signal torque as equations (3.8) and (3.12).

IV.   Application of Unified Approach for the 2-DOF revolute manipulator
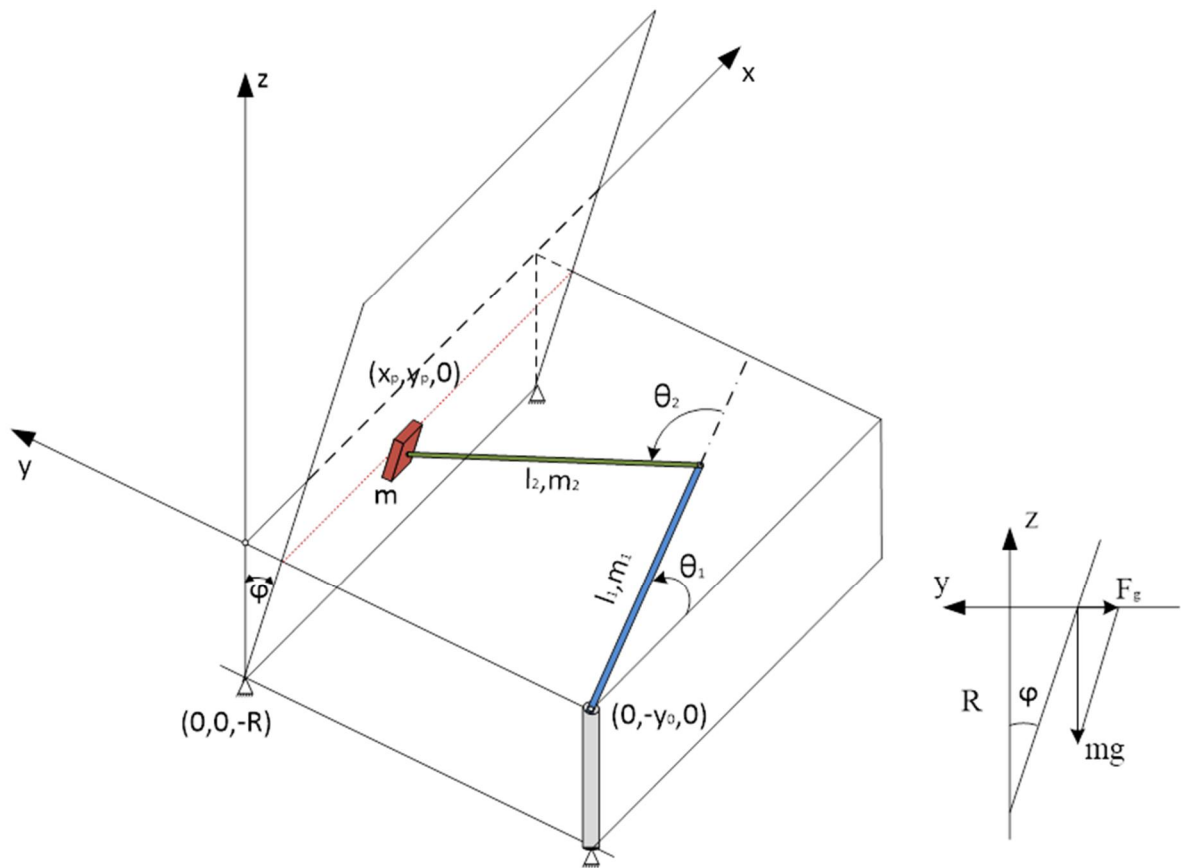
Fig. 72 Model of 2 DOF revolute manipulator.

4.1   Dynamic Modeling

The dynamic model of the robot interacting with its work-piece:

$$H(q)\ddot{q} + h(q,\dot{q}) = \tau + J^T(q)F \qquad (3.27)$$

The model of object dynamics:

$$M(q)\ddot{q} + L(q,\dot{q}) = S^T(q)F \tag{3.28}$$

Where $q = [\theta_1 \ \theta_2]^T$ is angular position vector of the robot.

In this content, the operational space approach [89] was used, the end-effector equations of motion can be written in the Cartesian coordinate frame. The dynamic models are transformed to Cartesian coordinate frame:

$$\Lambda(z)\ddot{z} + \nu(z,\dot{z}) = T + F \tag{3.29}$$

$$\mathcal{M}(z)\ddot{z} + \mathcal{L}(z,\dot{z}) = -F \tag{3.30}$$

Where the Cartesian coordinate $z = [x \ y]^T = \chi(q)$, the position coordinate are induced from angle vector.

The matrices $M(q)$ and $L(q,\dot{q})$ are constant matrices of inertia, viscous friction, and stiffness, respectively.

Assuming that all the functions in $(3.27 - 30)$ are continuously differentiable with respect to all variables with initial conditions $z(t_0) = z_0$ and $\dot{z}(t_0) = \dot{z}_0$, and the programmed motion $z_p(t)$ and the programmed interaction force $F_p(t)$ satisfy environment dynamic model (3.30), so the control objective is to achieve: $(z(t), \dot{z}(t), F(t)) \to (z_p(t), \dot{z}_p(t), F_p(t))$ when $t \to \infty$. These responses of the system are specified by the transient process synthesis.

4.2 Transient processes of motion and force

The transient processes of motion and contact force generally are determined by the equations:

$$\ddot{\eta} = P(\eta, \dot{\eta}) \tag{3.31}$$

$$\ddot{\mu} = Q(\mu, \dot{\mu}) \tag{3.32}$$

Where $\eta(t) = z(t) - z_p(t)$, $\mu(t) = F(t) - F_p(t)$, the P and Q are continuous functions and they are used to determine characteristics of the transient processes for stabilizing the motion and interaction force.

The P is the function of vectors η and $\dot{\eta}$ with Γ_1 and Γ_2, where Γ_1 and Γ_2 are constant coefficient matrices, the (3.31) can be rewritten as:

$$\ddot{\eta} = \Gamma_1 \dot{\eta} + \Gamma_2 \eta \tag{3.33}$$

As for the two-link revolute robot, the environment dynamics are depicted as:

$$F_y = (m + m_e)\ddot{y} + h_y \dot{y} - k_y y \tag{3.34}$$

$$F_x = m\ddot{x} + h_x \dot{x} + v_x(F_y - m_e \ddot{y})sign(\dot{x}) \tag{3.35}$$

The deviations of environment dynamics for positive velocity:

$$\mu_y = (m + m_e)\ddot{\eta}_y + h_y \dot{\eta}_y - k_y \eta_y \tag{3.36}$$

$$\mu_x = m\ddot{\eta}_x + h_x \dot{\eta}_x + v_x(\mu_y - m_e \ddot{\eta}_y) \tag{3.37}$$

We assume that the constant matrices of inertia, viscous friction, and stiffness matrices are: $M = \begin{bmatrix} m & v_x m \\ 0 & m + m_e \end{bmatrix}$; $L_h = \begin{bmatrix} h_x & v_x h_y \\ 0 & h_y \end{bmatrix}$; and $L_k = \begin{bmatrix} 0 & -v_x k_y \\ 0 & -k_y \end{bmatrix}$, respectively.

So the correspondence between motion deviation and force deviation can be expressed:

$$\mu = M\ddot{\eta} + L_h \dot{\eta} + L_k \eta \tag{3.38}$$

To get the transient process of interaction force, the approximation is applied for the linearized system with definitions $w = [\eta \quad \dot{\eta}]^T$, $u = [\mu \quad \dot{\mu}]^T$, $\Gamma = [\Gamma_1 \quad \Gamma_2]$ and $L = [L_k \quad L_h]$. So, the equations (3.33) and (3.38) can be rewritten as:

$$\dot{w} = \begin{bmatrix} 0 & I \\ \Gamma_2 & \Gamma_1 \end{bmatrix} w = \Gamma_\eta w \tag{3.39}$$

$$\mu = (M\Gamma + L)w = Cw \tag{3.40}$$

We obtain:

$$u = \begin{bmatrix} C \\ C\Gamma_\eta \end{bmatrix} w = \alpha w \tag{3.41}$$

Where $\alpha = \begin{bmatrix} M\Gamma_2 + L_k & M\Gamma_1 + L_h \\ (M\Gamma_1 + L_h)\Gamma_2 & (M\Gamma_1 + L_h)\Gamma_1 + M\Gamma_2 + L_k \end{bmatrix}$, assume that the matrix α is nonsingular, deriving from (3.39) and (3.41) we obtain $\dot{u} = Q_\mu u$ where $Q_\mu = \alpha\Gamma_\eta\alpha^{-1}$. So the transient process of contact force can be obtained:

$$\ddot{\mu} = Q_1\dot{\mu} + Q_2\mu \tag{3.42}$$

Where $[Q_2 \quad Q_1] = [\alpha_2 \quad \beta_2]\alpha^{-1}$, $\alpha = \begin{bmatrix} \alpha_0 & \beta_0 \\ \alpha_1 & \beta_1 \end{bmatrix}$, $\alpha_0 = L_k + M\Gamma_2$, $\beta_0 = L_h + M\Gamma_1$, $\alpha_{i+1} = \beta_i\Gamma_2$, $\beta_{i+1} = \alpha_i + \beta_i\Gamma_1$, $i = 0,1$. So the coefficients of function Q are approximated from the coefficients of the function P.

When $(\ddot{\eta}, \dot{\eta}, \eta) \to 0$ as $t \to \infty$, (3.36) and (3.37) can induce $(\ddot{\mu}, \dot{\mu}, \mu) \to 0$.

4.3   Simulation

4.3.1   Simulation Setup

As mentioned in the previous section, the Cartesian robot is described as Fig. 72 and its parameters are in Table 3. The robot consists of two revolute links on the plane and a flexible movement tool is mounted on the tip.

Table 3 Simulation parameters

Desired contact force (F0)	100 [N]
Horizontal velocity (V0)	80 [mm/s]
Mass of tool (m)	5 [kg]
Mass of link 1 (m1)	10 [kg]
Mass of link 2 (m2)	7 [kg]
Length of link 1 (l1)	1 [m]
Length of link 2 (l2)	1 [m]
Vertical distance of flat plane (R)	0.3 [m]
Robot foot in y-axis (y0)	1.4 [m]

The dynamics modeling of the Cartesian robot is depicted by the positive matrices of inertia moment, nonlinear functions of centrifugal, Coriolis' and gravitational moment and Jacobian matrix. All of these coefficients are induced by the angular position vector of the robot.

The relation between $z = [x \ y]^T$ and $q = [\theta_1 \ \theta_2]^T$ is:

$$z = \chi(q) = \begin{bmatrix} cos(\theta_1) + cos(\theta_1 + \theta_2) \\ sin(\theta_1) + sin(\theta_1 + \theta_2) - 1.4 \end{bmatrix} \tag{3.43}$$

The contact force vector is introduced in Cartesian space $F = \begin{bmatrix} F_x & F_y \end{bmatrix}^T$, in which the contact force F_y is a sum of the inertial, frictional and gravitational components:

$$F_y = 7.45\ddot{y} + 0.1\dot{y} - 163.5y \tag{3.44}$$

Where $k_y = \dfrac{mg}{R} = 163.5$ is environment stiffness coefficient, and $m_e = \dfrac{mR}{y_p} = 2.45$ is the support equivalent mass.

The horizontal component of contact force is a sum of the inertial and frictional forces:

$$F_x = 5\ddot{x} + 0.1\dot{x} + 0.01(F_y - 2.45\ddot{y})sign(\dot{x}) \tag{3.45}$$

The equations (3.44) and (3.45) are reformed from environment dynamics equation (3.30). For maintaining the constant contact force, the programmed contact force along the y-axis is set as constant.

$$F_{y_p}(t) = F_y^0 = F^0 = 100 \text{ (N)}$$

And the nominal motion along the x-axis:

$x_p(t) = x^0(t) = V_0 t, V_0 = 0.08$ (mm/s)

From (3.40), (3.41) we can determine the horizontal component of contact force F_x and vertical motion y_p:

$F_{x_p}(t) = F_x^0(t) = h_x V_0 + v_x F^0 = 1.008(N).$

And $y_p(t) = y^0(t) = -\dfrac{1}{k_y} F^0 = -0.61(m).$

4.3.2 Procedure Proposal

In order to implement the unified approach for synthesizing the force/position control law, the contact force, which acts on the dynamic car body, is studied through the

characteristics of its transient process. This process is induced by the sanding tool motion's transient process as mentioned before. The problem needs to be solved that is to find out the good form of the transient process of motion, which satisfies the exponential stability condition, so the function P in the equation (3.31) is investigated by being supposed as below:

$$\ddot{\eta}_x + 2\zeta_x\omega_x\dot{\eta}_x + \omega_x^2\eta_x = 0 \tag{3.46}$$

$$\ddot{\eta}_y + 2\zeta_y\omega_y\dot{\eta}_y + \omega_y^2\eta_y = 0 \tag{3.47}$$

In which, η_x, η_y are motion deviation between the real motion and programmed motion along x-axis, y-axis respectively. For generating the acceptable control model of the transient models in (3.46 – 47), the motion transient processes are analyzed in the s-space by using the Laplace transformation method.

From the equation (3.46), the Laplace transform of motion deviations can be rewritten as equation (3.48) with foreknown initial conditions, the same case for y-axis motion in the equation (3.47).

$$H(s) = \frac{0.05s + 0.1\zeta_x\omega_x}{s^2 + 2\zeta_x\omega_x s + \omega_x^2} \tag{3.48}$$

So the system has two poles and one zero, the trivial solution of zero is $s_0 = -2\zeta_x\omega_x$ and solutions of poles are $s_{1,2} = -\zeta_x\omega_x \pm \omega_x\sqrt{\zeta_x^2 - 1}$ respectively. The problem is considered as a simple second-order system. The root locus method is used to analyze the basic characteristics of the transient response of a closed-loop system is closely related to the location of poles in the s-plane. When the poles – in the left of the s-plane the system response – increases, similarly when the poles on the imaginary axis and in the right of s-plane the system response are neutral and increases respectively. For a linear system, the stability is related to the location of the roots of the characteristic equation. As the equation (3.48), the damping and nature undamped frequency varies the locations the system's poles are changed respectively.

[90] Through analyzing the characteristics of the transient process in root locus procedure, the rising time and delay time are proportional to damping ratio and inversely proportional to natural frequency. And based on the requirement of the transient time and damped state of the system, the damping ratio, and natural frequency can be tuned to generate the acceptable control model of the programmed interaction force with fast responses of step servo motors. In this case, the closed-loop root locus of such controller with $\zeta = 0.9, \omega = 8$ is examined as in Fig. 73. And the transient processes' responses of robot motion are shown in Fig. 74 with the acceptable specifications are expressed in Table 4.
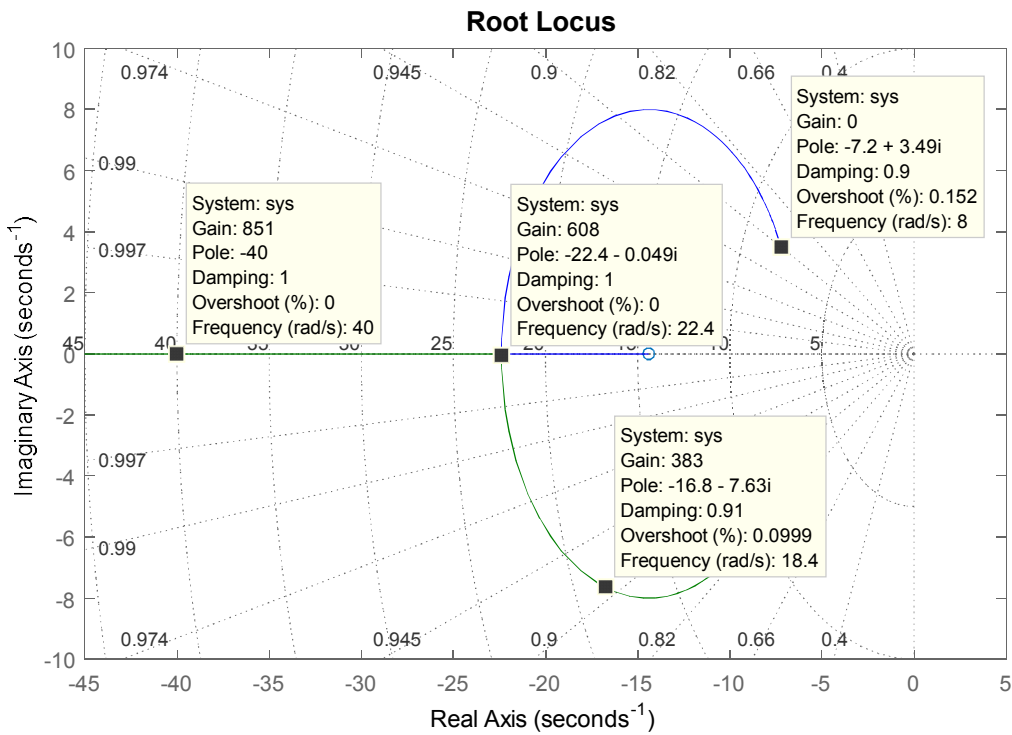
Fig. 73 Root locus for the revolute manipulator.

Table 4 Specifications of the transient process

Rising time (t_r)	365 [milliseconds]
Delay time (t_d)	200 [milliseconds]
Steady state error	2.926e-64 [m]

4.3.3   Results and Discussions

Basing on the above root locus, we can do tuning the damping ratio and frequency to get the acceptable responses for desired interaction control design.

In this proposal, the sanding motion is estimated with foreseen trajectory. In which the desired long velocity is proposed 80 mm/s along the x-axis and the y-direction desired position are constant depended on the desired interaction force.

T Where $\ddot{\eta}_x + 14.4\dot{\eta}_x + 64\eta_x = 0$ and $\ddot{\eta}_y + 14.4\dot{\eta}_y + 64\eta_y = 0$. The responses of motion and interaction force are obtained:
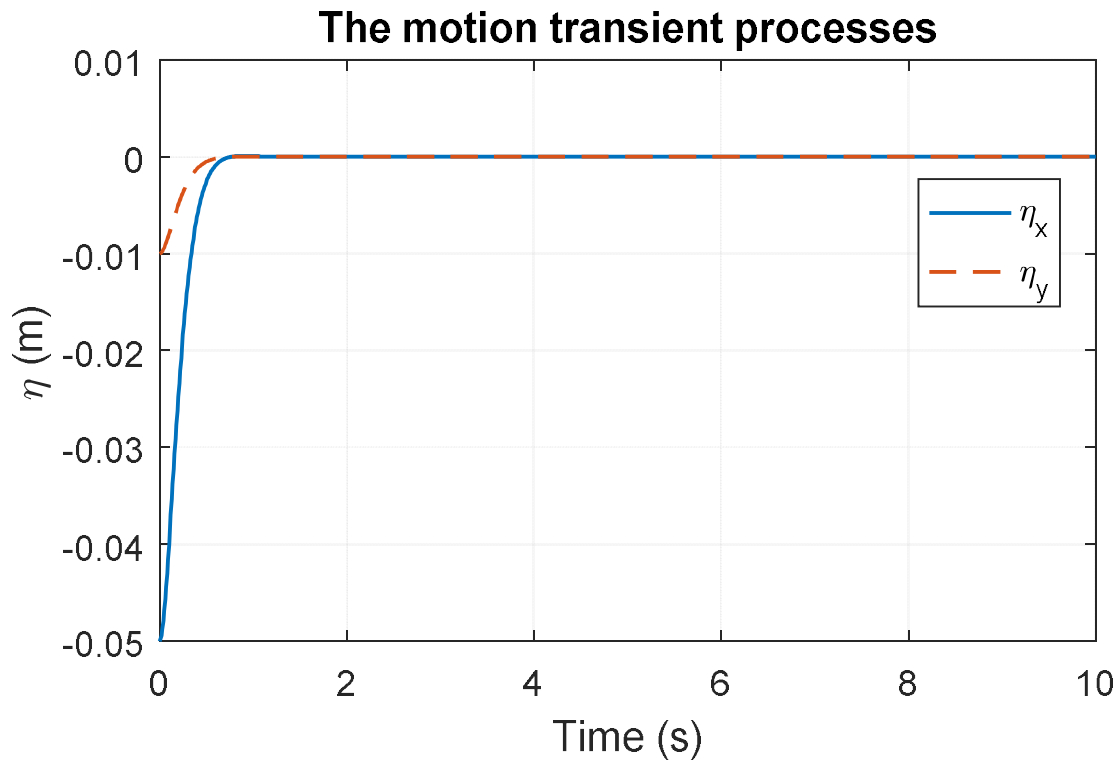
Fig. 74 The motion transient processes
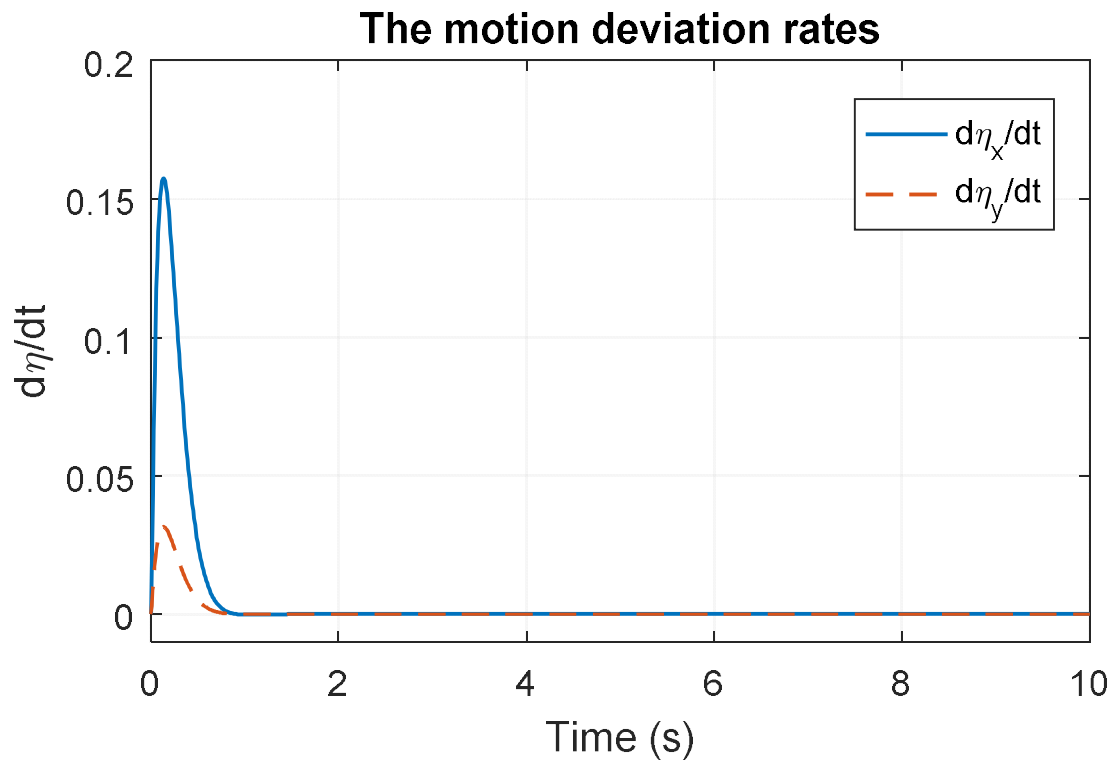
Fig. 75 The motion deviation rates.
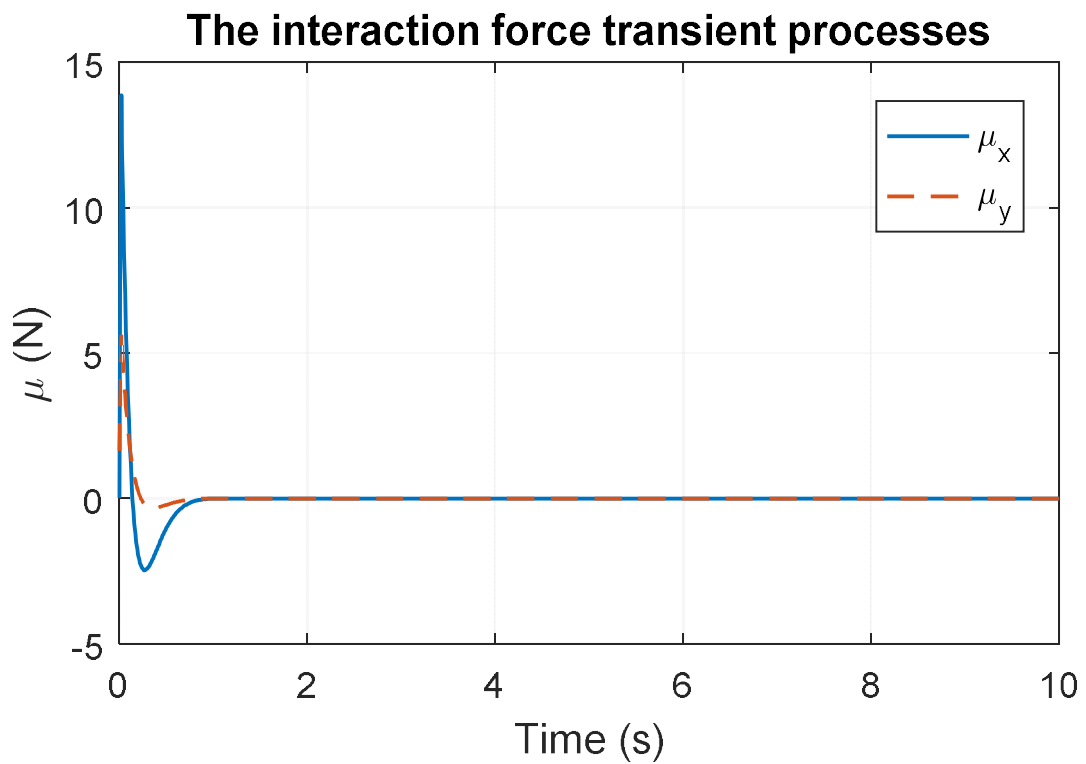
Fig. 76 The interaction force transient processes.

The x-axis component of interaction force
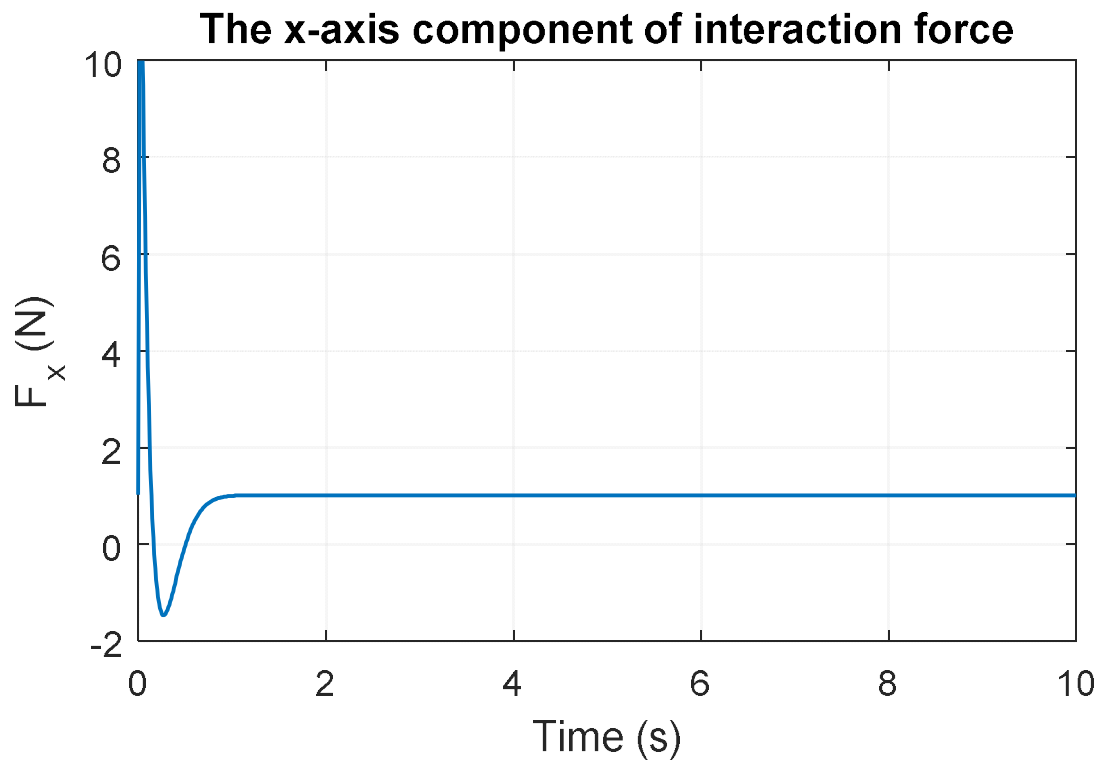
Fig. 77 The x-axis component of interaction force.

The interaction force
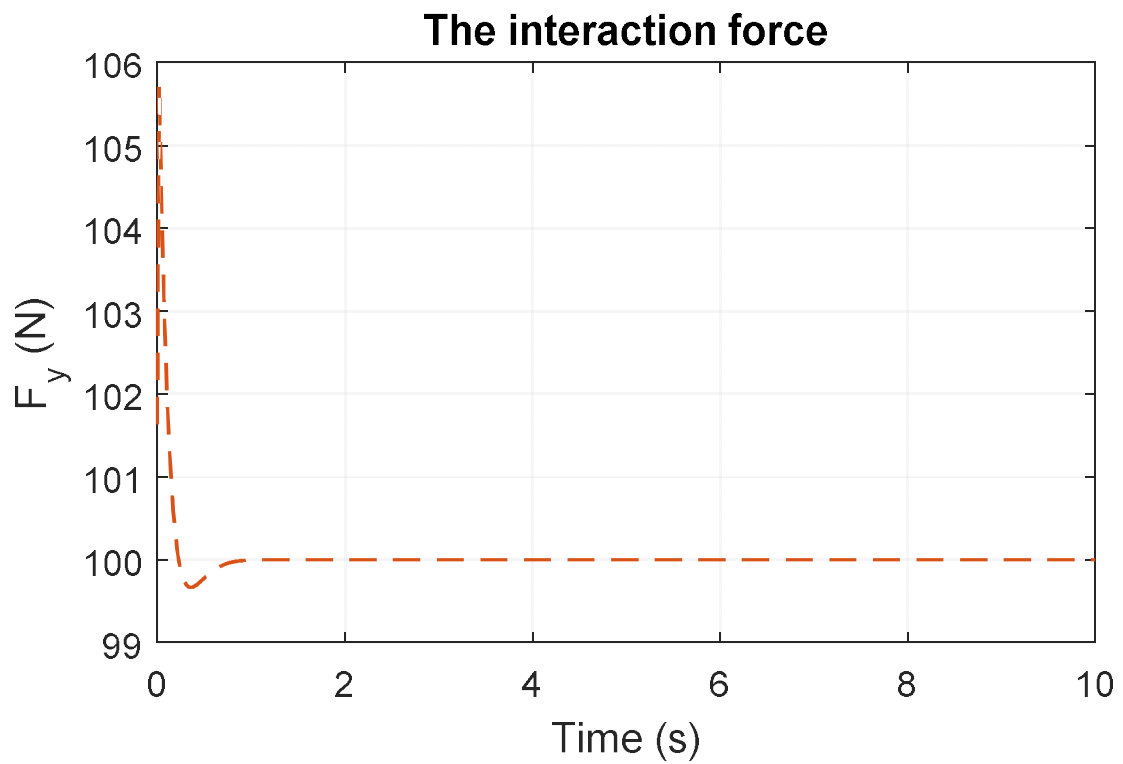
Fig. 78 The interaction force.

The angle of robot joint 1

Fig. 79 The angle of robot joint 1.
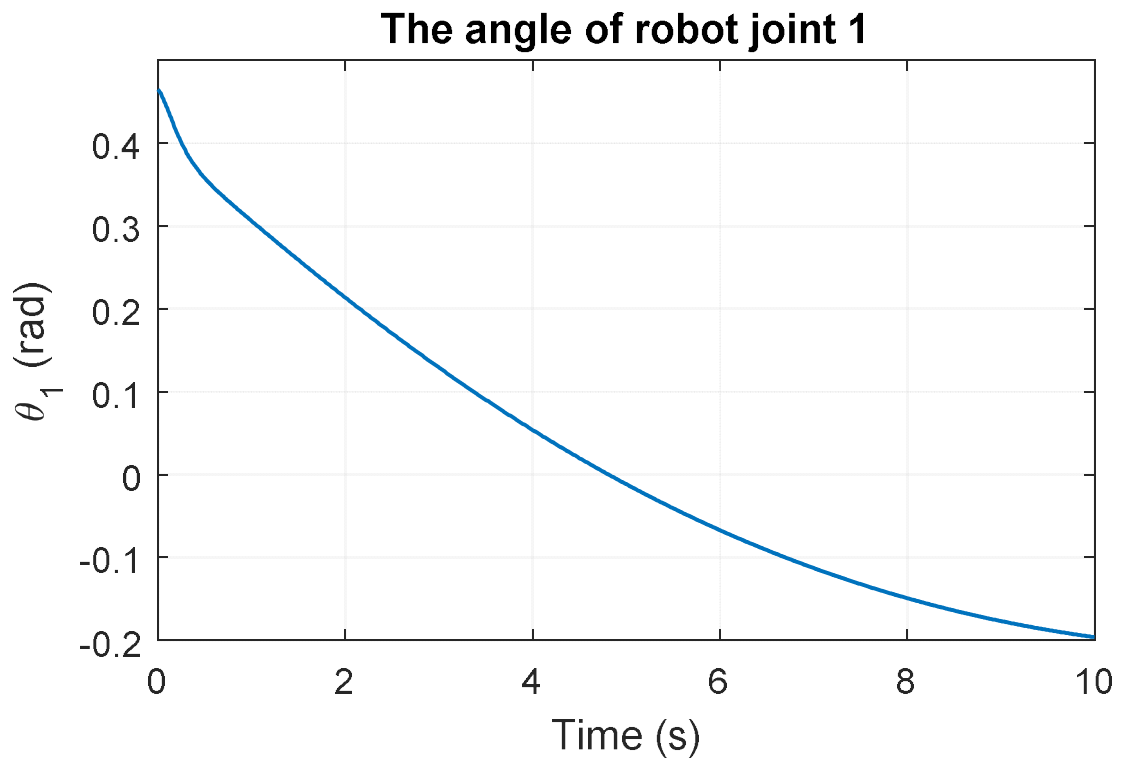
The angle of robot joint 2
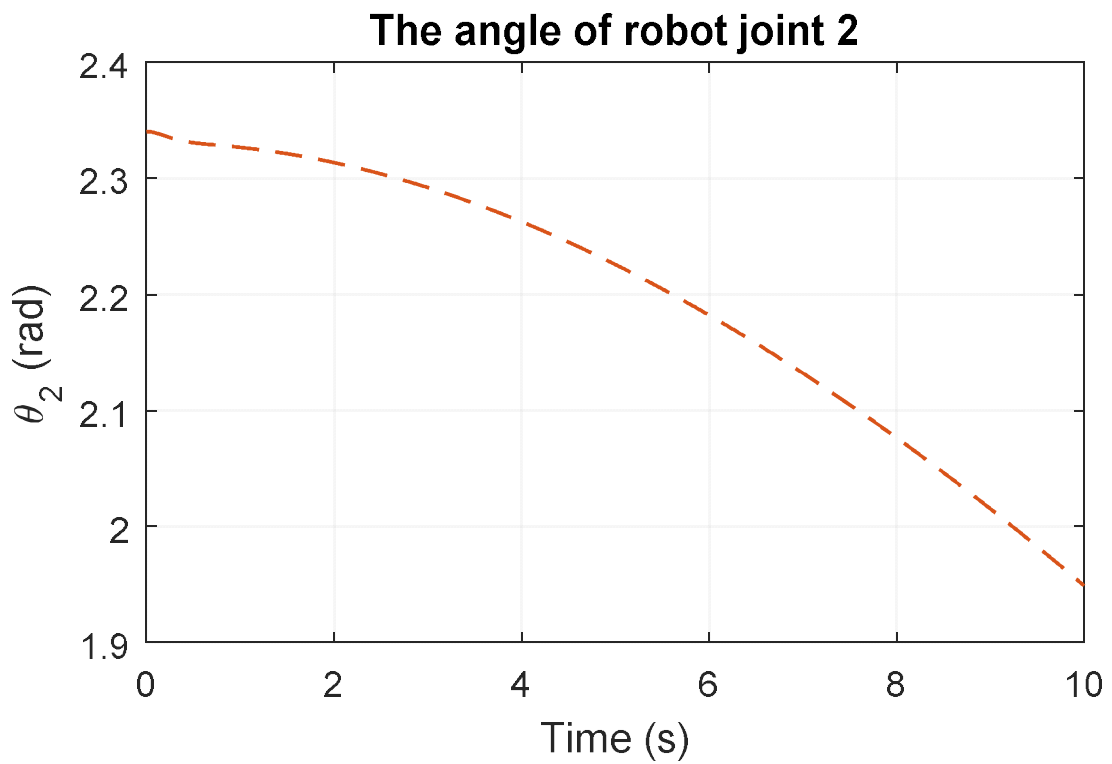
Fig. 80 The angle of manipulator joint 2.
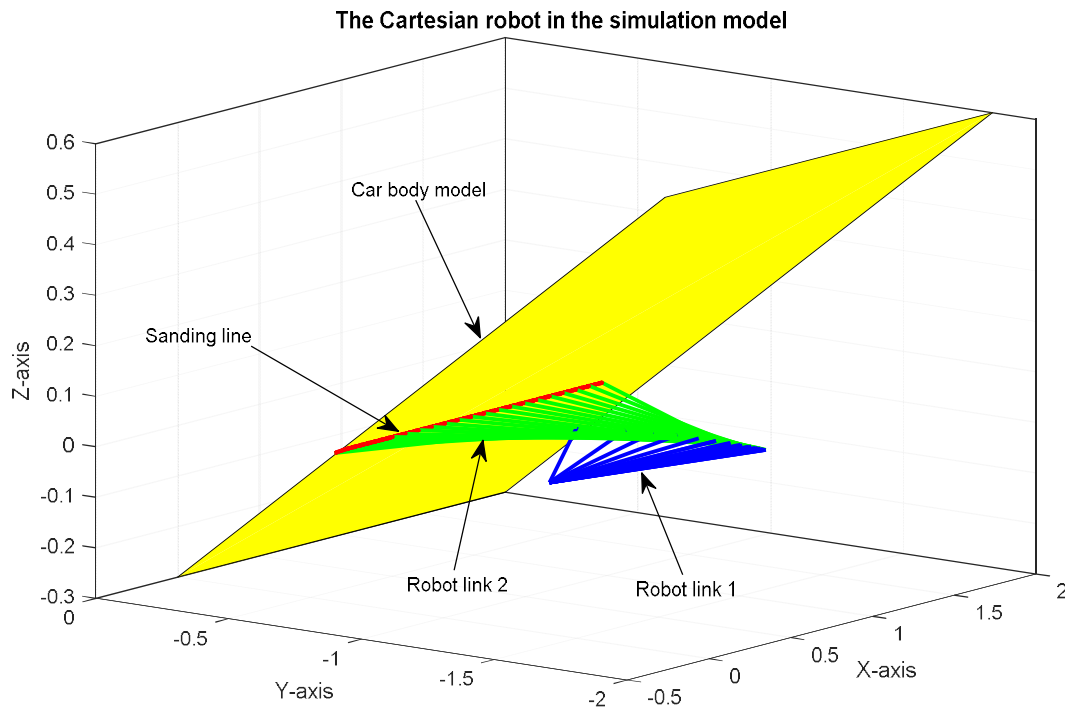
Fig. 81 The estimation of the Cartesian robot.

When such transient processes are applied, the response of interaction force reached the steady state adaptively. For adapting above responses, the joints' revolutions are estimated by using robotic invert kinematic as shown in Fig. 79, and Fig. 80.

The estimation of the Cartesian robot is shown as Fig. 81 based on the simulation data. The slope angle φ is calculated as -1.1148 rad, about -63.872 degree.

V.   Position Error-based Impedance Control Model for Deburring Robot

To realize the Target Impedance Model and apply the unified method, the experimental system is assembled as shown in Fig. 82. The measured motion and measured force are collected for estimating the coupled impedance model which is applied in the simulation. The actuators are driven by two step servo motors and are observed by encoders. The tool with force sensor is attached on the tip of vertical

actuator. The pseudo-work piece is a horizontal aluminum profile. The Arduino Uno board is used as the main controller.
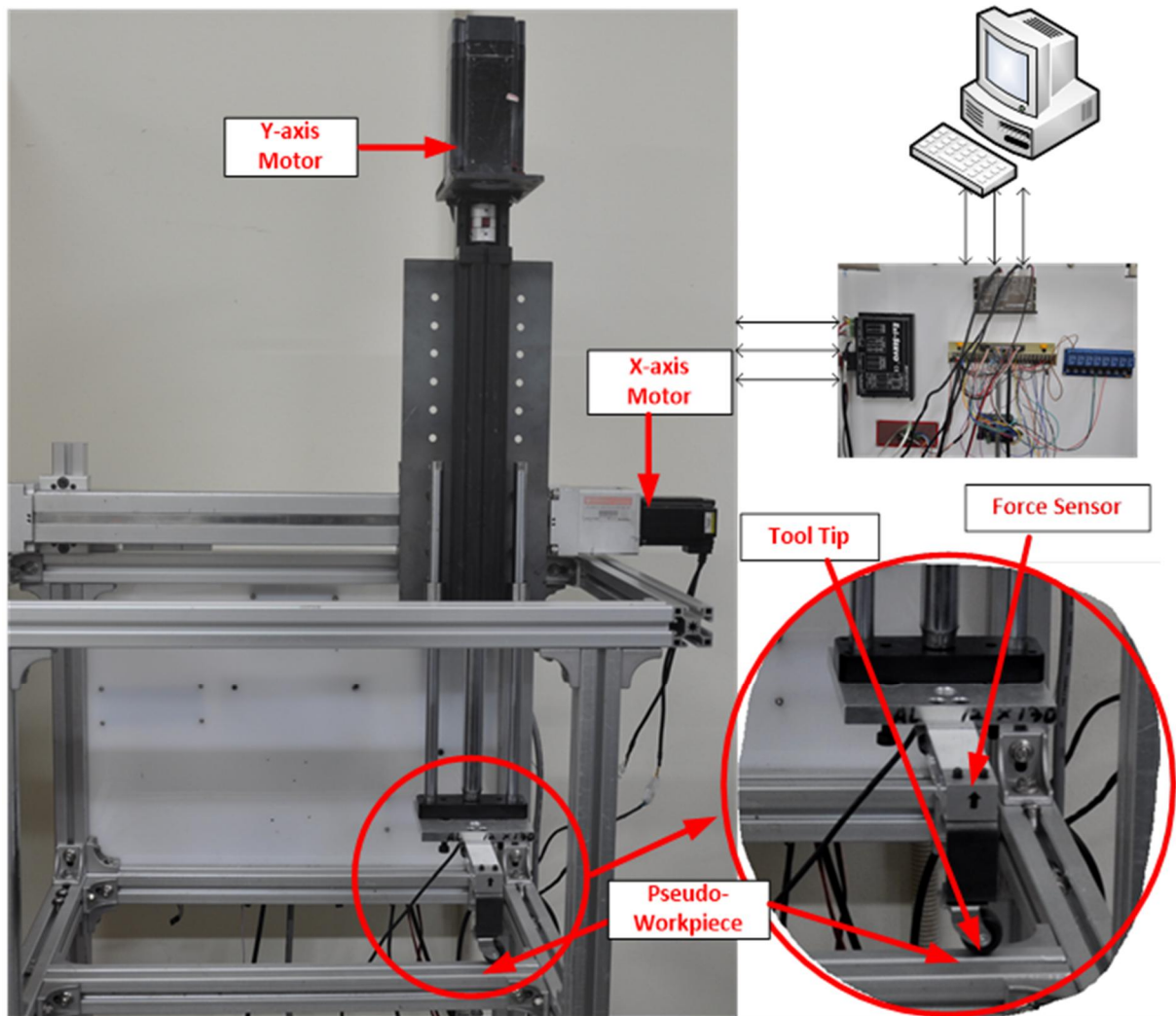
Fig. 82 Experimental Apparatus

5.1   Impedance System Behavior

In principle, there is an arbitrary functional form of the control input that describes a desired target impedance model, which is commonly adopted in the linear second-order differential equation form [91], describing the simple and well-understood decoupled mass-spring-damping mechanical system.

$$F = M_t(\ddot{y} - \ddot{y}_p) + B_t(\dot{y} - \dot{y}_p) + K_t(y - y_p) \qquad (3.49)$$

In s-domain

$$F(s) = (M_t s^2 + B_t s + K_t)(y - y_p) = Z_t(s)(y_p - y)$$

Where $Z_t(s) = -(M_t s^2 + B_t s + K_t)$ is the target robot impedance model, y_p is programmed tool position, y is the actual position, F is reaction force, and M_t, B_t, K_t are positive definite inertia, damping and stiffness matrices which define the target impedance model.
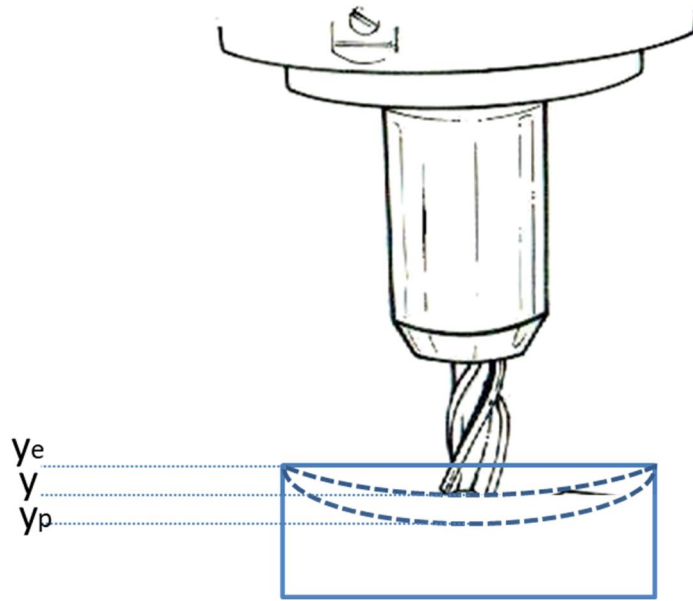
Fig. 83 Geometric model of deburring tool's penetration.

In the surface processing, when the working tool penetrates into the environment, the robot is controlled with desired motion y_p. The robot firstly contacts to the objective at position y_e and the penetration begins up, the interaction generates the reaction force on the robot. The depth of penetration is maintained at position y and this value depends on the environment stiffness [92]. The impedance control is classified into position-mode and force mode, but when applying for robotic control, the position-

mode is more advantageous on the reliability, simpler design, and implementation. Furthermore, sufficiently accurate and robust desired impedance behavior can be achieved. Therefore, the position-mode scheme is prioritized for the further considerations, as well as implementation and experiments with convenient industrial robotic systems.

The position error of the impedance model is presented in Fig. 84, the robot position control system consists of the following transfer function matrices: G_r position regulator, G_s robot plant, and G_e environment. The force feedback compensator G_f, Z_t the target impedance model, the reference position y_r is computed through position correction Δy_f, estimated the reaction force by feedback compensator.
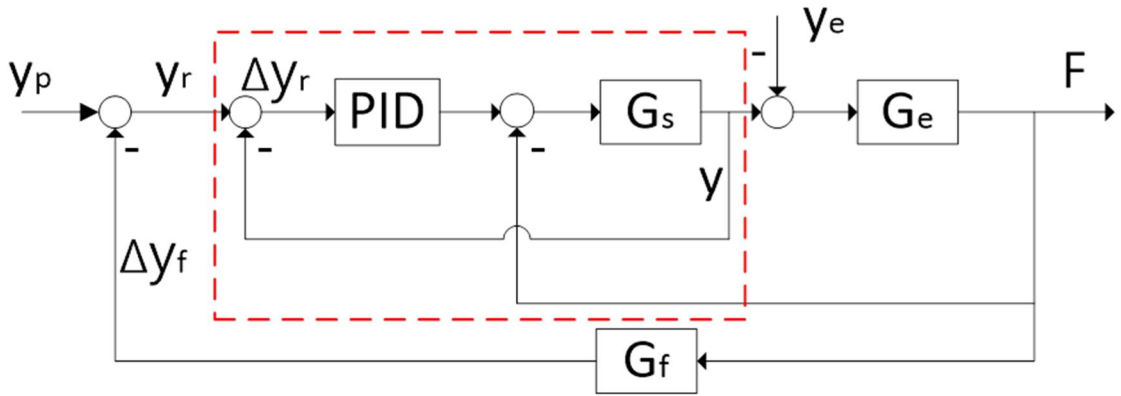
Fig. 84 The position error-based impedance control model.

In this control algorithm, the fundamental equations can be written:

$$\Delta F = F_p - F = G_t(y_p - y) - F = e_f \tag{3.50}$$

$$G_s^{-1}(s)y = G_r(y_r - y) - F = G_r e_p - F \tag{3.51}$$

$$y_r = y_p - \Delta y_f \tag{3.52}$$

$$\Delta y_f = G_f(s)F \tag{3.53}$$

Synthesis of all control loops, the penetration position under impedance control G_f (s) is:

$$y = G_p(s)y_p - G_p(s)G_f(s)F - S_p(s)G_s(s)F \tag{3.54}$$

where

$$G_p(s) = [G_s^{-1}(s) + G_r(s)]^{-1}G_r(s)$$

$$S_p(s) = [G_s^{-1}(s) + G_r(s)]^{-1}G_s^{-1}(s)$$

So, the position tracking error $e = y_p - y$:

$$e = S_p(s)y_p + S_p(s)G_s(s)F + G_p(s)G_f(s)F \tag{3.55}$$

Assuming that the internal position control system behaves as an ideal stiff servo, so the compensator ensures the desired impedance target inducing $G_p \approx I$ and $S_p \approx 0$. In this case, the reference position error is as small as possible [93].

Equation (3.55) can be rewritten as:

$$F(s) = \hat{G}_t(s)e(s) \tag{3.56}$$

where $\hat{G}_t^{-1} = G_p G_t^{-1} = G_p G_f$

In (3.56), the $F(s) = G_e(s)(y - y_e) = G_e(s)p(s)$ and $e = y_p - y = (y_p - y_e) - (y - y_e) = p_0 - p.$

Inducing the penetration model

$$p(s) = [I + \hat{G}_t^{-1}(s)G_e(s)]^{-1}p_0(s) \tag{3.57}$$

Substituting $p = G_e^{-1}(s)F$ into (3.57), the coupled impedance/admittance model is depicted:

$$F(s) \approx \left[I + G_e(s)\hat{G}_t^{-1}(s)\right]^{-1} G_e(s)p_0(s) \tag{3.58}$$

The penetration deviation is:

$$e(s) \approx [I + G_e^{-1}(s)G_t(s)]^{-1}p_0(s) \tag{3.59}$$

The coupled system stability is considered to determine the equilibrium state of target impedance model.

5.2   Target Impedance Model Realization

As a model at equation (3.58), the coupled impedance Z_c can be rewritten:

$$F(s) = Z_c(s)p_0(s) = \frac{G_t(s)G_e(s)}{G_t(s)+G_e(s)}p_0(s) \tag{3.60}$$

In this case the deform of the workpiece in slow motion of the robot is considered as quasi-static with dominating stiffness effects, so the coupled impedance is the transfer function induced by target impedance model $G_t(s)$ and environment stiffness K_e.

$$Z_c = \frac{K_e(M_t s^2 + B_t s + K_t)}{M_t s^2 + B_t s + K_t + K_e} \tag{3.61}$$

To realize the target impedance model, the penetration position p_0 and reaction force F are measured. In the experiment, the robot end-effector is moved manually to contact with surface [94], the step motor penetrates the tool by target penetration p_0 1 mm by 1 mm and the reaction force is measured simultaneously are shown as Fig. 85

.
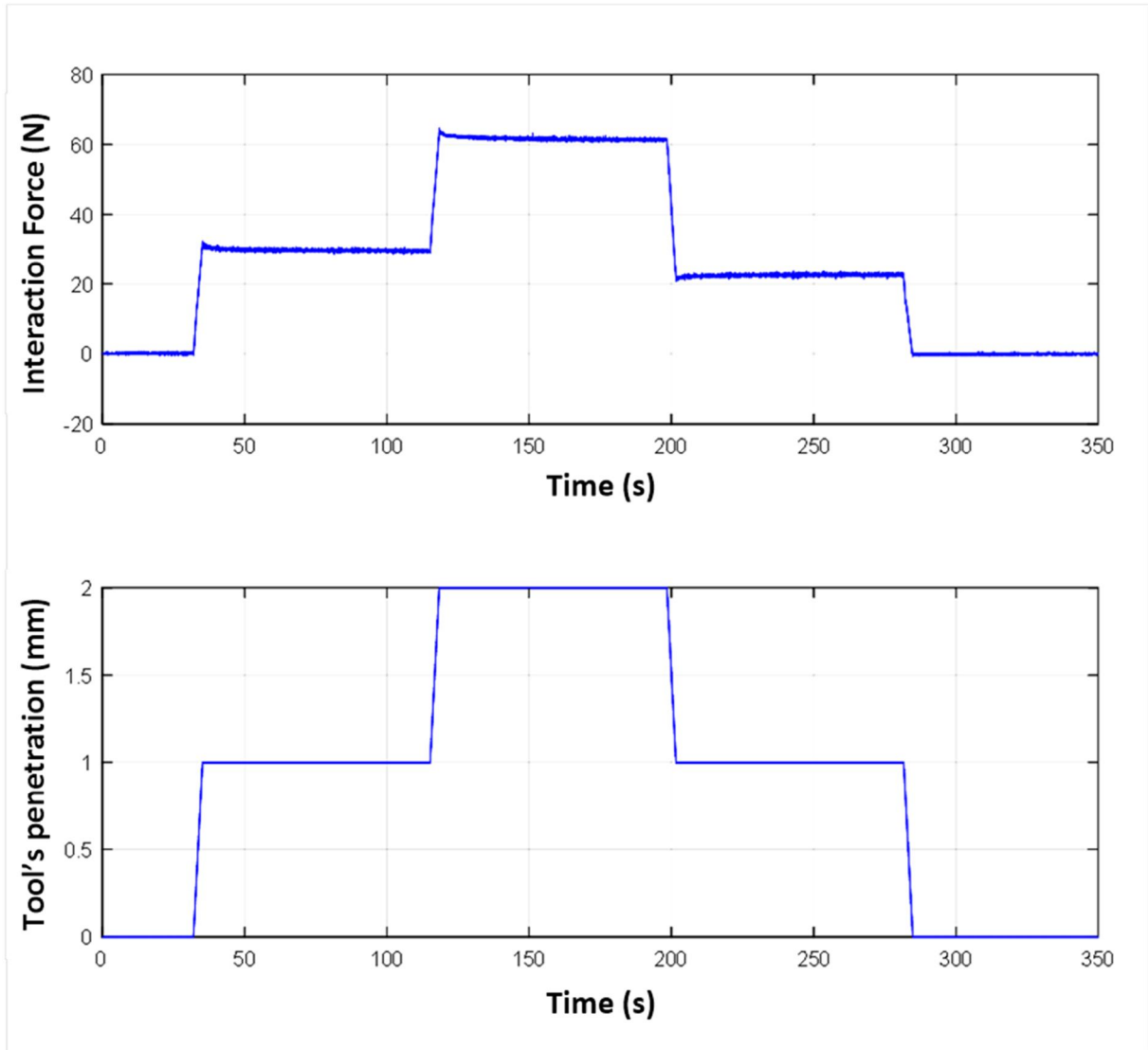
Fig. 85 The interaction force and tool's penetration are measured in the experiment.

The coupled impedance Z_c is estimated by MATLAB System Identification Toolbox with position input and force output as Fig. 85. And the numerator and denominator of Z_c are chosen as equation (3.61). The contact force is estimated with accuracy rate 92.93% compared with the measured value shown as Fig. 86.
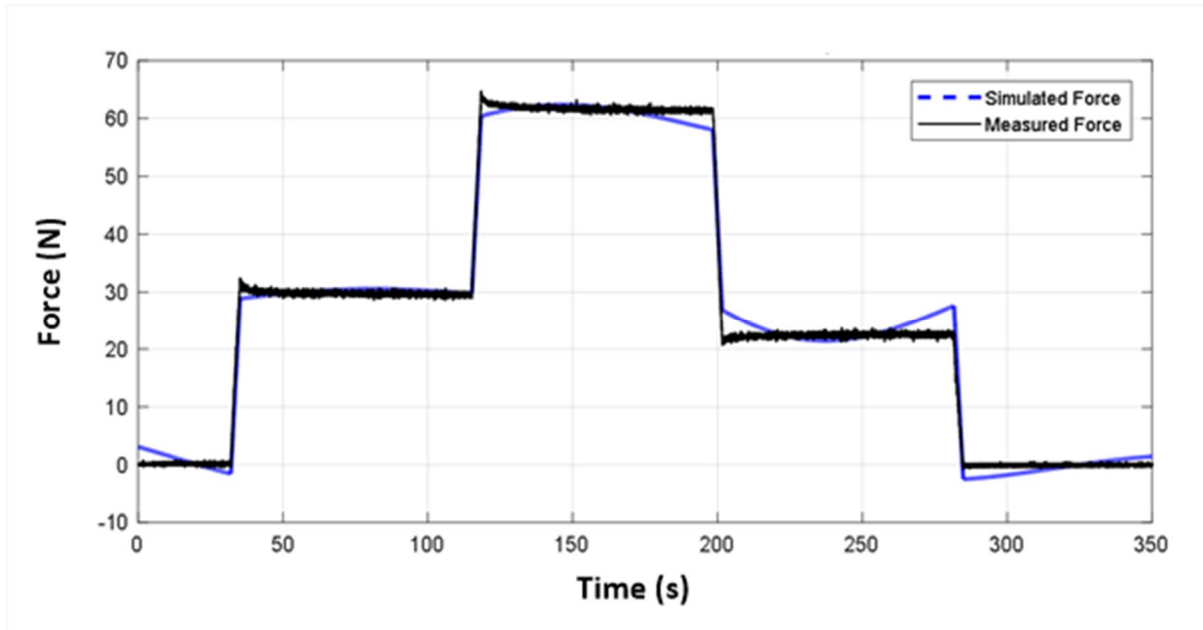
Fig. 86 Comparison of the measured force and simulated force.

At steady state, the nominal stiffness $K_0 = \frac{K_t K_e}{K_t + K_e}$ is approximated as 30,000 N/m.

5.3   Simulation of Position Error-based Impedance Control Model

The simulation aims to evaluate the impedance control performance when it is applied to the low-cost deburring system. As shown in Fig. 84, the position error based impedance control consists of the robot internal position control, this part is determined by motor specifications and PID control, and the environment dynamic without inertia and damping factors is determined by the coupled impedance Z_c using MATLAB System Identification Toolbox.

The internal position closed-loop control is experimented by Arduino, and simulated by MATLAB. The internal PID controller gets feedback by the encoder with 10,000/rev resolution, has good performance as Fig. 87.
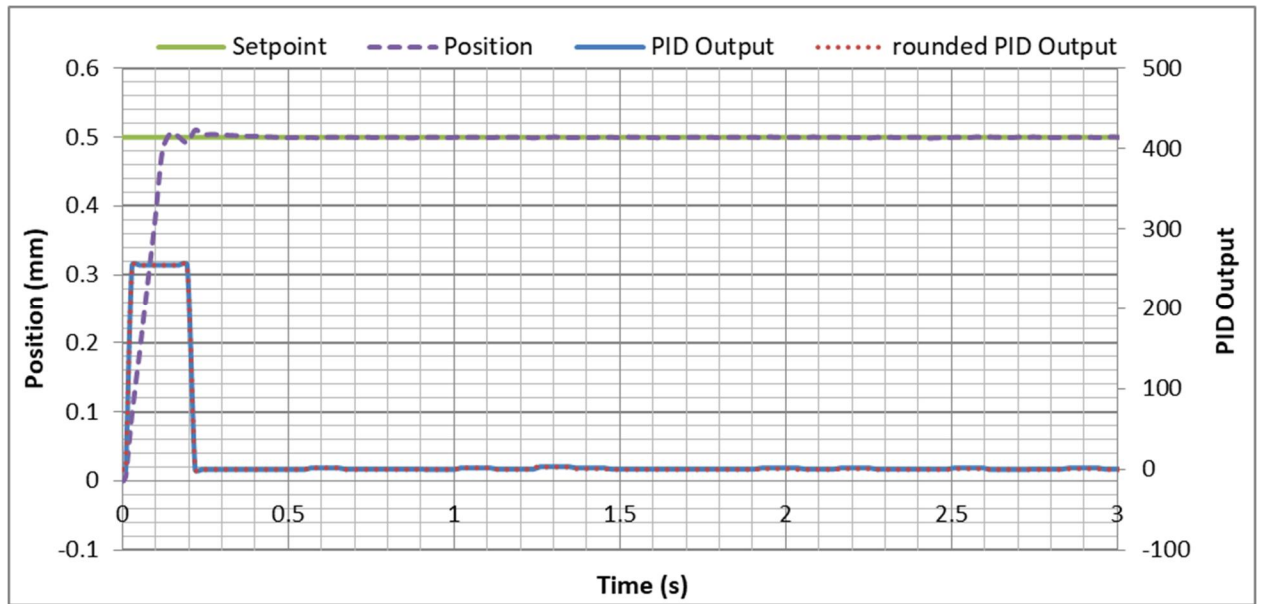
Fig. 87 The response of PID internal position control

The motor model with the specifications in Table 5 is used for simulation.

Table 5 Step motor specifications

Resistance per Phase (R)	0.8[Ω]
Inductance per Phase (L)	8.68 [mH]
Rotor Inertia (J)	5400 [g.cm2]
Holding Torque (T)	12 [N.m]

The simulation is carried out as Fig. 88, the responses of simulation is obtained by selecting the environment stiffness coefficient and tuning the target impedance model's inertia, damping ratio, and frequency coefficients.
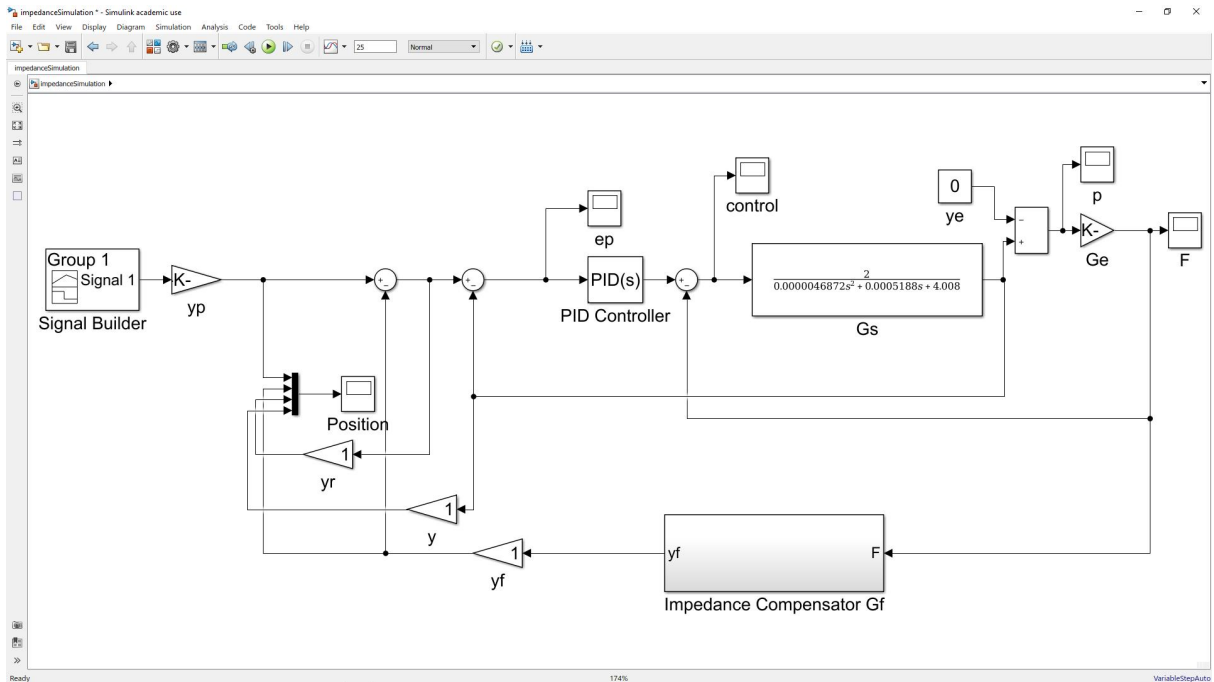
Fig. 88 Simulation of Position Error-based Impedance Control Model.

The simulation results are displayed in Fig. 89: the responses of contact force and position are shown for the low stiffness case and high stiffness case. Since the coupled impedance is around $K_0 = 30,000$ N/m when the system is stable, therefore the target impedance model's parameters need to be selected to obtain the desired contact force, in which the environment and target model's stiffness always satisfies $K_0 = \dfrac{K_t K_e}{K_t + K_e}$. The target impedance model's parameters are tuned inducing the correction position is varied, the instant robot position is regulated to ensure the desired penetration is maintained as desired. The Fig. 90 and Fig. 91 show the effects of damping coefficient and mass inertia.
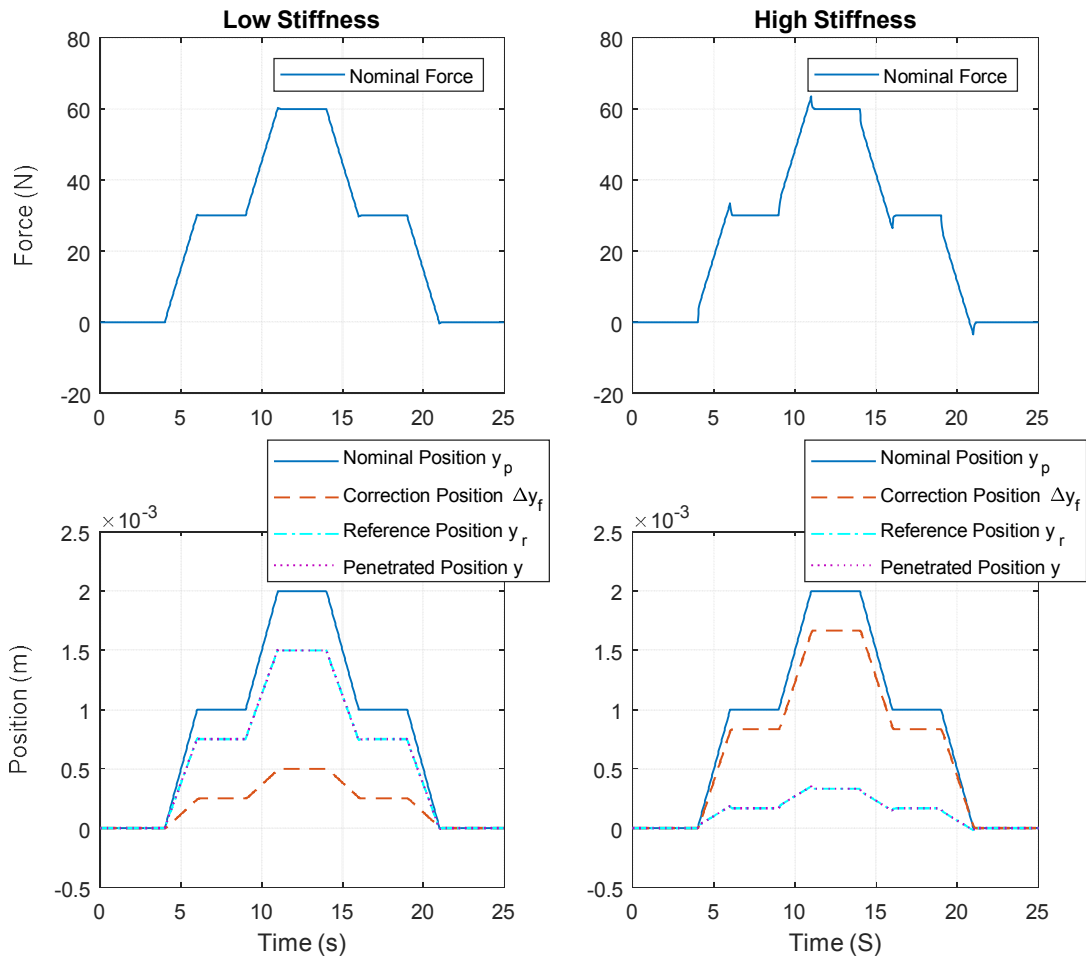
Fig. 89 The Responses of Target Impedance Model: Effect of Stiffness
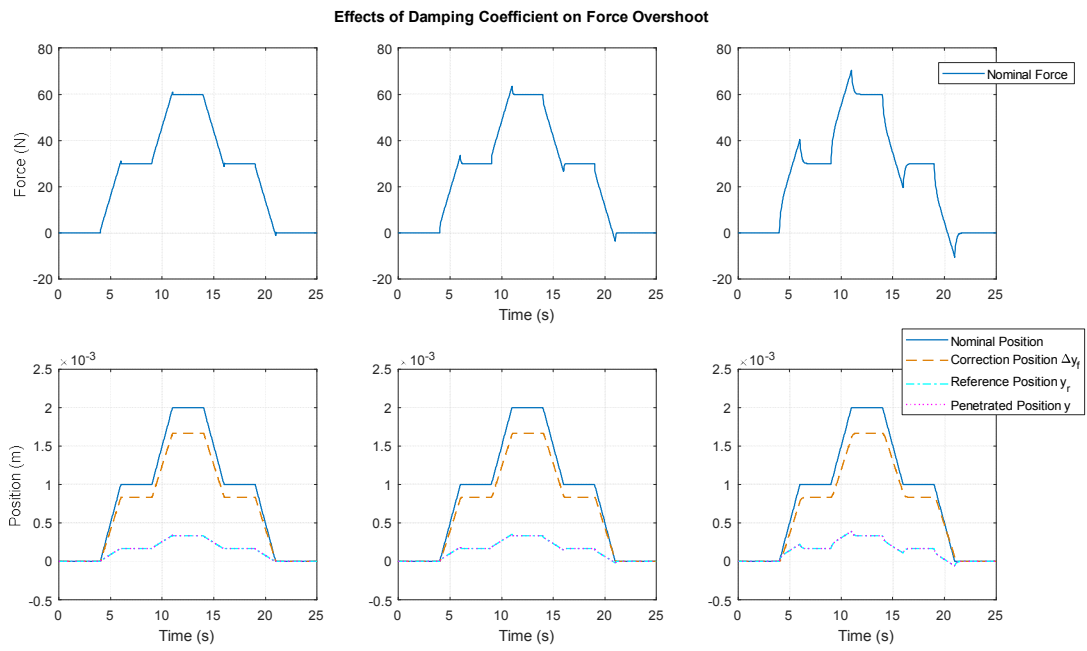
Fig. 90 The Responses of Target Impedance Model: Effect of damping
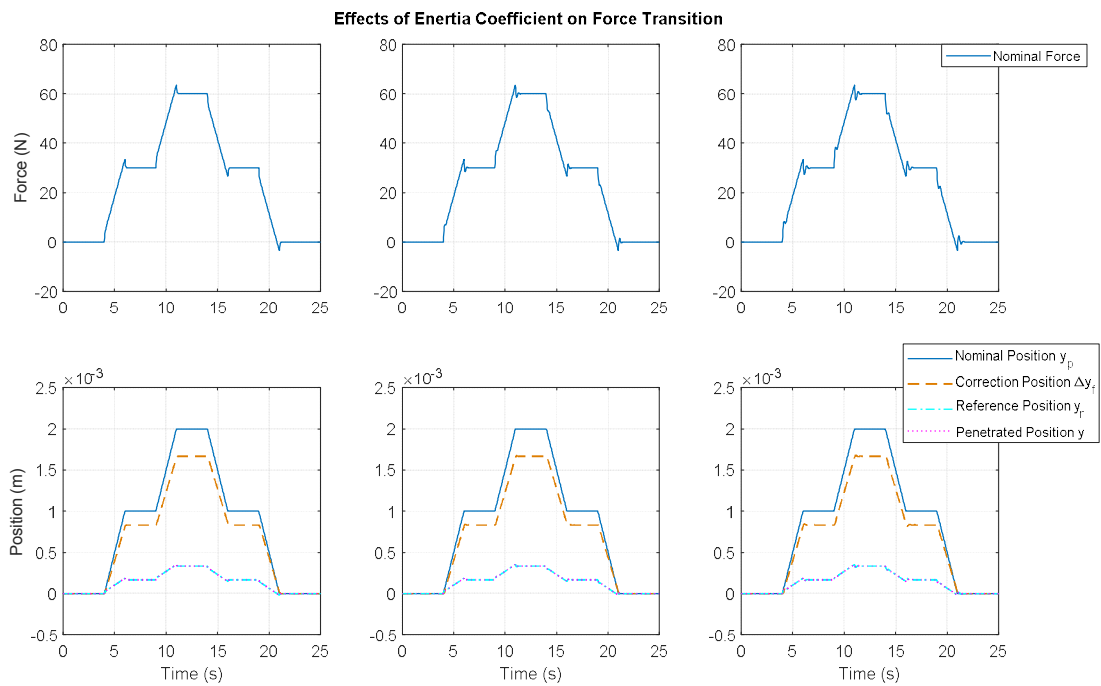
Fig. 91 The Responses of Target Impedance Model: Effect of mass inertia

The results show the robot actual motion y tracks accurately the nominal motion y_p in free space. After the contact, the Impedance Model generates the correction position

116

Δy_f, the internal position control tried to track the reference input $y_r = y_p - \Delta y_f$. The robot motion y was controlled to be close to the reference position y_r.

In the Fig. 90, the stiffness is kept constant as the left case of Fig. 89 and the damping coefficient is tuned with three different values. As the damping coefficient is tuned, the overshoot of the response force is also varied. Respectively, in the Fig. 91, the stiffness and damping coefficient are fixed, and only the mass inertia coefficient is tuned. When the mass inertia coefficient is increased, the force transition is oscillated and the settling time is lengthened. To control the desired contact force of deburring robot we could regulate the pertinent coefficients of impedance model.

The simulations of position error-based impedance control model showed the influence of the target impedance model on the response of the force. Actually, the workpiece can be made of different materials. Burrs also affect the action of the force. The target impedance model, which was proposed, can be used to control the desired force by regulating the robot tool's penetration to reduce the overshoot of force and stabilize the response of the force.

CHAPTER V PRACTICAL SYNTHESIS

OF IMPEDANCE CONTROL AND IDC

DEVICE FOR DEBURRING ROBOT

I.   Introduction

The realization of impedance control is described in chapter iv, the unified approach is applied for the robot in which the horizontal motion is driven with constant velocity and the vertical position is tracked the value computed from the desired force. The experiment system is designed basing on the unification of position and force. The servo step motors drive the motion of the robot. The x-axis motion is controlled with constant velocity by using PWM of 8-bit timer/counter0. The y-axis motion at current point is controlled respectively in order to x-axis's velocity and deburring profile's impact by using the PWM of 8-bit timer/counter2. The 10,000 revolutions encoder measures the position of the robot, and the PID controller is applied for robot position control. The strain gauge force sensor is used to measure the actual force. The deburring profile is proposed with variable curves for modeling of the deburring workpiece.
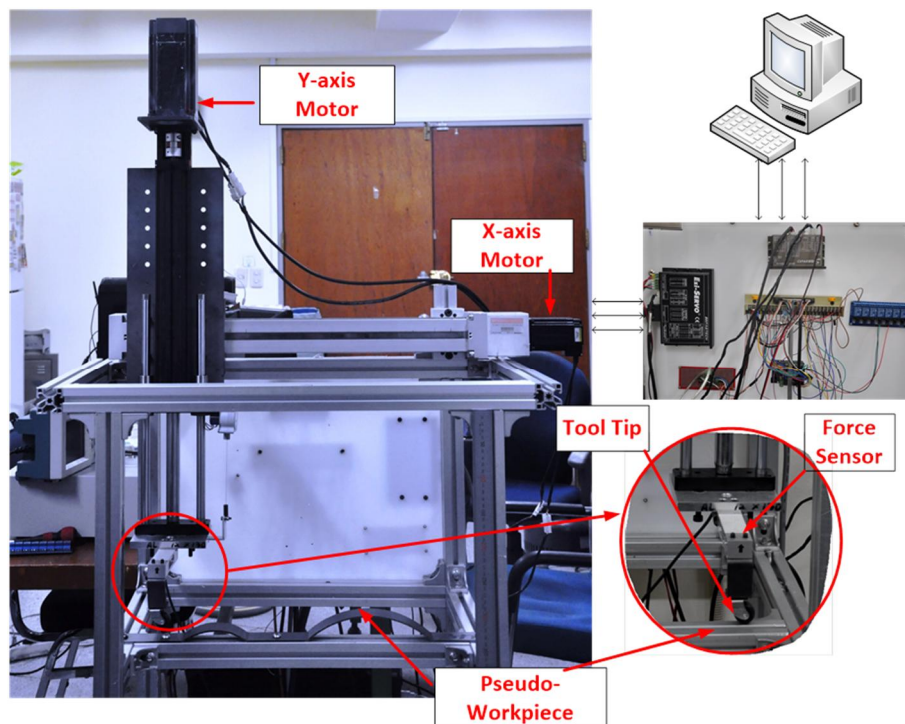
Fig. 92 The experiment system.

The experiment is carried out to control the actual force of deburring robot on the variable profile to track the desired value. As for impedance control, the position correction Δy_f is computed by using the impedance compensator function G_f by select the gain coefficient and the set force. The reference position is determined in according to the force sensor feedback. The internal position controller tracks the reference points at each time.
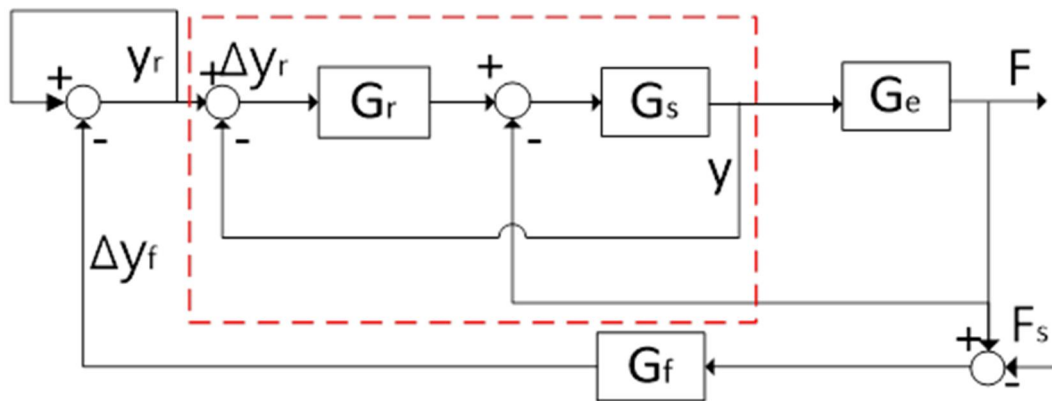
Fig. 93 The scheme of impedance control.

The responses of impedance control are shown in experiment results section. The system has the inherent properties because of the mechanical mechanism, and the position control is asynchronous. Especially the conflict at the gap points of deburring profile influences the response of the force. The chapter ii and iii presented the IDC device with the flexible mechanism. This device is attached between robot end-effector and tool to improve the contact force performance. The improvement is proved by experiment results.

II.   Experiment Processes and Results

The experiment is carried out to evaluate the impedance control for constant contact force control of the deburring robot. The IDC device's passive compliance is separately examined. The comparison of the impedance control of a deburring robot in

two cases of impedance control with IDC device and impedance control without IDC device is realized to evaluate the performance of IDC and impedance control.

2.1.   Application of impedance control without IDC device on the deburring profile

The application of impedance control without IDC device on the deburring profile is tested as Fig. 94.
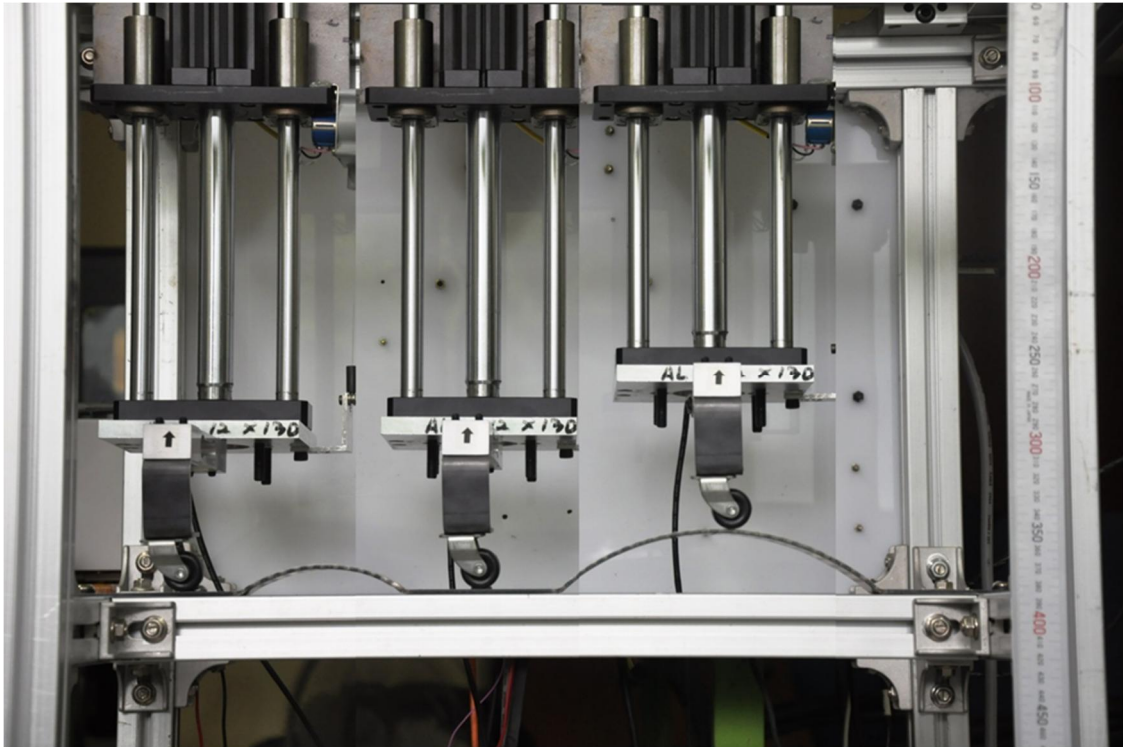
Fig. 94 Impedance control is tested on the deburring profile without IDC device. The trajectory of tooltip tracks well the deburring profile.
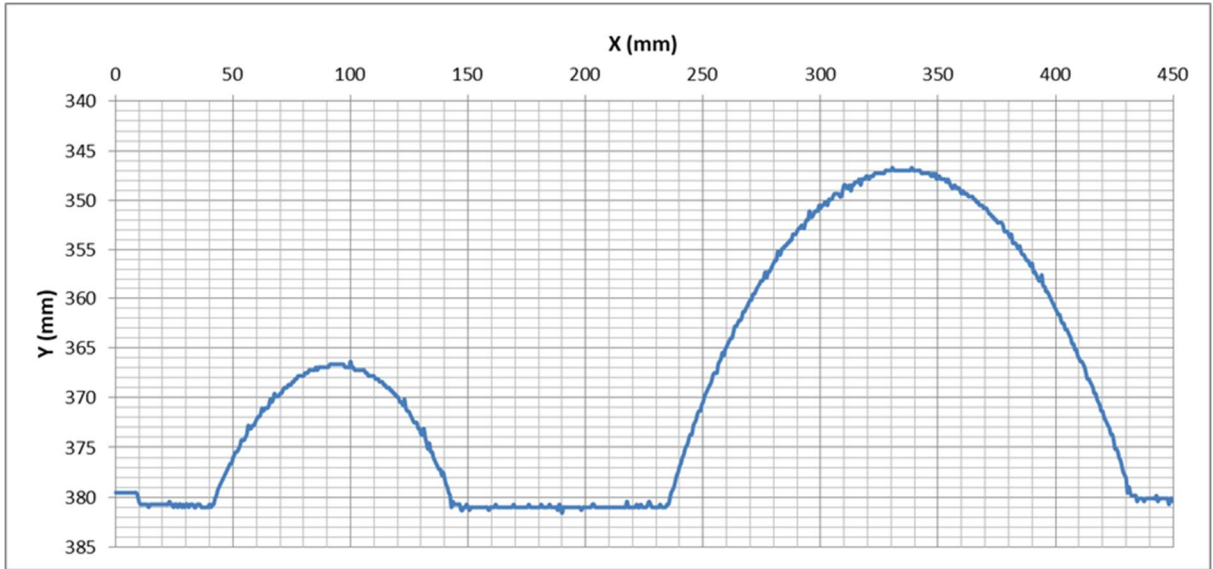
Fig. 95 The trajectory of the deburring tool in XY coordinates.
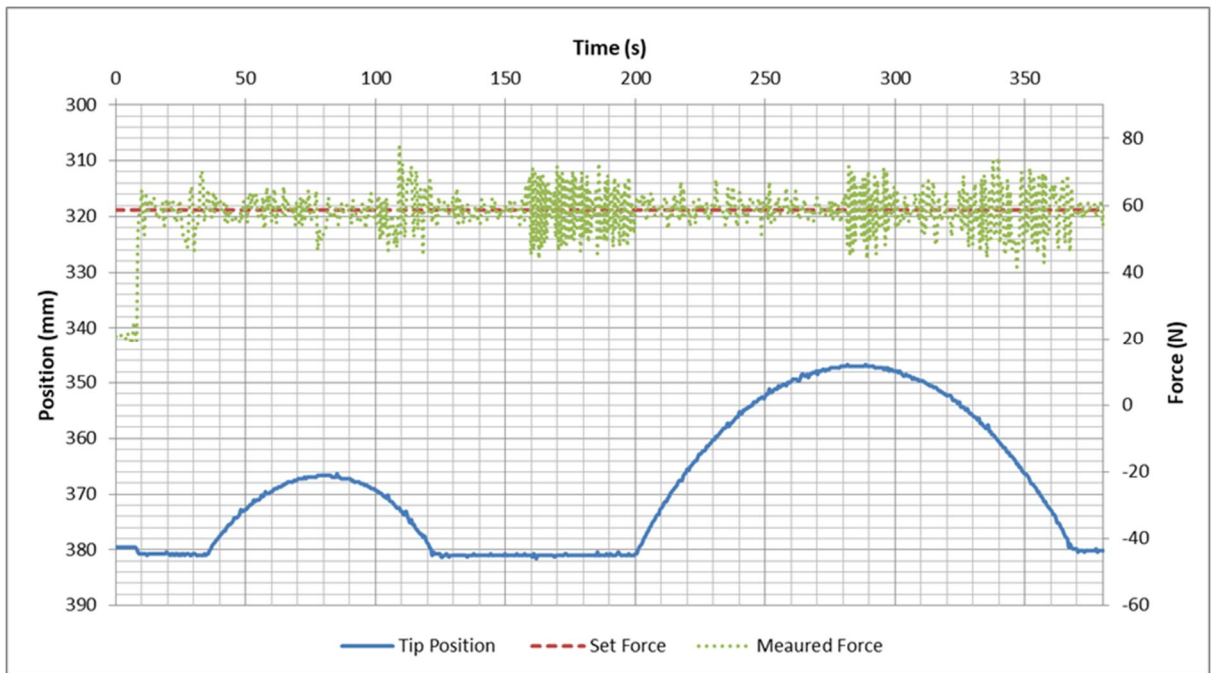
Fig. 96 Responses of robot motion and interaction force.

The actual force is abnormal at the gap of profile or at the unusual profile.

2.2.   Application of impedance control with IDC device on the deburring profile

The application of impedance control with IDC device is tested on the deburring profile as Fig. 97.
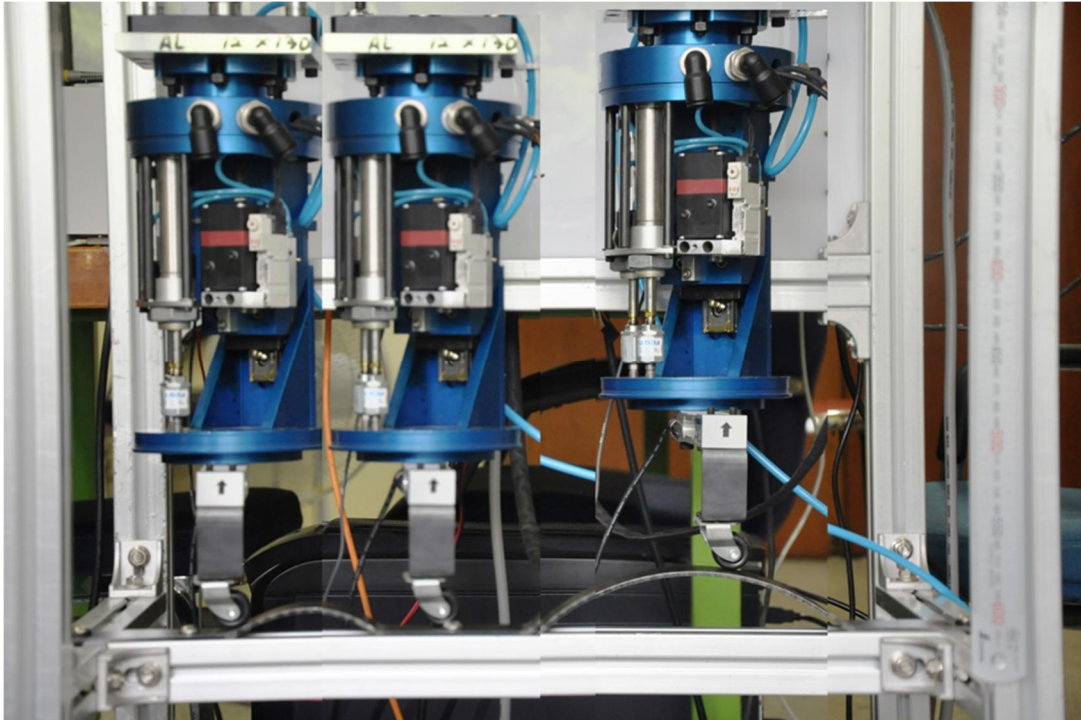
Fig. 97 Impedance control is tested on the deburring profile without IDC device.

    a.   The passive compliance of IDC device.

The passive compliance of IDC device is tested. The robot just moves in the horizontal. The IDC device is set with constant pressure, which is estimated from the desired value of actual force. The measured position and force reflected that the retract distance of IDC device effects on the interaction force when the robot contacts with the deburring profile.
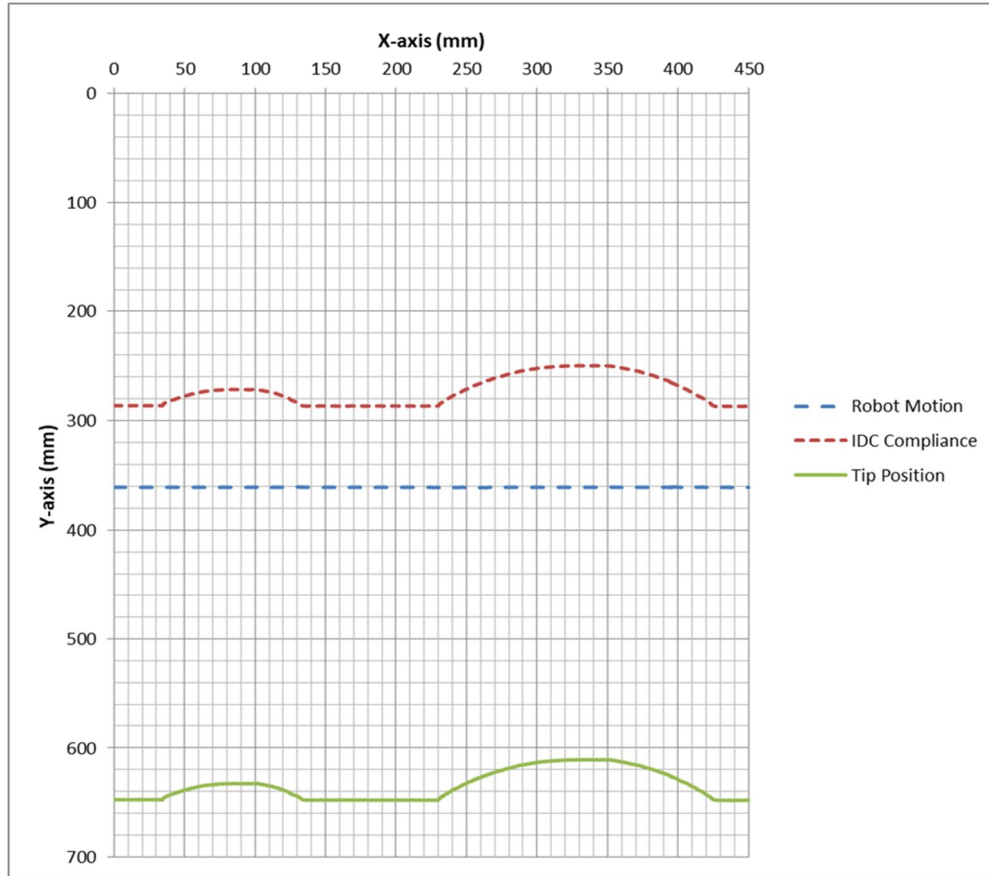
Fig. 98 The trajectories of the deburring tool, IDC compliance and robot motion in XY coordinates.
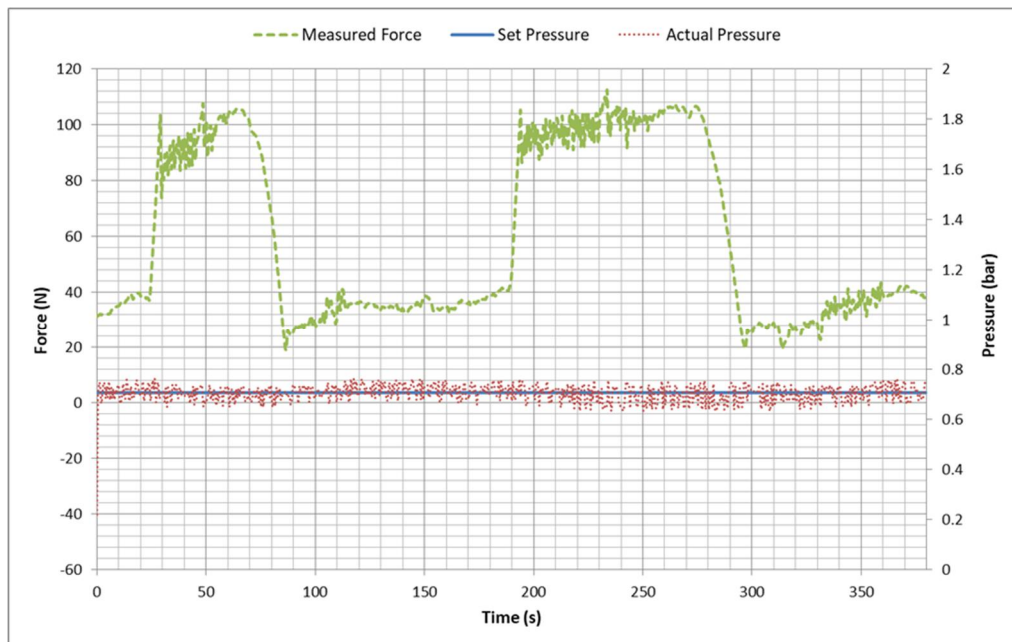
Fig. 99 Pressures of IDC device and the measured force.

b. Application of impedance control with IDC device on the deburring profile
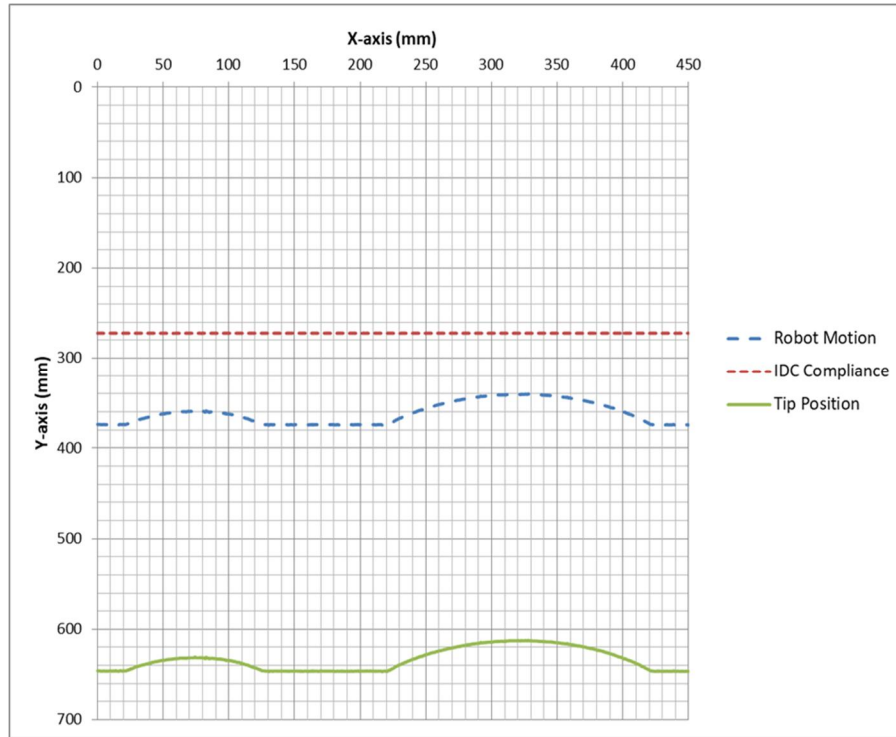
Fig. 100 The trajectories of the deburring tool, IDC compliance and robot motion in XY coordinates.
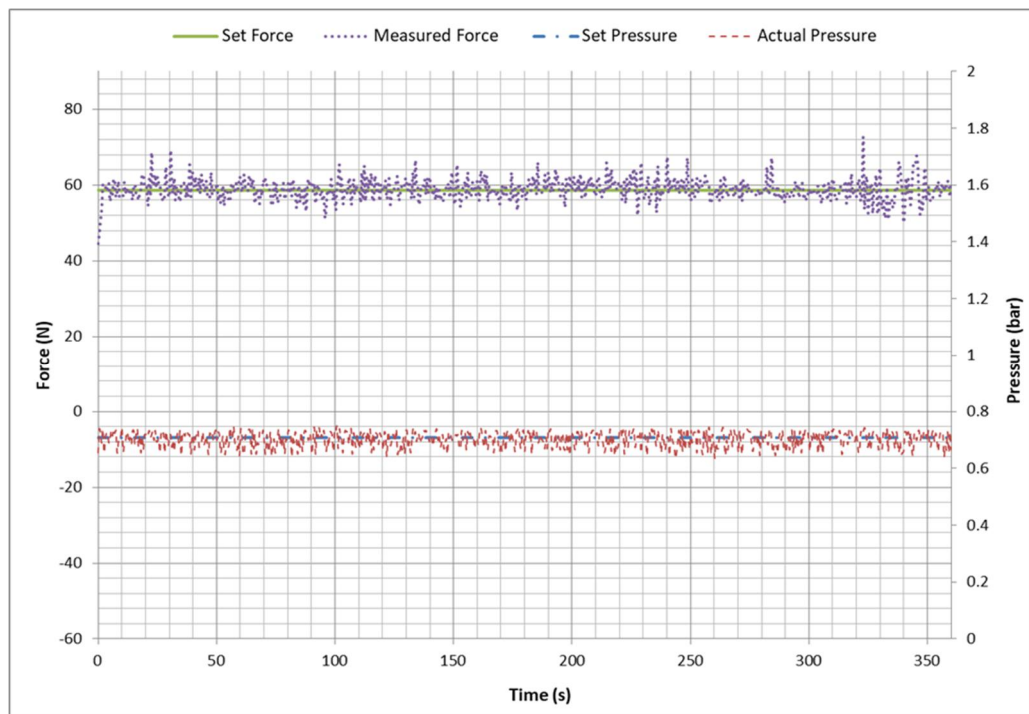
Fig. 101 Pressures of IDC device and the force responses.

125

2.3.   Comparison of the impedance control with IDC device and without IDC device.
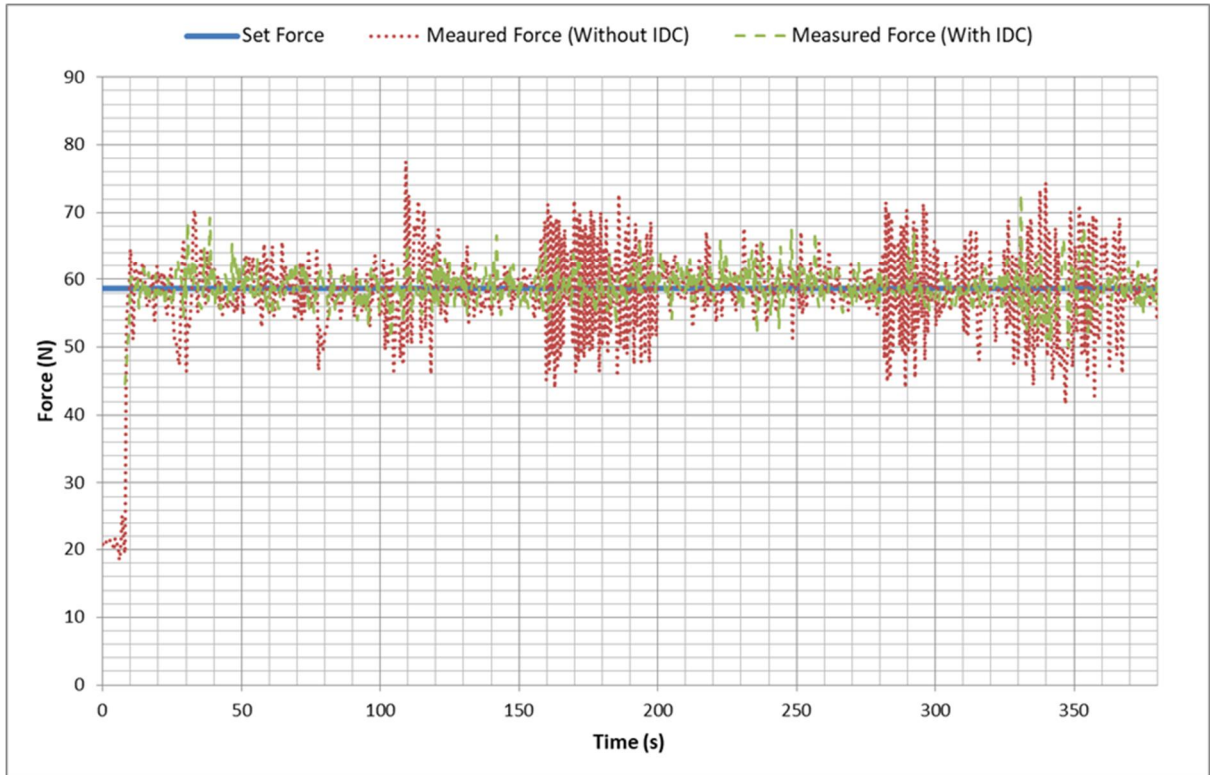
Fig. 102 Comparison of actual force responses.

The measurements are evaluated by using $L_2[e] = \sqrt{(1/T_f) \int_0^{T_f} |F - F_s|^2 \, dt}$ [95]. In which the scalar valued L_2 norm is used as an objective numerical measure of average tracking performance, where T_f is total time.

Table 6 Control performance evaluation

	Average Error ($\overline{F - Fs}$)		Standard errors ($L_2[e]$)	
	N	%	N	%
With IDC	0.19	0.33	2.76	4.71
Without IDC	-0.11	-0.19	5.62	9.58

III. Conclusion

The impedance control can control the actual force of deburring robot and well tracks the deburring profile respectively. The IDC device with flexible mechanism is controlled by the pneumatic system. However, the impedance control is applied to our experiment system, which remains inherent properties of the mechanical mechanism. The experiment showed that the passive compliance of IDC device can compensate the position and force control of impedance control. If the specific controller as active compliance controls the IDC device and impedance controller controls the deburring robot, the expected response of deburring robot will be optimistic.

CHAPTER VI CONCLUSION

In order to study the actual force control for the deburring robot, we presented two approaches. Two approaches are carried out in the different perspectives. In chapter ii and iii, the IDC device is designed with the specific controller for supporting the robot operation. The IDC device has a role like spring with the compliant mechanism. The main operation of such device is controlled by a pressure regulating valve and the cylinders' movement is feedback of position sensor. The force generation mechanism is modeled as mathematical modeling of pneumatic cylinders. The contact force is an equation of cylinders' movement and the supply pressure at the current point. The constant contact force is well assured by its controller and its sensors. For more detail, the pneumatic cylinders have the role of the air spring. The compliance of cylinders produces the active contact for preventing the collision in the processing. Likewise, such pneumatic cylinders are regulated by the pressure valve system, in which the directional solenoid valve can change the direction of cylinders for purpose of application such as pulling or pushing tasks, and the pressure regulating valve is used for generating the variable stiffness by regulating the air pressure. The first-order model is proposed for system modeling and verified by measurement. The motion of cylinders is animated by using the MATLAB/SimMechanics and the MATLAB simulation and Arduino-based experiment are used for evaluating the performance of IDC mechanism in order to control constant contact force.

In chapter iv, the relation between robot motion and contact force of a 2 DOF deburring robot is modeled by the affection of the robot dynamic modeling and the environment dynamic modeling. The unified position/force approach is applied in the transient processes shows that the stabilization of contact force is decided by the stabilization of robot motion. The contact force has an important role for deburring robot control in the surface processing. The contact force was evaluated by simulating the position-error-based impedance control model. The relative equation between the motion and the force is based on the robot dynamic model and environment dynamic model. The unified position/force method showed that the stabilization of contact force

is decided by the stabilization of robot motion in part. Basing on such findings, the target impedance model is realized by MATLAB System Identification Toolbox and evaluated by MATLAB/Simulink simulation from the experimental system's specifications. The simulation results reflected that the target impedance model could be used to regulate the deburring tool's penetration. Such penetration generates the desired force when robot works on the workpiece with variable materials, or when the burrs appear on the workpiece surface. The results also show the affection of estimated mass, damping and stiffness coefficients to the responses of the contact force such as the overshoot ratio, setting time, and the steady state.

On the transient processes, the continuous functions of motion deviation are defined in a form of the second-order differential equation. The function parameters are chosen by Root Locus analysis to stabilize the transition of robot motion. The continuous function of contact force deviation is derived through the motion deviation's function and dynamic model of the environment. The simulations of applications shows the responses of desired motion and force for robot system and it's environment when the stabilization of force and motion are synthesized simultaneously. Target impedance model proposed a the mass-damping-spring system-based variable stiffness model for the position error-based impedance control model to evaluate the response of contact force. In which, the internal position control of the robot is interfered by Arduino PID controller using interrupts and timers. The position error-based impedance control used such internal position control and realized-target impedance model and applied the unified approach for analyzing the effects of target impedance model on the responses of contact force such as target force, overshoot ratio, and stable state.

In chapter v, the impedance control is used for practical application of the deburring process. The experiment showed the impedance control is able to control the actual force and tracks the deburring profile. The inherent properties of robot motion and abnormality of the deburring robot could be compensated by controllable stiffness mechanism of IDC device.

Recent applications for constant contact force is developed as the flexible or active support component for the robot. In these trends, Toyota Corp developed a tool tracking mechanism [96] for controlling the end-effector to track the desired path so that a reaction force between workpiece and tool remains constant. In which, the target position is always determined independently of the last target position, no position error due to time delay affects a new target position even when the next target position is generated before the tool reaches the last target position. Thus, the robot is quick, responsive, and accurate when tracking at a constant operating speed. The automatic grinding apparatus [97], includes a constant rotating grinder regulated by load current, was developed by Aiko Engineering Co., Ltd. The automatic grinding apparatus starts the grinding motor at first, halting the travelling device at the initiation of grinding, permitting the grinder to approach the object to be ground after a time interval and starting the travelling device simultaneously or a little later after detecting that the grinding disk contacts the object to be ground, due to the variation of the load current of the grinding motor. This device is used to control the sliding device – for adjusting the distance between the tool and the object – to allow the load current of the grinding motor to be constant. The constant force device [98] was developed by University of Texas System to apply constant force from an actuator to a tool in contact with a work surface. The compliance and response of this device are controlled by adjustment of gas pressures in the pneumatic cylinder. The device automatically compensates for changes in desired (reference) tool force by adjusting gas pressures entering a pneumatic force generator to bring estimated applied tool force into substantial agreement with the reference tool force.

In previous researches, the actuator is focused to develop but I think of the workpieces. The workpieces are able to be active or still passive. In this chapter, I propose the integration motion/force mechanism of manipulation for the active actuator and the active workpiece which is mounted on the IDC device as in Fig. 103. For carrying out this propose, we have to build one control box to handle two tasks. The first is to do

131

the path planning task for tracking along the workpiece surface or required trajectories and the latter controls the compliant motion of the IDC device to maintain the constant contact force when robot contacts the workpieces.
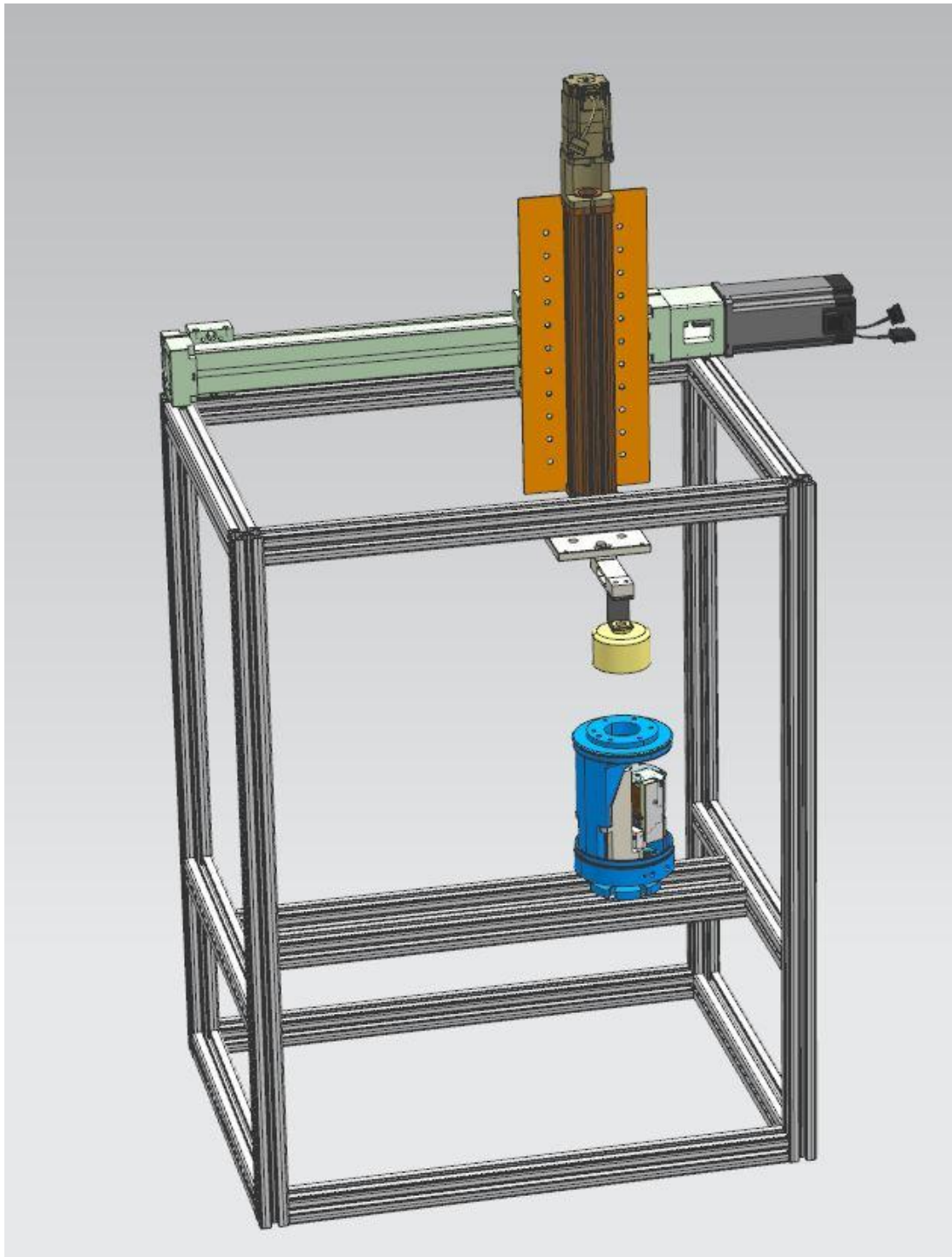
Fig. 103 Proposed system for an experimental deburring robot.

REFERENCES

[1] H. Kazerooni, J. Bausch and B. Kramer, "An Approach to Automated Deburring by Robot Manipulators," *ASME Journal of Dyn. Sys. Meas. and Control,* vol. 108, pp. 354-359, 1986.

[2] T. Yoshikawa, "Dynamic hybrid position/force control of robot manipulators description of hand constraints and calculation of joint driving force," *IEEE International Conference on Robotics and Automation,* pp. 1393-1398, 1986.

[3] T. M. Stepien, L. M. Sweet, M. C. Good and M. Tomizuka, "Control of Tool Workpiece Contact Force with Application to Robotic Deburring," *IEEE Journal of Robotics and Automation,* Vols. RA-3, pp. 7-18, 1987.

[4] H. Kazerooni and J. Guo, "Design and Control of the Active Compliant End-Effector," *American Control Conference,* pp. 845-850, 1987.

[5] G. M. Bone and M. A. Elbestawi, "Robotic Force Control for Deburring Using an Active End-effector," *Robotica,* vol. 7, pp. 303-308, 1989.

[6] B. M. Kramer and S. S. Shim, "Development of a system for robotic deburring," *Robotics and Computer-Integrated Manufacturing,* vol. 7, no. 3-4, pp. 291-295, 1990.

[7] S. Choudhary, "Force-position-velocity control of an industrial machine in computer integrated manufacturing," *16th Annual IEEE Conference of Industrial Electronics Society,* vol. 1, pp. 439-444, 1990.

[8] M. G. Her and H. Kazerooni, "Automated Robotic Deburring of Parts Using Compliance Control," *ASME Journal of Dynamic Systems, Measurement, and Control,* vol. 113, pp. 60-66, 1991.

[9] G. Bone, M. Elbestawi, R. Lingakar and I. Liu, "Force Control for Robotic Deburring," *ASME Journal of Dyn. Sys. Meas. and Control,* vol. 113, pp. 395-400, 1991.

[10] S. Liu and H. Asada, "Adaptive control of deburring robots based on human demonstration data," *International Conference on Industrial Electronics, Control, Instrumentation, and Automation,* pp. 946-952, 1992.

[11] M. A. Elbestawi, G. M. Bone and P. W. Tern, "An Automated Planning, Control, and Inspection System for Robotic Deburring," *CIRP Annals - Manufacturing Technology,* vol. 41, no. 1, pp. 397-401, 1992.

[12] Q. Li, Q. Tao, H. Cai and L. Hou, "Identification and smooth tracking control of robot force control system," *The IEEE International Symposium on Industrial Electronics,* vol. 1, pp. 337-341, 1992.

[13] D. Dornfeld, "Intelligent deburring of precision components," *International Conference on Industrial Electronics, Control, Instrumentation, and Automation,* pp. 953-960, 1992.

[14] M. H. Liu, "Robotic Deburring Based On Fuzzy Force Control," *The IEEE/RSJ International Conference on Intelligent Robots and Systems,* vol. 3, pp. 782-789, 1992.

[15] M. S. Ali, M. N. Noori and J. Turi, "Automatic deburring utilizing a real-time impedance control strategy," *Computers & Structures,* vol. 46, no. 3, pp. 561-571, 1993.

[16] D. Jeon and M. Tomizuka, "Learning hybrid force and position control of robot manipulators," *IEEE Transactions on Robotics and Automation,* vol. 9, no. 4, pp. 423-431, 1993.

[17] S. Liu and H. Asada, "Task-Level Robot Adaptive Control Based on Human Teaching Data and Its Application to Deburring," *American Control Conference,* pp. 1414-1417, 1993.

[18] Y. K. Hwang, P. C. Chen, A. A. Maciejewski and D. D. Neidigk, "A global motion planner for curve-tracing robots," *Proceedings of the IEEE International Conference on Robotics and Automation,* vol. 1, pp. 662-667, 1994.

[19] A. D. Lucas and C. Manes, "Modeling of robots in contact with a dynamic environment," *IEEE Transactions on Robotics and Automation,* vol. 10, no. 4, pp. 542-548, 1994.

[20] E. Tabarah, B. Benhabib and R. Fenton, "Motion Planning for Cooperative Robotic Systems Performing Contact Operations," *ASME Journal of Mechanical Design,* vol. 116, pp. 1177-1180, 1994.

[21] K. Shimokura and S. Liu, "Programming deburring robots based on human demonstration with direct burr size measurement," *IEEE International Conference on Robotics and Automation,* pp. 572-577, 1994.

[22] G. Bone and M. Elbestawi, "Sensing and control for automated robotic edge deburring," *IEEE Transactions on Industrial Electronics,* vol. 41, no. 2, pp. 137-146, 1994.

[23] J. M. Schimmels, "The use of compliance and constraint for improved robotic material removal processes," *IEEE International Conference on Robotics and Automation,* vol. 3, pp. 2627-2632, 1994.

[24] G. Ferretti, G. Magnani and P. Rocco, "On the Stability of Integral Force Control in Case of Contact With Stiff Surfaces," *ASME Journal of Dyn. Sys. Meas. and Control,* vol. 117, pp. 547-553, 1995.

[25] R. N. Tomastik, A. Enomoto and T. W. Engel, "Concept of Robotic Deburring Using Multipass Active Control," *Journal of Vibration and Control,* vol. 3, pp. 351-369, 1997.

[26] G. Bone and M. Elbestawi, "Dual-Sensor Based Robotic Deburring," *ASME Journal of Manufacturing Science and Engineering,* vol. 118, pp. 439-441, 1996.

[27] A. Abou-El-Ela and R. Isermann, "Fine motion control of robot manipulators in deburring applications utilizing cutting tool signals," *4th International Workshop on Advanced Motion Control,* pp. 86-91, 1996.

REFERENCES

[28] L. D. Joly, C. Andriott and V. Haywardt, "Mechanical analogies in hybrid position/force control," *Proceedings of International Conference on Robotics and Automation,* vol. 4, pp. 835-840, 1997.

[29] K. A. Hekman and S. Y. Liang, "Feed rate optimization and depth of cut control for productivity and part parallelism in grinding," *Mechatronics,* vol. 9, no. 5, pp. 447-462, 1999.

[30] F. Y. Hsu and L. C. Fu, "A new adaptive fuzzy hybrid force/position control for intelligent robot deburring," *IEEE International Conference on Robotics and Automation,* pp. 2476-2481, 1999.

[31] E. Aertbelien and H. Brussel, "An observation model and segmentation algorithm for skill acquisition of a deburring task," *IEEE/ASME International Conference on Advanced Intelligent Mechatronics,* pp. 635-640, 1999.

[32] R. Stango, L. Chen and V. Cariapa, "Automated Deburring with a Filamentary Brush Prescribed Burr Geometry," *ASME Journal of Manufacturing Science and Engineering,* vol. 121, pp. 385-392, 1999.

[33] Y. D. Lee, B. H. Kang and J. O. Park, "Robotic deburring strategy using burr shape recognition," *IEEE/RSJ International Conference on Intelligent Robots and Systems,* pp. 1513- 1518, 1999.

[34] S. F. Su, T. J. Horng and K. Y. Young, "Evolution-based virtual training in extracting fuzzy knowledge for deburring tasks," *IEEE International Conference on Robotics and Automation,* pp. 3855-3860, 2000.

e

[35] S. F. Hsu and L. C. Fu, "Intelligent Robot Deburring Using Adaptive Fuzzy Hybrid Position/Force Control," *IEEE Transactions on Robotics and Autiomation,* vol. 16, no. 4, pp. 325-335, 2000.

[36] S. C. Chen and P. C. Tung, "Trajectory planning for automated robotic deburring on an unknown contour," *International Journal of Machine Tools and Manufacture,* vol. 40, no. 7, pp. 957-978, 2000.

[37] L. Chen, R. Stango and V. Cariapa, "A Force-Control Model for Edge-Deburring with Filamentary Brush," *ASME Journal of Manufacturing Science and Engineering,* vol. 123, pp. 528-532, 2001.

[38] P. Pagilla and B. Yu, "An experimental study of planar impact of a robot manipulator," *IEEE International Conference on Robotics and Automation,* vol. 4, pp. 3943-3948, 2001.

[39] P. Pagilla and B. Yu, "Robotic Surface Finishing Processes Modeling Control and Experiments," *ASME Journal of Dyn. Sys. Meas. and Control,* vol. 123, pp. 93-102, 2001.

[40] A. Goradia, N. Xi and J. D. Tan, "Hybrid force/position control in moving hand coordinate frame," *7th International Conference on Control, Automation, Robotics and Vision,* pp. 1126-1131, 2002.

[41] C. Valente and J. Oliveira, "A New Approach for Tool Path Control in Robotic," *ABCM Symposium Series in Mechatronics,* vol. 1, pp. 124-133, 2004.

[42] G. Ziliani, G. Legnani and A. Visioli, "A Mechatronic Design for Robotic Deburring," *Proceedings of the IEEE International Symposium on Industrial Electronics,* pp. 1575-1580, 2005.

[43] X. Wang, Y. Wang and Y. Xue, "Adaptive Control of Robotic Deburring Process Based on Impedance Control," *IEEE International Conference on Industrial Informatics,* 2006.

[44] A. Robertsson, T. Olsson, R. Johansson, K. Nilsson, M. Haage, B. Lauwers, H. Baerdemaeker, T. Brogardh and H. Breantmark, "Implementation of Industrial Robot Force Control Case Study: High Power Stub Grinding and Deburring," *IEEE/RSJ International Conference on Intelligent Robots and Systems,* pp. 2743-2748, 2006.

[45] X. Wang, Y. Wang and Y. Xue, "Intelligent Compliance Control for Robotic Deburring Using Fuzzy Logic," *IEEE International Conference on Industrial Informatics,* pp. 91-96, 2006.

[46] C. Kim and J. H. Chung, "Modeling and Control of a New Robotic Deburring System," *ASME Journal of Manufacturing Science and Engineering,* vol. 129, pp. 965-972, 2007.

[47] F. Nagata, Y. Kusumoto, Y. Fujimoto and K. Watanabe, "Robotic sanding system for new designed furniture with free-formed surface," *Robotics and Computer-Integrated Manufacturing,* vol. 23, pp. 371-379, 2007.

[48] D. Buckmaster, W. Newman and S. Somes, "Compliant motion control for robust robotic surface finishing," *7th World Congress on Intelligent Control and*

Automation, pp. 559-564, 2008.

[49] C. H. Kim, J. H. Chung and D. H. Hong, "Coordination control of an active pneumatic deburring tool," *Robotics and Computer-Integrated Manufacturing,* vol. 24, no. 3, pp. 462-471, 2008.

[50] J. Wang, G. Zhang and T. Fuhlbrigge, "Force control technologies for new robotic applications," *IEEE International Conference on Technologies for Practical Robot Applications,* pp. 143-149, 2008.

[51] J. Y. Choi, Y. J. Choi and B. J. Yi, "Force sensor-less interaction force control in the de-burring task using dual-arm manipulation," *IEEE/RSJ International Conference on Intelligent Robots and Systems,* pp. 967-973, 2008.

[52] L. Liao, F. Xi and K. Liu, "Modeling and control of automated polishing/deburring process using a dual-purpose compliant toolhead," *International Journal of Machine Tools and Manufacture,* vol. 48, no. 12-13, pp. 1454-1463, 2008.

[53] Y. Zhu and E. Barth, "Passivity-Based Impact and Force Control of a Pneumatic Actuator," *ASME Journal of Dyn. Sys. Meas. and Control,* vol. 130, pp. 024501:1-7, 2008.

[54] M. Daniali and G. Vossoughi, "Intelligent active vibration control of constrained manipulaors in robotic deburring," *International Conference on Industrial Mechatronics and Automation,* pp. 76-80, 2009.

[55] S. H. Lee, C. J. Li, D. H. Kim, J. H. Kyung and C. S. Han, "The direct teaching

and playback method for robotic deburring system using the adaptive force-control," *IEEE International Symposium on Assembly and Manufacturing,* pp. 235-241, 2009.

[56] F. Xi, L. Liao and K. Liu, "Adaptive Control of Pressure Tracking for Polishing Process," *ASME Journal of Manufacturing Science and Engineering,* vol. 132, pp. 011015:1-12, 2010.

[57] T. Osada, K. Yano, N. Kato and M. Fofana, "On the Development of a Machining Support System to Improve Surface Finish," in *ASME Int. Mechanical Engineering Congress and Exposition*, USA, 2011.

[58] Y. H. Chen and C. C. Ian, "An Adjustable Constant-Force Mechanism for Adaptive End-Effector Operations," *ASME Journal of Mechanical Design,* vol. 134, pp. 031005:1-9, 2012.

[59] T. Diezt, U. Schneider, M. Barho, S. Oberer-Treitz, M. Drust, R. Hollmann and M. Fraunhofer, "Programming System for Efficient Use of Industrial Robots for Deburring in SME Environments," *ROBOTIK 2012; 7th German Conference on Robotics,* pp. 428-433, 2012.

[60] H. C. Song, B. S. Kim and J. B. Song, "Tool path generation based on matching between teaching points and CAD model for robotic deburring," *2012 IEEE/ASME International Conference on Advanced Intelligent Mechatronics (AIM),* pp. 890-895, 2012.

[61] F. Domroes, C. Krewet and B. Kuhlenkoetter, "Application and Analysis of Force Control Strategies to Deburring and Grinding," *Modern Mechanical Engineering,*

vol. 3, pp. 11-18, 2013.

[62] H. C. Song and J. B. Song, "Precision robotic deburring based on force control for arbitrarily shaped workpiece using CAD model matching," *Int. Journal of Precision Manufacturing,* vol. 14, no. 1, pp. 85-91, 2013.

[63] V. Parlaktaş, "Spatial compliant constant-force mechanism," *Mechanism and Machine Theory,* vol. 67, pp. 152-165, 2013.

[64] J. R. D. Posada, S. Kumar, A. Kuss, U. Schneider, M. Drust, T. Diezt and A. Verl, "Automatic Programming and Control for Robotic Deburring," in *47th International Symposium on Robotics*, Germany, 2016.

[65] F. Tian, C. Lv, Z. Li and G. Liu, "Modeling and control of robotic automatic polishing for curved surfaces," *CIRP Journal of Manufacturing Science and Technology,* vol. 14, pp. 55-64, 2016.

[66] W. Xu, "Robotic Time-Varying Force Tracking in Position-Based Impedance Control," *ASME Journal of Dyn. Sys. Meas. and Control,* vol. 138, pp. 091008:1-12, 2016.

[67] S. Liu and J. E. Bobrow, "An Analysis of a Pneumatic Servo System and Its Application to A Computer-Controlled Robot," *ASME Journal of Dynamic System, Measurement, Control,* vol. 110, pp. 228-235, 1988.

[68] J. E. Bobrow and F. Jabbari, "Adaptive Pneumatic Force Actuation and Position Control," *ASME Journal of Dynamic System, Measurement, Control,* vol. 113, pp. 267-272, 1991.

[69] B. W. McDonell and J. E. Bobrow, "Adaptive Tracking Control of an Air Powered Robot Actuator," *ASME Journal of Dynamic System, Measurement, Control,* vol. 115, pp. 427-433, 1993.

[70] P. K. Arun, J. K. Mishra and M. G. Radke, "Reduced Order Sliding Mode Control for Pneumatic Actuator," *IEEE Trans. Control Systems Technology,* vol. 2, no. 3, pp. 271-276, 1994.

[71] D. Ben-Dov and E. Salcudean, "A Force-Controlled Pneumatic Actuator," *IEEE Transactions of Robotic and Automation,* vol. 11, no. 6, pp. 906-911, 1995.

[72] A. M. Al-Ibrahim and D. R. Otis, "Transient Air Temperature and Pressure Measurements During the Charging and Discharging Processes of An Actuating Pneumatic Cylinder," in *Proceedings of the 45th National Conference on Fluid Power* , 1992.

[73] E. Richer and Y. Hurmuzlu, "A High Performance Pneumatic Force Actuator System: Part I-Nonlinear Mathematical Model," *ASME Journal of Dynamic Systems, Measurement, and Control,* vol. 122, pp. 416-425, 2000.

[74] J. Carneiro and F. Almeida, "Reduced-order Thermodynamic Models for Servo-Pneumatic Actuator Chambers," *Journal of System and Control Engineering,* vol. 220, no. 3, pp. 301-314, 2006.

[75] D. Dihovicni and M. Medenica, "Mathematical Modelling and Simulation of Pneumatic Systems," in *Advances in Computer Science and Engineering*, InTech, 2011, pp. 161-186.

[76] Y. Wang, H. Su, K. Harrington and G. S. Fisher, "Sliding Mode Control of Piezoelectric Valve Regulated Pneumatic Actuator for MRI-compatible Robot Intervention," in *Proceedings of ASME Dynamic Systems and Control Conference*, 2010.

[77] P. Bigras, K. Khayati and T. Wong, "Modified Feedback Linearization Controller for Pneumatic System with non-Negligible Connection Port Restriction," in *Proceedings of IEEE Int. Conf. on System, Manu. and Cybernetics*, Tunisia, 2002.

[78] N. H. Quach and M. Liu, "Transition from Free Motion Control to Constrained Force Control for Robot Manipulators," in *5th Asian Control Conference* , Melbourne, Australia, 2004.

[79] M. H. Raibert and J. J. Craig, "Hybrid Position/Force Control of Manipulators," *Trans. ASME J. of Dynamic System, Measurement and Control,* vol. 103, no. 2, pp. 126-133, 1981.

[80] Y. Ekalo and M. Vukobratovic, "Quality of Stabilization of Robot Interacting with Dynamic Environment," *Journal of lntelligent and Robotic Systems,* vol. 14, pp. 155-179, 1995.

[81] M. Vukobratovic and Y. Ekalo, "Unified Approach to Control Laws Synthesis for Robotic Manipulators in Contact with Dynamic Environment," *IEEE Int. Conference on Robotics and Automation,* pp. 213-229, 1993.

[82] V. C. Aitken and H. M. Schwartz, "On the Exponential Stability of Discrete-Time System with Applications in Observer Design," *IEEE Trans. on Automatic*

Control, vol. 39, no. 9, pp. 1959-1962, 1994.

[83] M. Vukobratovic, Applied dynamics of manipulation robots: modelling, analysis and examples, Berlin : Springer-Verlag , 1989.

[84] Y. Ekalo and M. Vukobratovic, "Robust and adaptive position/force stabilization of robotic manipulators in contact tasks," *Robotica,* vol. 11, no. 4, pp. 373-386, 1993.

[85] M. Vukobratovic, "The Role of Environment Dynamics in Contact Force Control of Manipulation Robots," *ASME J. Dyn. Sys., Meas., Control ,* vol. 119, no. 1, pp. 86-89, 1997.

[86] A. M. Lyapunov, "The general problem of the stability of motion," *International Journal of Control,* vol. 55, no. 3, pp. 531-534, 1992.

[87] R. D. Gregorio, "Dynamic Model and Performances of 2-DOF Mechanisms," *Robotica,* vol. 24, no. 1, pp. 51-60, 2006.

[88] T. C. Nguyen, W. J. Lee and Y. S. Yang, "A Study on the Interaction Control of Force and Motion between Tool and Workpiece," *Autumn Conference on Drive and Control,* pp. 157-161, 2016.

[89] O. Kathib, "A Unified Approach for Motion and Force Control of Robot Manipulator: The Operational Space Formulation," *IEEE Journal ob Robotics and Automation,* vol. 3, no. 1, pp. 43-53, 1987.

[90] T. C. Nguyen, W. J. Lee and Y. S. Yang, "Unified Approach for Force/Position

Control in the Vehicle Body Sanding Process," *Journal of Drive and Control,* vol. 14, no. 3, pp. 25-31, 2017.

[91] Z. Lu and A. A. Goldenberg, "Implementation of Robust Impedance and Force Control Using VSS Theory," *ASME Press Series: Proceedings of the International Symposia on Robotics and Manufacturing,* vol. 3, pp. 279-285, 1990.

[92] J. Maples and J. Becker, "Experiments in Force Control of Robotic Manipulators," *Proceedings of IEEE International Conference on Robotics and Automation.,* pp. 695-703, 1986.

[93] H. Kazerooni, "Contact Instability of the Direct Drive Robot when Constrainned by a Rigid Envinronment," *IEEE Transactions on Automatic Control,* vol. 35, no. 6, pp. 710-714, 1990.

[94] E. Lizama and D. Surdilovic, "Design G-Optimal Experiment for Robot Dynamics Identification," *Proceedings of IEEE Int. Conf. on Robotics and Automation,* pp. 311-316, 1996.

[95] L. Xu and B. Yao, "Adaptive Robust Precision Motion Control of Linear Motors with Negligible Electric Dynamics: Theory and Experiments," *IEEE Trans. Mechatronics,* vol. 6, no. 4, pp. 444-452, 2001.

[96] Y. Ishiguro, Y. Kato, C. Hayashi, M. Nakano, M. Koide, H. Moribe and T. Kuno, "Robot with controlled tool tracking displacement". US Patent 4,967,127, 30 10 1990.

n

[97] S. Yonaha, M. Chin and K. Yatsuda, "Automatic grinding apparatus". US Patent 5,299,389 , 05 04 1994.

[98] E. A. Erlbacher, "Method for applying constant force with nonlinear feedback control and constant force device using same". US Patent 5,448,146 , 05 09 1995.

PUBLICATIONS

JOURNALS

1. Q. H. Le, Y. M. Jeong, C. T. Nguyen and S. Y. Yang, "Development of a Virtual Excavator using SimMechanics and SimHydraulic", *J Korean Soc Fluid Power Constr Equip,* Vol. 10, No. 1, pp. 29-36, 2013.

2. C. T. Nguyen, Q. H, Le, Y. M. Jeong and S. Y. Yang, "A Study of Stability for Field Robot using Energy Stability Level Method", *J Korean Soc Fluid Power Constr Equip*, Vol. 11, No. 3, pp. 22-30, 2014.

3. Q. H. Le, Y. M. Jeong, C. T. Nguyen and S. Y. Yang, "Development of the Flexible Observation System for a Virtual Reality Excavator using the Head Tracking System", *Journal of Drive and Control,* Vol. 12, No. 2, pp. 27-33, 2015.

4. C. T. Nguyen, Q. H, Le, Y. M. Jeong and S. Y. Yang, "A Study on Modeling of Pneumatic System for an IDC Device", *Journal of Drive and Control*, Vol. 12, No. 3, pp. 11-17, 2015.

5. C. T. Nguyen, J. W. Lee and S. Y. Yang, "Unified Approach for Force/Position Control in the Vehicle Body Sanding Process", *Journal of Drive and Control*, Vol. 14, No. 3, pp. 25-31, 2017.

6. C. T. Nguyen and S. Y. Yang, "A Study of Force Control for Deburring Robot using Position Error-based Impedance Control Model", *Journal of Drive and Control*, Vol. 15, No. , pp. , 2018. (under-reviewed)

7. C. T. Nguyen and S. Y. Yang, "Practical Synthesis of Impedance Control and IDC Device for Deburring Robot", *Journal of Mechanical Science and Technology*, (will be submitted in July 2018).

CONFERENCES

1. J. W. Oh, Y. M. Jeong, G. Y. Kim, C. T. Nguyen and S. Y. Yang, "Automobile Transmission Valve Body Cover Automation System", KSAE Autumn Conference, pp. 57-64, 2015.

2. . U. Kim, J. W. Oh, C. T. Nguyen, Y. S. Kim, K, H, U and S. Y. Yang, "A Study on Development of the Automatic Painting Surface Inspection System", KSFC Spring Conference, pp. 123-126, 2015.

3. Q. H. Le, Y. M. Jeong, C. T. Nguyen and S. Y. Yang, "Study on Remote Control for Field Robot and Augmented Reality Vision Using Head Tracker System", KSFC Autumn Conference, pp. 65-70, 2014.

4. J. W. Oh, Y. M. Jeong, G. Y. Kim, C. T. Nguyen and S. Y. Yang, "Automobile Transmission Automation System", Drive and Control Autumn Conference, pp. 93-99, 2015.

5. C. T. Nguyen, Q. H. Le, Y. M. Jeong and S. Y. Yang, "A Study on Modeling of Pneumatic System for an IDC Device", Drive and Control Spring Conference, 109-114, 2015.

6. C. T. Nguyen, Y. M. Jeong and S. Y. Yang, "Study of the Stability for Field Robot", ICROS Conference No. 42, pp. 406-407, 2013.

7. C. T. Nguyen, Y. H. Lee and S. Y. Yang, "Study on Turn-over Stability for Filed Robot with Swinging Manipulator", Drive and Control Spring Conference, pp. 111-115, 2015.

8. Q. H. Le, Y. M. Jeong, C. T. Nguyen and S. Y. Yang, "Study on Intuitive Configuration of Joystick for Operator in Flattening Task of Excavator", KSFC Autumn Conference, pp. 11-15, 2013.

9. J. W. Oh, T. W. Kim, C. T. Nguyen, Y. S. Kim and S. Y. Yang, "A Study on Development of an Oil Mist Collecting Simulator of Vacuum Systems", Drive and Control Spring Conference, pp. 145-149, 2015.

10. Q. H. Le, S. W. Choi, T. U. Kim, C. T. Nguyen, J. W. Lee and S. Y. Yang, "A Study on Trajectory Tracking Control of Field Robot", Drive and Control Autumn Conference, 119-123, 2016.

11. C. T. Nguyen, J. W. Lee and S. Y. Yang, "A Study on the Interaction Control of Force and Motion between Tool and Workpiece", Drive and Control Autumn Conference, pp. 157-161, 2016.

12. Q. H. Le, S. W. Choi, C. T. Nguyen and S. Y. Yang, "Development of Intuitive Configuration of Joystick in Grading Task of Excavator", Drive and Control Spring Conference, pp. 101-105, 2017.

13. C.T. Nguyen, J.W. Lee and S.Y. Yang, "Unified Approach for Force/Position Control in the Car Body Sanding Process", Drive and Control Spring Conference, pp. 149-155, 2017.

14. Q. H. Le, S. W. Choi, C. T. Nguyen and S. Y. Yang, "Simulation of Hydraulic System for Double Arm Excavator in Disaster Environment", Drive and Control Autumn Conference, pp. 53-59, 2017.

15. C. T. Nguyen, Q. H. Le, Y. M. Jeong, Y. S. Kim and S. Y. Yang, "Study of Development of Intelligent Deburring Control (IDC) Device Applied for Surface Processing", KSME Spring Conference, pp. 18-18, 2014.

16. Q. H. Le, J. I. Bae, Y. M. Jeong, C. T. Nguyen and S. Y. Yang, "Development of the Flexible Observation System for a Virtual Reality Excavator using the Head Tracking System", 15th ICCAS, pp. 841-846, 2015.

17. C. T. Nguyen, K. T. Park and S. Y. Yang, "A Study of Stability for Field Robot using Energy Stability Method", 14th ICCAS, pp. 331-337, 2014.

18. C. T. Nguyen. J. H. Ko, Y. H. Lee and S. Y. Yang, "The Energy Stability Margin for Tracked Vehicle Mounted Manipulator", 13th ICCAS, pp. 1156-1159, 2013.

19. Q. H. Le, Y. M. Jeong, C. T. Nguyen and S. Y. Yang, "Control of Virtual Excavating System base on Real-Time Simulation", 12th ICCAS, pp. 703-707, 2012.

r

20. Q. H. Le, Y. M. Jeong, C. T. Nguyen and S. Y. Yang, "A Study on Real-Time Simulation and Control of Virtual Excavator", ICMT Conference, pp. 382-387, 2012.

21. Q. H. Le, Y. M. Jeong, C. T. Nguyen and S. Y. Yang, "The Architecture of the Remote Control System for Excavator", ICROS Autumn Conference, 2012.

22. . H. Le, Y. M. Jeong, C. T. Nguyen and S. Y. Yang, "A Study on Remote Control with Flexible Vision System for Field Robot using Head Tracking System", ICMT Conference, pp. 34-40, 2014.

23. S. Y. Yang, Q. H. Lee, C. T. Nguyen and Y. M. Jeong, "Study on Remote Control for Field Robot and Augmented Reality Vision using Head Tracker System", JFPS Conference, pp. 747-751, 2014.

24. C. T. Nguyen, I. H. Kim and S. Y. Yang, "Impact Energy-based Study of Stability for Field Robot", ICMT Conference, pp. 200-204, 2013.

25. C. T. Nguyen, T. U. Kim, J. W. Lee and S. Y. Yang, "Study on Interaction Control for Contact Robotics", ICMT Conference, pp. 125-129, 2017.

LIST OF PROJECT

번호	과제명	사업명	연구기간	참여기관
1	차륜형장갑차 가변피스톤형 유압펌프 개발	구매조건부 신제품개발사업	2016.09.22 ~2018.03.21	피엠씨
2	선박 기관실용 1.5톤 지능형 Manipulator 기술개발	지역주력산업 육성사업	2017.06.01 ~2018.05.31	영광공작소
3	재난·재해 대응 특수목적 기계용 핵심요소부품 및 시스템개발	산업핵심기술 개발사업	2015.07.01 ~2018.04.30	한국생산기술연구원 건설기계부품연구원 수산중공업
4	데이터처리율 향상을 위한 사물인터넷기반의 공정품질관리 시스템	산학공동기술 개발지원사업	2017.06.01 ~2018.05.31	ING KOREA
5	EV/PHEV용 VCU 개발에 관한 연구	산학협력선도 대학육성사업	2016.07.01 ~2016.12.31	정우테크
6	자율주행자동차 경진대회 차량제작 지원	기타사업	2016.01.26 ~2017.01.31	현대엔지비㈜
7	블랙박스(RC-100)금형 시제품 해석	기타사업	2016.01.25 ~2016.04.24	㈜에이티엠

t

8	차량 3D CAD 설계정보와 로봇 비젼시스템을 이용한 도장표면 불량 검출 및 마킹 자동검사 시스템 개발	중소기업융복합기술개발사업	2014.12.22 ~2016.12.21	㈜에이티엠
9	안전로컬분전함개발	기업부설연구소지원사업	2014.11.01 ~2016.10.31	맵시전자
10	루프 캐리어 개발사양 선정을 위한 시뮬레이터 개발	산학협력선도대학육성사업	2015.07.01 ~2015.12.31	주경산업
11	자동차 미션 사이드커버 자동화 조립시스템 개발	구매조건부신제품개발사업	2014.12.01 ~2015.11.30	㈜화인
12	중전기 및 2차 전지 생산공정의 진공펌프를 위한 수·유분 미스트 제거시스템 개발	산학공동기술개발지원사업	2014.12.01 ~2015.11.30	㈜엠벡
13	로봇을 이용한 차량 도장 표면검사 시스템 개발을 위한 선행 기술 조사	기타사업	2014.11.03 ~2015.01.30	㈜에이티엠
14	지능형제어를 통한 자동차부품의 정밀 디버링 기술 개발	지역특화산업육성사업	2013.06.01 ~2015.05.31	㈜유창파워텍 이든모터스㈜ ㈜세원물산
15	교통약자를 위한 휠체어 수납 시스템 개발에 관한 연구	산학협력선도대학육성사업	2014.08.01 ~2015.01.31	㈜유창파워텍

16	자동차 차제조립용 지그 설계 자동화 프로그램 개발	산학공동기술 개발지원사업	2013.11.01 ~2014.10.31	하이인텍
17	중형 지게차 TCU 개발에 관한 연구	기타사업	2013.09.02 ~2014.03.31	㈜엠에스정밀
18	연료효율 향상을 위한 가감속 제어 시스템 개발	산학협력선도 대학육성사업	2013.08.01 ~2014.01.31	포텐
19	톱 루프&매니퓰레이터 호이스트 타입 승용차량 휠체어 수납 및 이송장치 개발	현장맞춤형 기술개발사업	2013.06.11 ~2014.04.23	이든모터스㈜
20	CTIS(공기압조절장치)기능을 가진 2차 감속 조향 구동허브 개발	지역산업 기술개발사업	2012.12.01 ~2013.11.30	신정개발특장차㈜